5. RESEARCH ACTIVITIES

5.1 NUCLEAR PHYSICS

As Indian National Gamma Array (INGA) experimental campaign is in TIFR, very few experiments were done in GDA beamline. The experiments were done using GDA with CPDA for 'l' distribution experiment, and Perturbed angular distribution system.

The GPSC facility has been used for many user experiments on studies of heavy ion induced fusion-fission dynamics by measuring fission fragment angular distribution and mass distribution. Two large area multi-wire proportional counter (MWPC) are used for detection of complimentary fragments in coincidence and an array of hybrid detector telescope (gas ionization & Silicon detector) was used for particle identification and angular distribution measurements.

The existing neutron array facility consisting of 24 liquid scintillators and two MWPC detectors for fission fragment setup has been used in user experiments measuring pre- & post scission neutron multiplicity from heavy ion induced fission. The neutrons were detected in coincidence with fission fragments. A series of experiments were performed in this year and the analysis of data from these experiments is currently in progress. This facility will soon be replaced by the large array of neutron detectors (DST project) being setup at IUAC.

The recoil spectrometer HYRA in the gas filled mode has been successfully used for several experiments for the study of fusion-fission dynamics near the Coulomb barrier. In conjunction with the 32-element NaI detector sum-spin spectrometer from TIFR installed at the target position the angular momentum effects in reaction dynamics were probed.

Giant resonances in middle mass nuclei were studied through fusion reactions with the spin spectrometer in coincidence with the large NaI(Tl) detector HIGRASP and also a novel LaBr + NaI detector developed at TIFR to probe the shape evolution effects at high excitations in nuclei.

5.1.1 SADDLE POINT SHELL CORRECTION ENERGIES FROM PRE-SCISSION NEUTRON MULTIPLICITIES

Golda K.S.[1,2], A. Saxena[3], K. Mahata[3], P. Sugathan[1], A. Jhingan[1], V. Singh[4], R. Sandal[4], S. Goyal[5], J. Gehlot[1], A. Dhal[1], B.R. Behera[4], R.K. Bhowmik[1], V.K. Mittal[2] and S. Kailas[3]

[1]Inter University Accelerator Centre, Aruna Asaf Ali Marg, New Delhi 110067, India
[2]Department of Physics, Punjabi University, Patiala, Punjab 147002, India
[3]Nuclear Physics Division, Bhabha Atomic Research Centre, Mumbai 400085, India
[4]Department of Physics, Panjab University, Chandigarh 160014, India
[5]Department of Physics and Astrophysics, University of Delhi, New Delhi 110007, India

The quantitative determination of fission barrier height is the key to understand dynamics of heavy ion fusion-fission process and the prediction of super heavy elements. However, very few attempts have been made to extract the shell correction to the fission barrier from the experimental fission data in heavy ion induced fusion-fission reactions. It has been shown that [1] the shell corrections at saddle point is necessary to explain the measured fission cross-sections, the evaporation residue cross sections and the pre-scission neutron multiplicity data simultaneously in mass 200 region. With this motivation, we carried out measurements of neutron spectra for $^{12}C+^{194,198}Pt$ systems [2].

The statistical model code PACE2 with modified level density and fission barrier prescription [1] was used to extract the shell correction values from the experimental observables. Energy dependent shell

corrections were used to obtain level density parameter at equilibrium ($\tilde{a}_n$) and saddle point ($\tilde{a}_f$). Further details can be found in Ref. [1]. The fission barrier is calculated by adding the shell correction at ground state (Δ_n) and that at saddle point (Δ_f) to the liquid drop component of fission barrier. The Δ_f is assumed to be $k_f \times \Delta_n$ where k_f is determined by fitting the experimental data. In Fig. 1 the experimental pre-scission neutron multiplicities are compared with the statistical model (SM) predictions as described above also fitting simultaneously fusion and fission excitation functions. The bottom panels of Fig.1 shows how good the SM calculations (continuous line) using the best fitted (k_f , $\tilde{a}_f/\tilde{a}_n$) parameters match with the experimental fusion (filled diamond) and fission (filled uptriangle) excitation functions [3]. To understand the effects of shell correction at saddle point satisfying the fission excitation functions, the SM calculations have been carried out with different conditions to estimate the average pre-scission neutron multiplicity. As can be seen from Fig. 1 the calculated neutron multiplicities without any shell correction at the saddle point (k_f=0.0) under predict the experimental values. Whereas, the calculated neutron multiplicities with full shell corrections at the saddle point (k_f = 1.0, dotted line) over predict the measured data. As the excitation energy of the fissioning system increases, the dynamical effect comes into picture which eventually increases the number of neutrons emitted before scission. Hence the simultaneous fitting of fusion and fission cross sections and pre-scission neutron multiplicity to obtain the best fitted (k_f , $\tilde{a}_f/\tilde{a}_n$) values was done at the lower two excitation energies. Thus obtained k_f was used to estimate the saddle point shell correction and thereby to determine the fission barrier height. The uncertainties in the fitted parameters are obtained by minimizing the χ^2 and are <6%. It is interesting to note that in case of $^{12}C+^{198}Pt$ system the best fitted value of (k_f , $\tilde{a}_f/\tilde{a}_n$) thus obtained could satisfactorily explain the pre-scission multiplicity at the highest excitation energy also. However it under predicts the data at the highest energy for $^{12}C+^{194}Pt$ system. A fission delay of 30×10^{-21} s was incorporated to estimate the dynamical correction in the pre-scission neutron multiplicity [1]. The data shown with open circles in Fig. 1 are obtained by considering the dynamical effect. It shows that the inclusion of fission delay is essential to satisfactorily explain the measured pre-scission multiplicities at the highest excitation energy for the $^{12}C+^{194}Pt$ system. However, the incorporation of dissipative effects are not required to explain the experimentally measured pre-scission multiplicities for $^{12}C+^{198}Pt$ system in the energy domain under consideration. Hence it could be conjectured that dissipation effects are felt for shell closed nuclei only at higher excitation energy compared to nuclei away from closed shell.

To conclude, we have determined the shell correction energies within an uncertainty of 6% at the saddle point by measuring the average pre-scission neutron multiplicities for $^{12}C+^{194}Pt$ and for $^{12}C+^{198}Pt$ systems. It has been demonstrated that the introduction of shell correction of 70% at the saddle point potential energies with respect to the ground state shell correction value is crucial for the description of the measured pre-scission neutron multiplicities and the difference in their values for the two systems.

We gratefully acknowledge Dr. S.S. Kapoor for the stimulating discussions and critical suggestions.

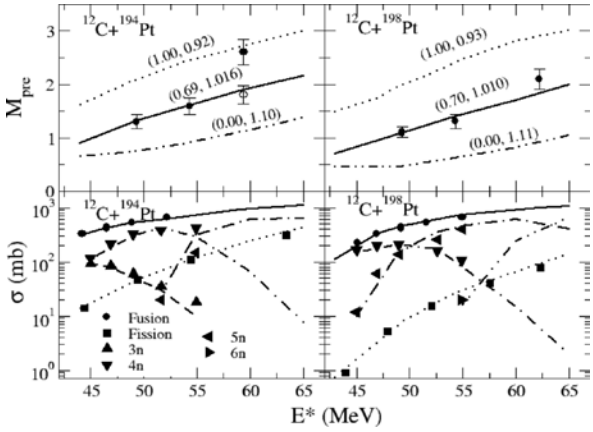

Fig. 1: Experimental pre-scission neutron multiplicities, fusion,fission and ER excitation functions along with the statistical model results.

REFERENCES:

[1] K. Mahata et al., Phys. Rev. C 74, 041301 (2006).
[2] Golda K.S. Et al., DAE Symp. on Nucl. Phys.,Vol. 55, 262 (2010).
[3] A. Shrivastava et al., Phys. Rev. C 63, 054602 (2001).

5.1.2 EVAPORATION RESIDUE SPIN DISTRIBUTION FOR $^{31}P+^{170}Er$

Gayatri Mohanto[1], N. Madhavan[1], S. Nath[1], J. Gehlot[1], I. Mazumdar[2], A. Jhingan[1], Jhilam Sadhukhan[3], Ish Mukul[1], Maninder Kaur[4], Varinderjit Singh[4], T. Varughese[1], D.A. Gothe[2], P.B. Chavan[2], A.K. Sinha[5], R.K. Bhowmik[6], A. Roy[1], S. Pal[3] and V.S. Ramamurathy[7]

[1]Inter University Accelerator Centre, Aruna Asaf Ali Marg, New Delhi 110067, India
[2]Tata Institute of Fundamental Research, Homi Bhabha Road, Mumbai 400005, India
[3]Variable Energy Cyclotron Centre, 1/AF Bidhan Nagar, Kolkata 700064, India
[4]Department of Physics, Panjab University, Chandigarh 160014, India
[5]UGC-DAE CSR, Kolkata Centre, 3/LB-8, Bidhan Nagar, Kolkata 700098, India
[6]Department of Physics, Guru Ghasidas University, Bilaspur, Chhatisgarh 495009, India
[7]National Institute of Advanced studies, Bengaluru 560012, India

Effect of shell closure on fusion-fission dynamics has been an interesting topic of research. Shell closure of either of reaction partners [1] and shell closure of Compound Nucleus (CN) have been found to affect the reaction dynamics [2-4]. We chose evaporation residue (ER) spin distribution as a tool to study fusion-fission dynamics and effect of CN shell closure, if any. ER spin distribution gives information of partial waves which survived fission. We studied two reactions namely, $^{30}Si+^{170}Er$ and $^{31}P+^{170}Er$, forming CN ^{200}Pb and ^{201}Bi respectively. These two CNs have same number of neutrons but one has proton shell closure (Z = 82) and the other one has Z = 83. The objective was to compare ER spin distributions for CN ^{200}Pb and ^{201}Bi at similar excitation energies.

The experiment was carried out at Inter University Accelerator Centre. ^{30}Si and ^{31}P beams of energies from 146 MeV to 188 MeV were provided by Pelletron + LINAC facility. Target of ^{170}Er of thickness 130 μg/cm^2, sandwiched between two carbon layers of thicknesses 45 and 23 μg/cm^2, was used in the experiment. The HYbrid Recoil mass Analyzer (HYRA) [5] was used to select ERs. ERs were detected at the focal plane with the help of a Multi Wire Proportional Counter (MWPC) of area 6" × 2" followed by a double sided silicon strip detector with 16 strips at each side [6]. HYRA was operated in gas-filled mode, with helium gas at a pressure of 0.15 Torr. Gamma-rays were detected with the help of TIFR 4π spin spectrometer [7] coupled to HYRA [8]. The complete array of the spin spectrometer consists of 32 NaI detectors (12 pentagonal detectors and 20 hexagonal detectors). Out of 32, 29 detectors were used in this experiment covering a solid angle of 91% of 4π sr giving an absolute efficiency of 77%. 2 pentagonal detectors were removed for beam entrance and exit and one hexagon was removed for inserting the target ladder. Time of flight of ERs from target chamber to focal plane was of the order of 1.5 μs. Pulsed beam of repetition rate 2 μs was taken and Time to Amplitude Converter (TAC) was set between the anode signal of MWPC and the RF signal from beam pulsing system. The TAC spectrum allowed separation of ERs from other contaminants. Time-of-flight (TOF) gate was put on the multiplicity to get ER-gated experimental multiplicity (gamma-fold) distribution. Data were collected in beam-off condition too in order to quantify background in first few folds which could help in incorporating appropriate corrections to ER-gated fold distribution.

ER gate was put on experimental gamma-fold to clean other non-compound events. 1-4 folds were contaminated by huge background and had to be determined by extrapolation for further analysis. Fold distributions were fitted to get gamma-multiplicity distributions using the procedure described in Ref. [9]. Further analysis is in progress.

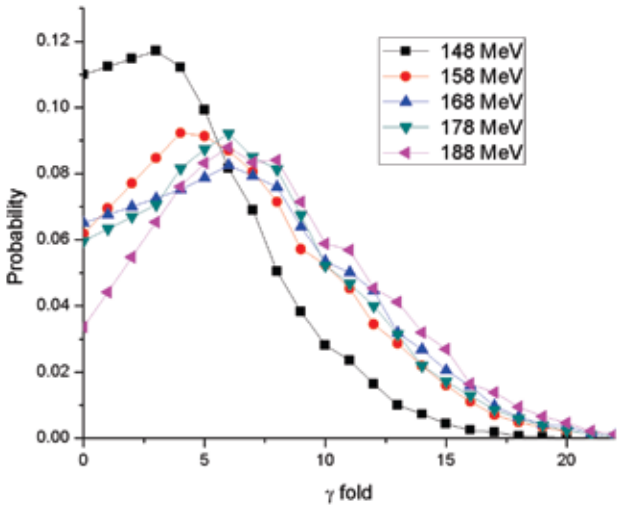

Fig1. Experimental gamma-fold distributions for $^{31}P+^{170}Er$ at five different beam energies.

REFERENCES:

[1] K. Sataou et al., Phys. Rev. C 65, 054602 (2002).
[2] A. Shrivastava et al., Phys. Rev. Lett. 82, 699 (1999).
[3] S. Nath et al.,Phys. Rev. C 81, 064601 (2010).
[4] S. Nath et al., Nucl. Phys. A 850, 22 (2011).
[5] N. Madhavan et al., Pramana -J Phys 75, 317 (2010).
[6] A. Jhingan et al., DAE Symp. on Nucl. Phys. Vol. 56, 1096 (2011).
[7] G. Anil kumar et al., Nucl. Instr. Meth. A 76, 611 (2009).
[8] N. Madhavan et al., EPJ Web of Conferences 17, 14003 (2011).
[9] G. Mohanto et al., EPJ Web of Conferences 17, 16007 (2011).

5.1.3 MODELING OF INCOMPLETE FUSION AT $E_{lab} \approx$ 4-8 MEVA

R. Kumar[1], Vijay R. Sharma[2] and R.K. Bhowmik[3]

[1]Inter University Accelerator Centre, Aruna Asaf Ali Marg, New Delhi 110067, India
[2]Accelerator Laboratory, Department of Physics, Aligarh Muslim University, Aligarh 202002, India
[3]Department of Physics, Guru Ghasidas University, Bilaspur, Chhatisgarh 495009, India

The dynamics of incomplete fusion (ICF) has been extensively investigated in heavy ion (HI) induced reactions at energies near and/or above the Coulomb barrier, where ICF is found to compete with complete fusion (CF) at energies 4-7 MeV/A. However, the complex mechanism of incomplete mass transfer is still not well understood and, thus, continues to be an active area of investigations. Recently, it was observed in several studies that the projectile, before its break-up, loses a significant amount of energy in the interaction with the target nucleus and later, there may be complete and/or partial momentum transfer [1]. As HI reactions are associated with large angular momentum, therefore, a proper understanding of entrance channel partial waves is important in the study of ICF.

In order to emphazise the relative contribution of CF and ICF in terms of partial waves, an attempt has been made to carry forward Wilczynski model [2] at beam energies ≈ 4-7 MeV/A by assuming a Fermi-like function (f) i.e. $f_l=1/(1+\exp((l_p-l_c)/\Delta)$, where the symbols have their usual meaning [3]. The data of the experiments carried out for $^{14}N+^{169}Tm$, $^{16O}+^{169}Tm$, $^{12}C+^{159}Tb$ and $^{16}O+^{159}Tb$ systems at the Inter University Accelerator Center (IUAC), New Delhi, using recoil-catcher technique followed by offline gamma-spectroscopy have been used to obtain the fusion cross-sections. The details of the experiments are given elsewhere [4-6]. The partial cross-sections have been calculated using the code PACE which uses Bass fusion cross-sections. The transmission probability associated with the partial waves can be calculated

using the one dimensional barrier penetration model (BPM). To the best agreement experimental excitation functions have been obtained for the values of a=A/8.0 MeV^{-1} and the value of the diffuseness parameter has been set to 0.2 for the calculations. In order to account for CF cross-section 'σ_{CF} ' and ICF cross-section 'σICF ', the Bass fusion cross-section formalism was normalized with the presently assumed fermi-like function (f_l). For CF cross-section; $\sigma_{CF} = \sigma l.fl$ and for ICF cross-section; $\sigma_{ICF} = \sigma l .(1-f_l)$. Based on the above presently assumed prescription, a FORTRAN based Multi-step pArtial Reaction Cross-section (MARC) code has been developed, which is able to reproduce relative yields of CF and ICF. Further, cross-sections obtained using the MARC program are plotted against normalized values of angular momentum (Fig. 1(a)-1(d)).

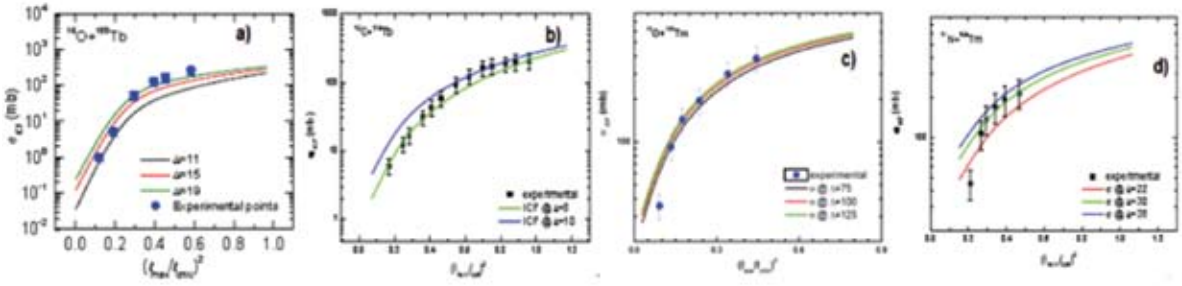

Fig. 1. Theoretical incomplete fusion (ICF) cross section at different diffuseness parameter 'Δ' as a function of normalized angular momentum.

REFERENCES:

[1] P.P. Singh et al., Phys. Rev C. 77, 014607 (2008).
[2] J. Wilczynski et al., Phys. Rev. Lett. 45, 606 (1980); Nucl. Phys. A 373, 109 (1982).
[3] R. Kumar, Vijay R. Sharma et al., Nucl. Phys. Symp. Vol. 56, 614 (2011).
[4] Abhishek Yadav et al., Phys. Rev. C 85, 034612 (2012).
[5] Manoj K. Sharma et al., Nucl. Phys. A 776, 83 (2006).
[6] R. Kumar et al., communicated to Phys. Rev. C (2012).

5.1.4 SEARCH FOR QUASIFISSION IN ASYMMETRIC REACTION FORMING ^{250}Cf COMPOUND SYSTEM

C. Yadav[1], R.G. Thomas[1], R.K. Choudhury[1], P. Sugathan[2], A. Jhingan[2], S. Appannababu[2], E. Prasad[3], K.S. Golda[2], D. Singh[2], Ish Mukul[2], J. Gehlot[2], H.J. Wollershiem[4]

[1]Nuclear Physics Division, Bhabha Atomic Research Centre, Mumbai 400085, India
[2]Inter University Accelerator Centre, Aruna Asaf Ali Marg, New Delhi 110067, India
[3]Department of Physics, University of Calicut, Calicut 673635, India
[4]GSI, Darmstadt, Germany

In the early eighties of the last century, it was first recognized that the observation of fission fragments in heavy ion induced reaction does not necessarily originate from fission decay of a compound nucleus formed by fusion of projectile and target nuclei [1]. The process responsible for this observation is a non-equilibrium fission process called quasifission, which is associated with the incomplete relaxation in the mass asymmetry within the time available for the reaction. Though much progress in the description of this process, which is also expected to play a critical role in the synthesis of heavy and superheavy nuclei via fusion of heavy nuclei, have been achieved over the years, a comprehensive understanding of this complex processes is yet to be reached [2]. Of late, several measurements have shown unexpected presence of quasifission even in less fissile and asymmetric systems (i.e., systems with fissility < 0.8) [3-5].

The main motivation of this present work was to study the onset of quasifission process in the fissility region > 0.8. It was observed that angular distribution of fission fragments produced in reactions in this fissility region showed anomalously large anisotropies at sub-barrier energies as compared to SSPM,

implying presence of pre-equilibrium fission (PEF) [6]. In order to find the experimental evidence of mass equilibration/non-equilibration in the reactions with fissility ~0.86, we carried out measurements of mass angle and mass ratio distributions at the 15UD Pelletron accelarator facility of Inter University Accelarator Centre (IUAC), New Delhi, for the $^{12}C+^{238}U$ and $^{18}O+^{232}Th$ reactions, forming the same compound nucleus ^{250}Cf (fissility = 0.86), at similar excitation energy and angular momentum. The measurements were carried out in the energy range $E_{c.m.}/V_b \sim 0.88 - 1.1$, where $E_{c.m.}$ is the energy in center-of-mass frame and V_b is the Coulomb barrier. We used pulsed beams of ^{12}C (E_{lab} = 61-76 MeV) and ^{18}O (E^{lab} = 80-96 MeV) with a pulse width of ~1 ns and pulse separation of ~250 ns, bombarded on a ^{238}U target of thickness 108 μg/cm^2, sandwiched between carbon backings of ~20 μg/cm^2 and ^{232}Th target of thickness 150 μg/cm^2 on a carbon backing of thickness 30 μg/cm2, respectively. Fission fragments produced in the reactions were detected by a pair of large area Multi-Wire Proportional Counters (MWPC) with the active area of 20 cm × 10 cm, kept at mean fission fragment folding angle. The distance of forward detector from target was 58 cm and that of backward detector from target was 36 cm. Two silicon surface barrier detectors were also placed at 10^0 with respect to beam direction for beam monitoring purpose. Time distribution of fission fragments were recorded by taking the start signal from MWPC's anode and a delayed stop signal from RF. The time distribution spectra were then converted to time of flight (TOF) spectra after appropriate calibration. The calibrated position spectra along with TOF spectra were then used to deduce the velocity of complimentary fragments. In the analysis, the velocities of fissioning system in the reaction plane and perpendicular to it was used to separate the full momentum transfer (FMT) events and nucleon transfer induced fission (TF) events.

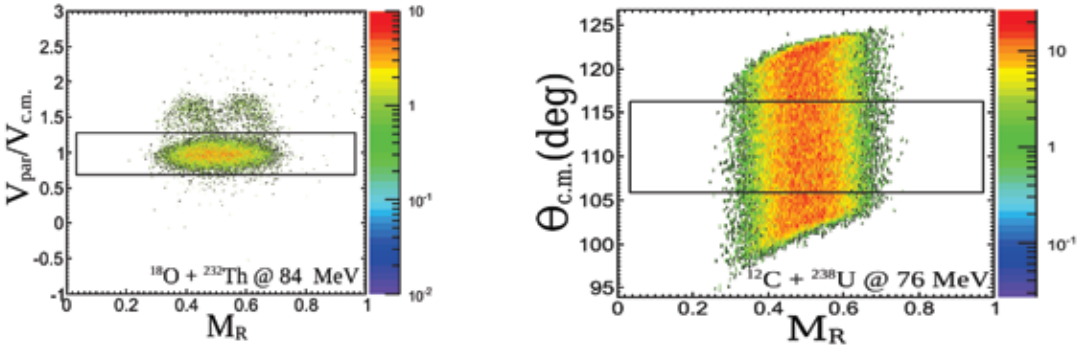

Fig. 1: The left panel shows scatter plot of mass-ratio MR versus parallel velocity component (relative to velocity in the c.m. frame) of the fissioning nuclei for $^{18}O+^{232}Th$ reaction at 84 MeV. The TF events are clearly separated from FMT events as seen in the above figure. The software cut (as shown) is used to select only the FMT events. The right panel shows experimental mass angle distribution of FMT events for $^{12}C+^{238}U$ reaction at 76 MeV. The cut as shown in figure was imposed to obtain the mass ratio distributions.

Using the conservation of linear momentum, the mass ratio was then obtained from the relation [7],

$$M_R = M_2 / (M_1+M_2) = V_{1cm} / (V_{1cm} + V_{2cm}) ;$$

where V_{1cm} and V_{2cm} are c.m. velocity vectors of fission fragments with mass M_1 and M_2 respectively. In Fig. 1, the plots of mass ratio M_R against parallel velocity component of fissioning nuclei relative to c.m. velocity V_{CM} of fissioning nuclei, is shown. It is seen that FMT events and TF events are clearly visible. It is found that the contribution from transfer fission events increases as the beam energy fall through Coulomb barrier for both the systems. For further analysis we put the gate on FMT events to get the mass angle distribution of fusion-fission events. The mass angle distributions of FMT events for $^{12}C+^{238}U$ system is shown in the right panel of Fig. 1. We have seen that there is no correlation between mass ratio M_R (mass of one fragment divided by total mass) with emission angle of fission fragments, for both the systems at all the energies studied. The rectangular gates as shown in the right panel of Fig. 1 are imposed in mass angle distribution plots of both the systems at all energies to obtain mass ratio distributions unbiased from the geometrical limitation of the detectors.

The plot of standard deviations of extracted mass ratio distributions against compound nucleus excitation

energy is shown in Fig. 2. It can be seen that the width of mass distributions for $^{18}O+^{232}Th$ system is consistently higher than that of $^{12}C+^{238}U$ system at all excitation energies. The higher variance of mass distributions for the more symmetric system as compared to the asymmetric system is an indication of presence of quasifission in the more symmetric system (i.e., in $^{18}O+^{232}Th$ reaction) in addition to PEF [6-8].

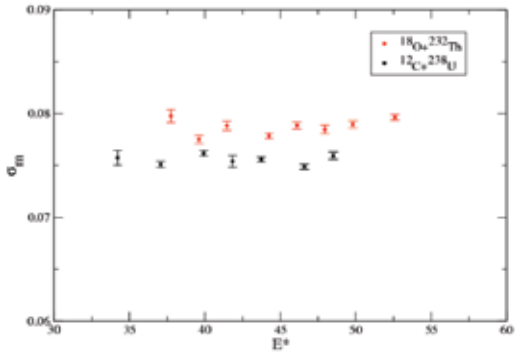

Fig. 2: Plot of standard deviation σ_m against compound nucleus excitation energy in MeV.

REFERENCES:

[1] W.J. Swiatecki, Phys. Scr. 24, 113 (1981).
[2] P. Armbuster, C.R. Physique 4, 571 (2003).
[3] R. Rafiei et al, Phys. Rev. C 77, 024606 (2008).
[4] R.G. Thomas et al, Phys. Rev. C 77, 034610 (2008).
[5] E. Prasad et al, Phys. Rev. C 81, 054608 (2010).
[6] V.S. Ramamurthy et al, Phys. Rev. Lett 54, 178 (1985).
[7] D.J. Hinde et al, Phys. Rev. C 53, 1290 (1996).
[8] R.G. Thomas et al, Phys. Rev. C 67, 041601 (2003).

5.1.5 STUDY OF FISSION FRAGMENT ANGULAR DISTRIBUTION FOR ^{19}F + $^{194, 196,198}Pt$ REACTIONS AT NEAR AND ABOVE BARRIER ENERGIES.

Varinderjit Singh[1], B.R. Behera[1], Maninder Kaur[1], A. Jhingan[1,2], P. Sugathan[2], D. Siwal[3], M. Oswal1, S. Goyal[3], K.P Singh, A. Saxena[4] and S. Kailas[4]

[1]Department of Physics, Panjab University, Chandigarh 160014, India
[2]Inter University Accelerator Centre, Aruna Asaf Ali Marg, New Delhi 110067, India
[3]Department of Physics and Astrophysics, University of Delhi 110007, India
[4]Nuclear Physics Division, Bhabha Atomic Research Centre, Mumbai 400085, India

From the study of light particles emitted in heavy-ion induced fusion-fission reactions, the importance of dissipation in fusion-fission dynamics is well established. Experimental signature of large dissipation is observed through large excess in pre-fission neutrons, gamma-ray multiplicities from the compound nucleus, giant dipole resonance (GDR), light charged particles and evaporation residue [1-2]. Back *et al*. [3] reported that in order to reproduce evaporation residue cross-sections for ^{224}Th and ^{216}Th nuclei, a larger dissipation strength was required for former in comparison to later. They concluded that nuclear dissipation had possible relation with neutron closed shell $N_C = 126$ [3]. It is to be noted that this conclusion was drawn from one observable sensitive to nuclear dissipation (i.e. evaporation residue). So it is desirable to do a consistent analysis for other observables like pre-scission neutron multiplicity, fission and ER cross section to establish the role of neutron shell closure in the dissipation strength. With this motivation in our mind, we have decided to perform a simultaneous analysis of neutron multiplicity, fission cross-section and evaporation residue cross-section for $^{19}F+^{194,196,198}Pt$ ($N_c = 126, 128, 130$) systems at excitation energy range 46 - 91.8 MeV. Here we report the preliminary results of our fission fragment angular distribution measurement.

The experiment was carried out at the general purpose scattering chamber (GPSC), using DC beam of ^{19}F (energy varies from 90.5 to 118.7 MeV) delivered by the 15 UD Pelletron at IUAC, New Delhi. ^{19}F beam was bombarded on ^{194}Pt, ^{196}Pt and ^{198}Pt targets of thicknesses ~ 1.75 mg/cm^2. Fission fragments were detected using two different detector set-ups kept on both arms of the scattering chamber on the ether sides of beam direction. On one arm of scattering chamber, two Si surface barrier telescope detectors (SSBD) were placed at a distance of 13 cm (collimator size 5 mm) each with angular separation of 24^0. On the other arm, three hybrid telescope (ΔE gas and E SSBD) detectors were kept at a distance of 28 cm (collimator size 10 mm) each with angular separation of 12^0 between two adjacent detectors. The two SSB detectors were kept at ± 10^0 with a distance of 70 cm (collimator size 1 mm) for monitoring and normalization purpose. The trigger to the data acquisition system was generated using the OR timing signals of two detector set-ups along with the monitor detectors.

The experimentally measured fission yield of each detector was normalized using the inter detector normalization, and the beam energy loss in the half target thickness were taken into account. The experimental fission fragment angular distribution was transformed from laboratory to center-of-mass frame using Viola systematics [4] for symmetric fission. The experimentally obtained angular distribution was fitted by chi-square minimization procedure using the theoretical angular distribution of fission fragments given by

$$W(\theta) \propto \sum_{J=0}^{\infty}(2J+1)T_J \frac{\sum_{K=-J}^{J}\frac{1}{2}(2J+1)\left|d^J_{0K}(\theta)\right|^2 \exp[\frac{-K^2}{2K_o^2}]}{\sum_{K=-J}^{J}\exp[\frac{-K^2}{2K_o^2}]}$$

where T_J is the transmission coefficient for fusion of J^{th} partial wave and K_o is the standard deviation of the K distribution. In this minimization procedure the K_0 was treated as free parameter. The fitted angular distribution for ^{19}F + ^{198}Pt at beam energy of 116.8 MeV for SSB telescope detectors is shown in Fig. 1.

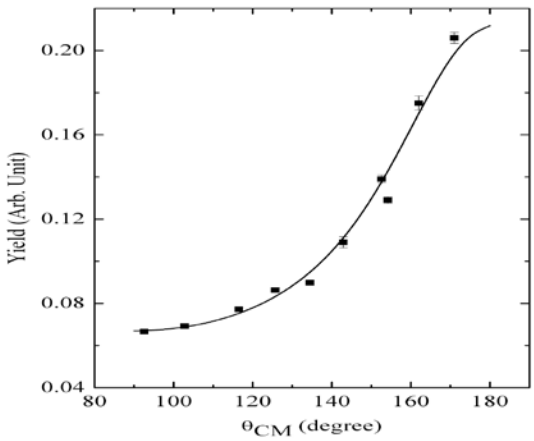

Fig. 1. Fission fragment angular distribution for ^{19}F + ^{198}Pt @ 116.8 MeV is shown (solid square) and lines are the values obtained by W(θ) fitting.

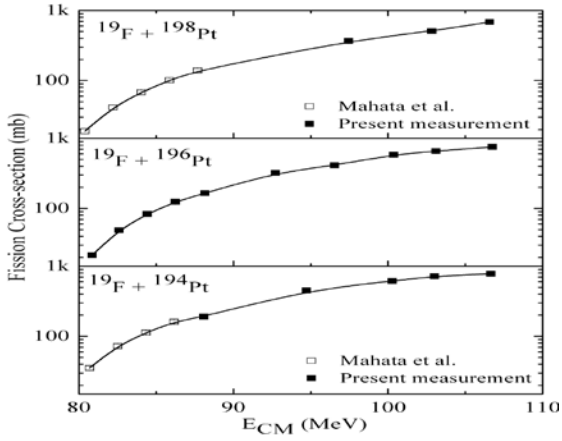

Fig. 2. Preliminary fission cross-sections of the present experiment.

Fission cross-sections were obtained using the following expression

$$\sigma_{fission} = \frac{1}{2}\frac{Y_{fiss}}{Y_{mon}}\frac{\Omega_{mon}}{\Omega_{fis}}\sigma_{ruth}$$

where Ω_{fiss} and Ω^{mon} are solid angle subtended by fission and monitor detector, respectively and σ_{ruth} is Rutherford cross-section in mb. The fission cross-section obtained from both detector set-up are shown in Fig. 2. It had been observed that the fission cross-section obtained by both the detector set-up agree within ± 5 % with each other. Further theoretical calculations are in progress.

REFERENCES:

[1] D. Hilscher et al., Ann. Phys. Fr. 17, 471 (1992).
[2] Peter Paul et al., Annu. Rev. Nucl. Part. Sci. 44, 65 (1994).
[3] B.B. Back et al., Phys. Rev. C 60, 044602 (1999).
[4] V.E. Viola et al., Phys. Rev. C 31, 1550 (1985).
[5] K. Mahata et. al., Phys. Rev. C 65, 034613 (2002).

5.1.6 THE STUDY OF $^{12}C(^{6}LI,d)^{16}O^*$ REACTION AT 20 MEV IN RELATION TO THE $^{12}C(\alpha\gamma)$ REACTION

S. Adhikari[1], C. Basu[1], P. Sugathan[2], A. Jhingan[2], K.S. Golda[2], A. Babu[2], D. Singh[2], S. Ray[3] and A.K. Mitra[1]

[1]Nuclear Physics Division, Saha Institute of Nuclear Physics, Kolkata 700064, India
[2]Inter University Accelerator Centre, New Delhi 110067, India
[3]Physics Department, Ramakrishna Mission Vivekananda University, Belur, Howrah 711202, India

The $^{12}C(^{6}Li,d)^{16}O$ reaction has considerable importance in the study of both nuclear physics and nuclear astrophysics [1]. In the context of nuclear physics this reaction is not very well understood at this energy regime. The main reason for this is the loosely bound nature of the ^{6}Li projectile that makes it very difficult to decipher the reaction mechanism in an inclusive measurement. The availability of sophisticated coupled reaction channel models in recent times makes it possible to look into this reaction in an appropriate way. Of particular importance is the effect of breakup of ^{6}Li on the other reaction process such as alpha transfer. The understanding of the reaction mechanism of the $^{12}C(^{6}Li,d)^{16}O^*$ reaction is important for its application in nuclear astrophysics. It is well known that the $^{12}C(\alpha\gamma)$ reaction at 300 keV determines the ^{16}O to ^{12}C abundance at the end of helium burning in stars. The direct measurement of the rate or astrophysical S-factor for the $^{12}C(\alpha\gamma)$ reaction at 300 keV is almost impossible. As such indirect methods that involve population of ^{16}O states (relevant for the alpha capture process) using a different reaction viz. alpha transfer reactions on ^{12}C are utilized. It is therefore important to extract the one step alpha transfer component in the reaction that is related to the alpha spectroscopic properties of the ^{16}O states. With these objectives in mind we have carried out a measurement of the deuteron angular distributions from the $^{12}C(^{6}Li,d)^{16}O$ at 20 MeV.

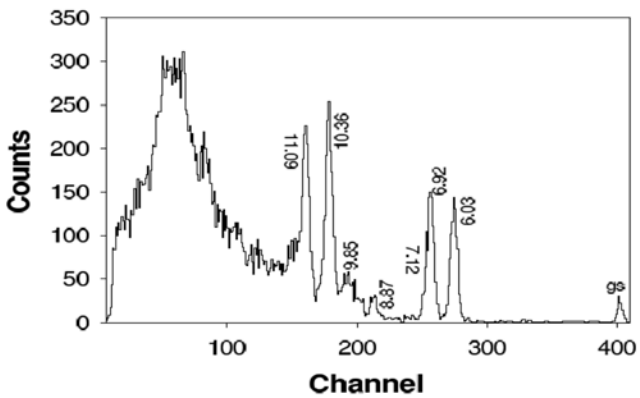

The experiment [2] was carried out using the ^{6}Li beam of the IUAC Pelletron facility during June-July 2011. A 200 $\mu g/cm^2$ natural carbon target was used in the experiment. Standard solid state silicon detectors were used for particle identification and measurement of angular distributions at various angles. The reaction products were measured from 27 deg to 150 deg inside the general purpose scattering chamber (GPSC). In Fig. 1, we show the measured spectrum of deuterons at 45 deg from the reaction. Several discrete states of ^{16}O are seen to be populated in the reaction. The seven states that are found to be strongly populated are the gs., 6.13 (3^-), 6.92 (2^+), 7.12 (1^-), 8.82 (2^-), 9.84 (2^+), 10.36 (4^+) and 11.09 (4^+) MeV. The angular distribution for each of the strongly populated states has been analyzed in terms of the different possible reaction modes. The contribution of deuteron from the de-excitation of the ^{18}F and subsequent compound nuclei has been estimated from Hauser Feshbach theory. The compound nuclear components are unable to reproduce the shape of the angular distributions. The direct alpha transfer and indirect alpha

transfer are examined using the latest version of CRC code FRESCO. The comparison between the single step alpha transfer and indirect transfer has been also examined. The alpha spectroscopic properties and their potential dependence will also be examined.

REFERENCES:

[1] Sucheta Adhikari and Chinmay Basu, Phys. Lett. B 704, 308 (2011).
[2] S. Adhikari et al., Proc. of the DAE Symp. on Nucl. Phys. 56, 616 (2011).

5.1.7 FIRST MEASUREMENT OF GDR γ-RAYS FROM ^{196}Hg IN A NOVEL LaBr+NaI SPECTROMETER

Indranil Mazumdar[1], D.A. Gothe[1], N. Madhavan[2], S. Nath[2], J. Gehlot[2], T. Varughese[2], P.B. Chavan[1], P. Sugathan, I. Mukul[2], G. Mohanto[2], M. Kaur[3] and V. Singh[3]

[1]Tata Institute of Fundamental Research, Mumbai 400005, India
[2]Inter University Accelerator Centre, New Delhi 110067, India
[3]Department of Physics, Panjab University, Chandigarh 160014, India

We report about the first measurements of high energy Giant Dipole Resonance (GDR) gamma-rays spectra using a combined assembly of large LaBr and NaI detectors. The measurements are part of an ongoing effort to carry out a systematic investigation of rare shape-phase transitions in hot-rotating heavy (A~190) nuclei [1]. In this experiment we aimed to carry out exclusive measurement of phase-space selected GDR gamma-rays from highly excited ^{196}Hg compound nucleus. The compound nucleus ^{196}Hg was populated at two different beam energies by bombarding a self-supporting and enriched target of ^{180}Hf using ^{16}O beam from the 16 MV Pelletron accelerator at the IUAC, New Delhi. The selection of the beam energies, 85 and 100 MeV, was governed by finite temperature potential energy surface (FTPES) calculations predicting definite shape-phase transitions between 1 to 2 MeV temperature for the ^{196}Hg nucleus. The GDR gamma-rays were measured in two independent high energy gamma-rays spectrometers, namely, the HIGRASP [2] and a combined assembly of LaBr and NaI detectors, kept on opposite sides of the beam line. The combined assembly comprised of a large cylindrical LaBr detector fitted inside a 2π thick NaI(Tl) annulus. The front surface of the NaI(Tl) annulus was shielded by 8 inches thick annular lead shielding. The energy signal from the combined assembly was derived by adding the signals from the LaBr and the NaI(Tl). A large square plastic scintillator detector was placed over the assembly for rejecting the cosmic rays. The high energy gamma-rays were detected in coincidence with the low energy discrete gamma-rays, detected in the TIFR 4π spin spectrometer [3]. The GDR spectra were measured at two different angles with respect to the beam direction for each of the two beam energies. The neutron-gamma separation was carried out by TOF technique and the pileup events were rejected by zero-crossover technique. Fig. 1 presents the GDR spectra measured in the LaBr+NaI assembly for both the beam energies at 90^0 with respect to the beam line. Similar spectra were also extracted for the measurements carried out at the back angle (120^0). The pronounced GDR bumps for both the energies are prominent with respect to the exponentially falling low energy parts (solid line) of the spectra. The expected higher yield of high energy gamma-rays for 100 MeV over 85 MeV is seen after normalizing the spectra around 4-5 MeV. Fig. 2 presents the ratio of the GDR gamma-rays measured at 90 and 120 degrees with respect to the beam direction for 100 MeV beam energy. The pattern of the angular anisotropy is significant and hints towards either non-collective prolate or collective oblate shape of the nucleus. The measurements demonstrate the efficacy of the combined assembly of LaBr and NaI detectors for measuring high energy gamma-rays. Detailed analysis of the data is in progress and will be reported elsewhere.

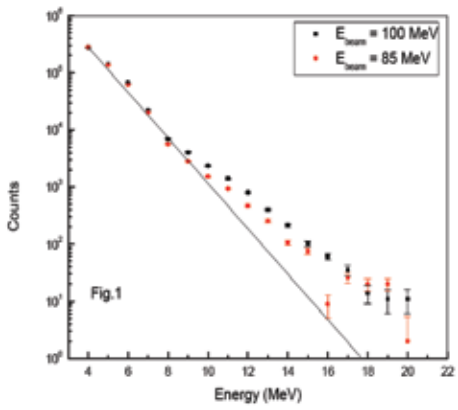

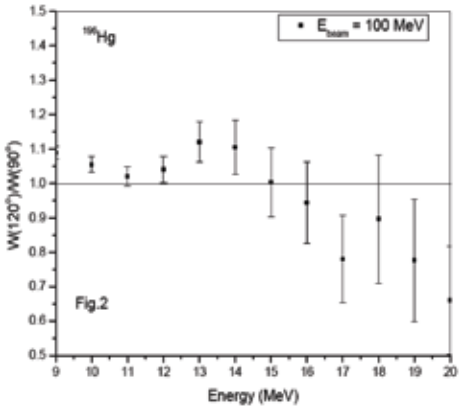

5.1.8 EVAPORATION RESIDUE CROSS-SECTION MEASUREMENTS FOR ^{19}F + $^{194, 196,198}Pt$ REACTIONS

Varinderjit Singh[1], B.R. Behera[1], N. Madhavan[2], Maninder Kaur[1], S. Nath[2] , J. Gehlot[2], T. Varughese[2], I. Mukul[2], G. Mohanto[2], A. Jhingan[2], S. Goyal[3], Jhilam Sadhukhan[4], A. Kumar[1], K. P. Singh[1], S. Santra[5], A. Saxena[5], S. Pal[4] and S. Kailas[5]

[1]Department of Physics, Panjab University, Chandigarh 160014, India
[2]Inter University Accelerator Centre, Aruna Asaf Ali Marg, New Delhi 110067, India
[3]Department of Physics and Astrophysics, University of Delhi 110007, India
[4]Variable Energy Cyclotron Centre, 1/AF, Bidhan Nagar, Kolkata 700064, India
[5]Nuclear Physics Division, Bhabha Atomic Research Centre, Mumbai 400085, India

The advent of heavy-ion accelerators opened up a new opportunity to study the heavy ion induced fusion-fission and fusion-evaporation reactions. The study of light particles emitted in a heavy ion induced reaction helped in understanding the nature of dissipation in these reactions. Thoennessen *et al*. [1] studied a large set of experimental data and concluded that the dissipation is not present at all values of excitation energy but, there is certain threshold above which it comes into picture. Neutron, charged particle multiplicity, evaporation residue cross-section and fission cross-section are the important probes to study the nuclear dissipation. Back *et al*. [2] reported that in order to reproduce evaporation residue cross-sections for ^{224}Th and ^{216}Th nuclei, a larger dissipation strength was required for former as compared to the latter. They concluded that nuclear dissipation has possible relation with neutron closed shell N_C=126. It is to be noted that this conclusion was drawn from one observable sensitive to nuclear dissipation (i.e. evaporation residue). Hence, it is desirable to do a consistent analysis for other observables like pre-scission neutron multiplicity, fission and ER cross section to establish the role of neutron shell closure in the dissipation strength. With this motivation in our mind, we decided to perform a simultaneous analysis of neutron multiplicity, fission cross-section and evaporation residue cross-section for ^{19}F + $^{194,196,198}Pt$ (N_c = 126, 128, 130) systems at excitation energy range 46 - 91.8 MeV. Here, we report the preliminary results of our evaporation-residue cross-section measurements.

The experiment was carried out at HYbrid Recoil mass Analyzer (HYRA) using Pelletron + LINAC accelerator at IUAC, New Delhi. Pulsed beam of ^{19}F with repetition rate of 4 μs and energy varying from 101 to 137.3 MeV, was bombarded on isotopically enriched targets of ^{194}Pt (96.5 % enrichment), ^{196}Pt (94.6 % enrichment) and ^{198}Pt (91.6 % enrichment). The ^{198}Pt and 196Pt targets were of thickness 170 μg/cm^2 on 20 μg/cm^2 C backing each and ^{194}Pt target was of thickness 265 μg/cm^2 with 10 μg/cm^2 C backing. The targets were placed at the center of 120 mm diameter scattering chamber and two Si surface barrier detectors were mounted at ± 23^0 (at a distance of 23 mm) with respect to beam direction. These detectors were used to monitor the beam flux and to normalize the ER yield to obtain absolute ER cross-section.

In this experiment, the first stage of HYRA [3, 4] was operated in gas-filled mode at 0.15 Torr He gas. This stage has the configuration QQ-MD-Q-MD-QQ, where QQ is quadruple doublet, MD is magnetic dipole and Q is quadruple singlet. The gas-filled HYRA was isolated from the beam line vacuum with the help of a self supporting Ni foil of thickness 1.3 mg/cm^2. The focal plane detector system consisted of a position sensitive MWPC followed by a two dimensional position sensitive Si detector. A time-of-flight spectrum was generated using anode signal of MWPC as start and RF of pulsed beam as stop. Further a two dimensional plot was generated using TOF and energy loss signal of MWPC. It provides a clean separation of ER from other background components as shown in Fig. 1.

The total ER cross-section can be obtained using the expression

$$\sigma_{ER} = \frac{Y_{ER}}{Y_M} \frac{\Omega_M}{\eta_{HYRA}} \left(\frac{d\sigma}{d\Omega}\right)_{Ruth}$$

where Y_{ER} is evaporation residue counts, Y_M is monitor counts, ΩM is solid angle of monitor detector, η_{HYRA} is HYRA transmission efficiency and $(d\alpha/d\Omega)_{Ruth}$ is Rutherford cross-section in mb. The transmission efficiency is the ratio of the ER detected at focal plane to the total number of ER produced at target position. The transmission efficiency of HYRA for the present systems have not been measured presently, so we are able to obtain the relative behavior of ER cross-section for the three systems under study as shown in Fig. 2. The relative yield shown here is normalized with the angular acceptance at lowest energy.

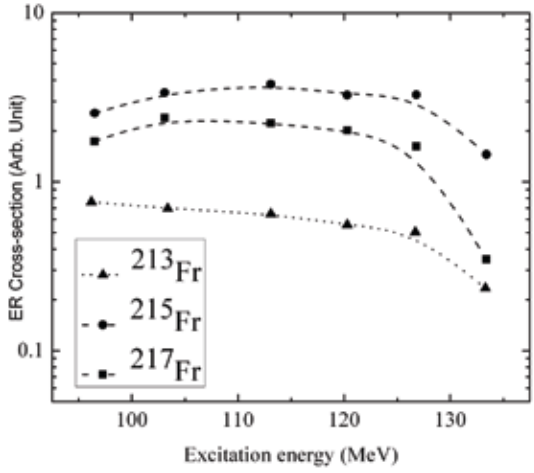

Fig. 1. Two dimensional plot of energy loss in MWPC vs TOF at 96.5 for $^{19}F + ^{194}Pt$ system.

Fig. 2. Relative ER cross-section of the different Fr isotopes under study.

The data analysis is in progress and attempts are being made to obtain the transmission efficiency and absolute cross-section.

REFERENCES:

[1] M. Thoennessen et al., Phys. Rev. Lett. 71, 4303 (1993).
[2] B.B. Back et al., Phys. Rev. C 60, 044602 (1999).
[3] N. Madhavan et al., EPJ Web of Conferences 17, 14003 (2011).
[4] N. Madhavan et al., DAE Symp. on Nucl. Phy. 55, 658 (2010).

5.2 MATERIALS SCIENCE

There were about hundred experiments in materials science beam line in beam hall I and a few experiments in materials science beam line in beam hall II. One experiment each was performed using in-situ X-ray diffraction setup and online Quadrupole Mass Analyzer. A test experiment on in-situ X-ray reflectivity was performed by Prof. Ajay Gupta, CSR-DAE Indore. The ion beam irradiation experiments werer mainly concerned with electronic sputtering, ion beam mixing, ion beam modification of materials etc.

Silver-silica nanocomposite was studied under SHI irradiation for correlation between surface plasmon resonance of metal particles and electronic sputtering of metal content. It was shown that the SPR can be tuned by ion fluence. SHI induced mixing was studied at the interfaces of Pb/Te and Bi/Te and a large mixing was observed, revealed by RBS. The phase of PbTe and Bi_2Te_3 were formed due to mixing. Lattice defects and structural strain induced by SHI irradiation of nanocrystalline ZnO thin films were studied. The decomposition of Zn silicate phase was studied under SHI irradiation. The influence of doping of nanocrystalline ZnO on SHI induced modifications was investigated. The conducting nanochannels were reported in SHI irradiated piezoelectric polymer subjected to functionalization.

SHI irradiation of SnO_2 films showed sputtering and decrease in crystallinity and resistance. PbTe thin films were shown to have enhancement in thermoelectric properties under SHI irradiation whereas the performance deteriorate under thermal annealing. Enhancement in sensing of LPG was observed in nanocrystalline ZnO thin films after SHI irradiation.

SHI induced modifications in Ti doped In_2O_3 films, multiferroic thin films, Polyethererketone PEEK films, etc. were studied. Transport properties of YBCO/Ag composite thin films were studied under 200 MeV Ag ion irradiation. SHI irradiation effects on optoelectronic properties of ZnS-TiO_2 core shell quantum dots were investigated.

Schottky devices using ZnO nanorods were shown to have rectifying response as a result of irradiation by 80 MeV O ions. Electrical characteristics of bipolar transistors and I-V characteristics of NPN rf power transistors were studied under ion irradiation. In-situ electrical characterizations were performed during O ion irradiation of 200 GHz SiGe HBTs.

5.2.1 IN-SITU ELECTRICAL CHARACTERIZATION OF 100 MeV O^{7+} ION IRRADIATED 200 GHz SiGe HBTS

K. C. Praveen[1], N. Pushpa[1], John D. Cressler[2], H. B. Shiva[1], Ambuj Tripathi[3] and A. P. Gnana Prakash[1]

[1]Department of Studies in Physics, University of Mysore, Manasagangotri, Mysore-570006
[2]School of Electrical and Computer Engineering, Georgia Institute of Technology, Atlanta, GA, 30332, USA
[3]Inter-University Accelerator Centre, Aruna Asaf Ali Marg, New Delhi -110067, India

The present work assesses the potential use of radiation tolerant silicon-germanium heterojunction bipolar transistors [SiGe HBTs] in front-end electronics for emerging high energy physics experiments. The SiGe HBTs are considered for the possible use in the upgrade of the Silicon Strip Detector and Liquid Argon Calorimeter of the ATLAS detector as part of the Large Hadron Collider (LHC), CERN, Geneva, Switzerland [1]. In order to understand the high dose effects, SiGe HBTs were irradiated with 100 MeV O^{7+} ions up to a total dose of 100 Mrad with a beam current of 0.3 p-nA (particle-nano Ampere). The dc I-V characteristics such as Gummel characteristics, excess base current ($\Delta I_B = I_{B\text{-}Post} - I_{B\text{-}Pre}$), current gain ($\beta$), output characteristics, neutral base recombination (NBR) and avalanche multiplication of carriers (M-1) were studied before and after irradiation. Some of the important results are discussed in this report. Fig. 1(a) shows the forward mode Gummel characteristics for 100 MeV O^{7+} ion irradiated 200 GHz SiGe HBT. At low injection levels, the base current (I_B) increases monotonically with increasing O^{7+} ion total

dose. The increase in I_B shows that the degradation is similar to the conventional degradation mechanism observed in silicon bipolar transistors [2]. The irradiation-induced damage in the emitter-base (EB) spacer oxide increases the emitter-base depletion region. The recombination current in the depletion region can be observed as an additional I_B in the lower emitter base voltage (V_{BE}) regime. However, the collector current (I_C) does not change with increase in O^{7+} ion total dose because the recombination in the depletion region does not affect the flow of electrons through the base. Therefore only the pre-irradiation IC is shown in the forward-mode Gummel plot. Fig. 1(b) shows the dc current gain (β) for the 100 MeV O^{7+} ion-irradiated SiGe HBT. As expected, the current gain decreases with O^{7+} ion total dose, because the I_B increases monotonically after O^{7+} ion radiation. Since the I_B starts increasing for the lower V_{BE} the peak current gain (β) shifts towards higher V_{BE} or higher I_C. The radiation-induced G/R centers decrease the minority-carrier lifetime which in turn decrease the current gain. The decrease in minority carrier lifetime is the dominant mechanism for gain degradation in addition to G/R centers created in the EB spacer oxide. Fig. 1(c) shows the neutral base recombination (NBR) for SiGe HBT before and after irradiation. The change in base charge after irradiation can be experimentally estimated by observing the slope of I_B as a function of V_{CB} at fixed V_{BE}. The slope of the NBR curve at lower VCB is almost same for prerad and 100 Mrad curve. There is negligible amount of displacement damage in the base region of SiGe HBT even after 100 Mrad total dose of O^{7+} ion irradiation. The I-V characteristics show that the performance of SiGe HBT is acceptable even after irradiating O^{7+} ion up to 100 Mrad of total dose. Though the deterioration observed in SiGe HBT is significant after O^{7+} ion irradiation, SiGe HBTs can be considered for use in the design of front-end readout ASICs for use in an upgraded LHC.

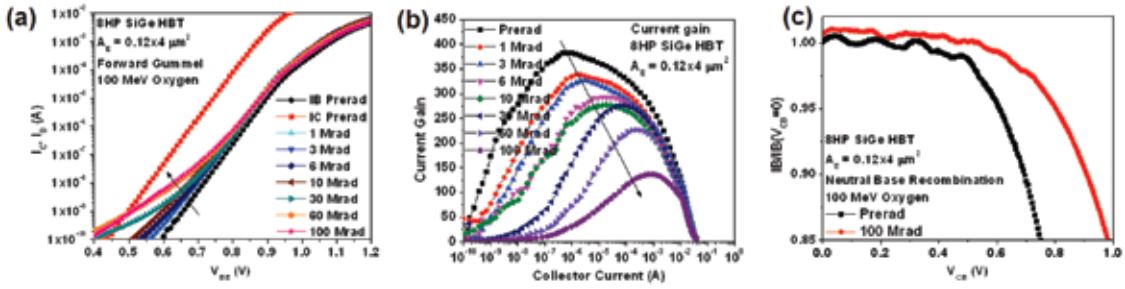

Fig. 1. (a) Forward mode Gummel characteristics (b) Variation of current gain for different total doses (c) NBR curves

REFERENCES

[1] K. C. Praveen, N. Pushpa, P. S. Naik, J. D. Cressler, Ambuj Tripathi, A. P. Gnana Prakash, Nucl. Instr. and Meth. B. 273 (2011) 43.

[2] A. P. Gnana Prakash, A. K. Sutton, R. M. Diestelhorst, G. Espinel, J. Andrews, B. Jun, J. D. Cressler, P. W. Marshall, and C. J. Marshall, IEEE Trans. Nucl. Sci. 53(6) (2006) 3175.

5.2.2 IN-SITU STUDY OF CURRENT TRANSPORT ACROSS Pt/n-Si (100) SCHOTTKY JUNCTION DURING 100 MeV Ni^{+7} ION IRRADIATION

Shammi Verma[1], Kumsi C. Praveen[2], Tanuj Kumar[1] and Dinakar Kanjilal[1]

[1]Inter-University Accelerator Centre, Aruna Asaf Ali Marg, New Delhi -110067, India
[2]Department of Studies in Physics, University of Mysore, Mysore-570006, India

Metal-Semiconductor (M-S) contacts are the fundamental part of the semiconductor devices. Formation of a controlled junction barrier known as Schottky barrier at these M-S interfaces is important from physics as well as technological point of view [1-2].

In-situ current-voltage (I-V) measurements of Pt/n-Si (100) Schottky Barrier (SB) diode were carried out during 100 MeV Ni^{+7} beam irradiation (Fig. 1). The diode was fabricated by depositing 100nm of Pt metal as a 2 mm circular dot on chemically cleaned and etched n-Si (100) of resistivity ~1 Ω-cm. The effect of ion beam on the electrical parameters like ideality factor (η) and Schottky Barrier Height (SBH) (ϕ_B) of SB

diode is assessed from their thermionic emission current-voltage equation [3]. SBH decreases slowly with fluence from its "pre-rad" value but there is almost no change in SBH and ideality factor for ion fluence ranging 5×10^{12} to 5×10^{13} ions/cm^2. This has been explained on the basis that after certain fluence there is equilibrium in two competing processes: defects creation and annealing by ion beam [4]. Considering cluster defects of size 10 nm diameter [5] in Si, an area of 2 mm will need about 4×10^{12} ions/cm^2 to get all filled by such cluster defects. So after this overlapping fluence there is saturation in device parameters. The reverse current is increased by about two orders of magnitude at fluence 5×10^{13} ions/cm^2 which corresponds to an exposure of a few decades in Low Earth Orbit [LEO]. The device Pt/n-Si (100) can, therefore, function reliably for a few decades in such radiation environments. The irradiation induced diffusion of Schottky metal into semiconductor and creation of trap centres at metal-semiconductor interface are supposed to be the most plausible mechanisms for these deviations in SB diode characteristics.

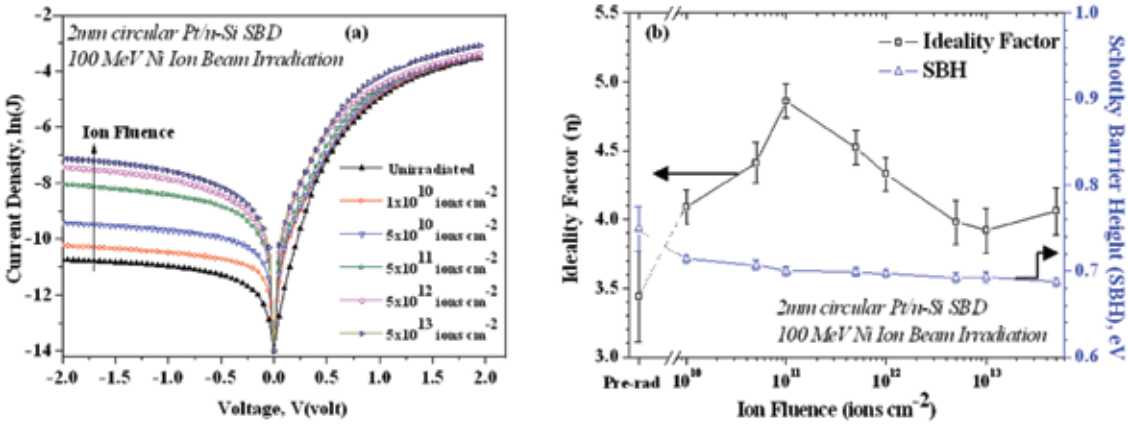

Fig. 1. (a) Experimentally observed I-V characteristics of the 2mm Pt/n-Si (100) Schottky Barrier Diodes at different ion fluences of 100 MeV Ni ion beam, (b) Variation of ideality factor (η) and Schottky Barrier Height (SBH) of Pt/n-Si (100) SBD with different ion fluences of 100 MeV Ni ion beam.

REFERENCES

[1] D. V. Lang, J. Appl. Phys., 45 (1974) 3014
[2] D. K. Schroder, *"Semiconductor Material and Device Characterization"*, New Jersey, Wiley Interscience (2006)
[3] E. H. Rhoderick, IEEE Proc., 129 (1982) 1
[4] R. Singh, S. K. Arora, and D. Kanjilal, Mat. Sci. Semicon. Proc., 4 (2001) 425–432
[5] Krzysztof Iniewski, *"Radiation Effects in Semiconductors"*, New York, CRC Press (2011)

5.2.3 FORMATION OF PbTe LAYER BY ION BEAM INDUCED INTERFACE MIXING

Srashti Gupta[1], D.C. Agarwal[2], S.K. Tripathi[3], S. Neeleshwar[1], S.A. Khan[2], S.K.Srivastava[4], and D.K. Avasthi[2]

[1]USBAS, G.G.S. Indraprastha University, Delhi-110075, India
[2]Inter-University Accelerator Centre, Aruna Asaf Ali Marg, New Delhi -110067, India
[3]Department of Physics, Panjab University, Chandigarh-160 014, India
[4]Department of Physics and Meteorology, Indian Institute of Technology, Kharagpur -721302, India

PbTe is a low band gap (0.25 eV at 0 K) semiconductor having applications in the field of IR photo detector and ultrahigh density optical data storage and thermoelectric devices etc [1, 2]. Doped PbTe powder with small grain size is synthesized by conventional methods like mechanical alloying, Bridgeman method, etc. Oxidation of PbTe is main drawback during synthesis. Ion beam mixing is one of the potential tools to make alloys with desired properties. In the present work, the formation of PbTe film using high energy heavy ion beam induced mixing of Te/PbO bilayer system is investigated.

Te/PbO bilayer samples were prepared by thermal evaporation of Pb (~ 28 nm) and Te (~ 14 nm) on quartz substrates and (~ 8-10 nm Te/PbO bilayer) on TEM Cu grids at a pressure ~ 2×10^{-5} mbar at room temperature; Te was the top layer. These bilayer samples were irradiated by 100 MeV Ag^{7+} ions with ~ 1 pnA ion current at different fluences ranging from 3×10^{12} to 1×10^{14} ions/cm^2. Pristine and irradiated samples were characterized by RBS, and TEM with SAED. RBS was performed using 2 MeV He^+ ions at scattering angle of 165° at IUAC. The RUMP simulation was used for the analysis of RBS spectra and to generate the depth profiles. TEM microscopy was performed using FEI TECNAI 20 microscope operated at 200kV at IIT Roorkee.

RBS spectra of the pristine sample, and of the samples irradiated by 100 MeV Ag ions at different fluences ranging from 3×10^{12} to 1×10^{14} ions/cm^2, are shown in Fig. 1. In the pristine sample, two separate peaks are observed for Pb and Te. RBS spectra and subsequent RUMP analyses show significant mixing at the fluence 1×10^{13} ions/cm^2 with unusually higher mixing rate ~1648 nm^4. The mixing rate (1648 nm^4) obtained in the present case is at least an order of magnitude higher than the mixing rates reported in other systems such as metal oxide/Si [Fe_2O_3/Si, NiO/Si, TiO_2/Si; mixing rate k < 10 nm^4], metal/semiconductor [Cu/Ge and Ni/Si; mixing rate k ≤ 140 nm^4], metal/metal [Ti/Fe and Ti/Au; mixing rate k ≤ 155 nm^4] [3-5].

SAED patterns taken from transmission electron microscopy (TEM) of the pristine and 1×10^{14} ions/cm^2 irradiated samples, prepared on Cu grids, confirms the formation of the PbTe phase after irradiation and is in good agreement with the RBS results. The formation of PbTe is shown to be a consequence of inter-diffusion of Pb and Te during transient molten phase by the considerations of the thermal spike model.

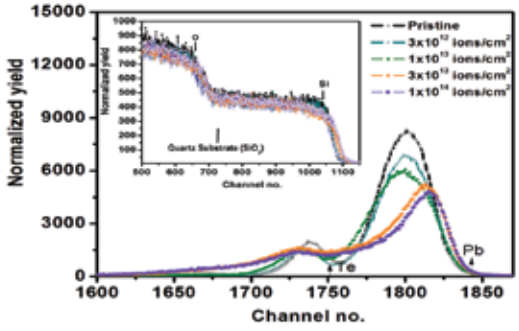

Fig. 1. RBS spectra of pristine and irradiated with 100 MeV Ag ions at fluence 3×10^{12}, 1×10^{13}, 3×10^{13}, 1×10^{14} ions/cm^2 of bilayer (Te/PbO) samples, the inset shown RBS spectra with quartz substrate.

REFERENCES

[1] F. Felder, A. Fognini, M. Rahim, M. Fill, E. Muller, and H. Zogg, Phys. Proce. 3 (2010) 1121
[2] H. S. Lee et al, App. Phy. Lett. 85 (2004) 2782
[3] S. Kumar, R.S. Chauhan, S.A. Khan, W. Bolse, and D.K. Avasthi, Nucl. Instr. & Meth. B. 244 (2006) 194
[4] B. Schattat, W. Bolse, S. Klaumünzer, F. Harbsmeier, and A. Jasenek, Nucl. Instr. & Meth. B. 191(2002) 577
[5] S. Kraft, J. Appl. Phys. 91 (2002) 1129

5.2.4 ION BEAM MIXING IN Bi/Te THIN FILM SYSTEM

Th. Diana[1], D. C. Agarwal[2], P. K. Kulriya[2], S. K. Tripathi[3], H. Nandakumar Sarma[1] and D. K. Avasthi[2]

[1]Department of Physics, Manipur University, Imphal – 795003
[2]Inter-University Accelerator Centre, Aruna Asaf Ali Marg, New Delhi -110067, India
[3]Department of Physics, Panjab University, Chandigarh – 160014

Bi and Te thin films were deposited over cleaned Si (100) substrate by thermal evaporation. The bilayer system were irradiated using 100 MeV Ag and 100 MeV Ni ions delivered by 15 UD Pelletron facility in IUAC under the fluences 3×10^{12} – 6×10^{13} ions/cm^2. The samples were also annealed at 200°C in Ar gas atmosphere to induce interfacial reaction between the layers.

The pristine and irradiated samples were characterized with grazing incidence X-ray diffractometer (XRD) using Bruker D8 Advance diffractometer, Digital Instruments Nanoscope IIIa Atomic force microscopy (AFM) and Rutherford backscattering spectroscopy (RBS). Electrical measurements like IV characteristics and RT measurements were performed for the pristine and irradiated samples in the temperature range liquid nitrogen to 300 K.

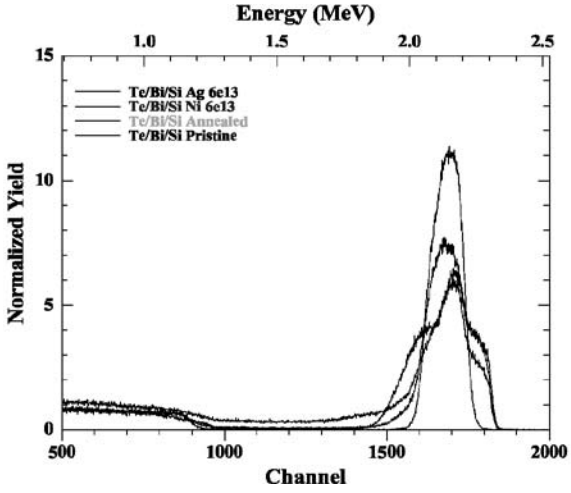

Fig. 1. RBS spectra of pristine, annealed, 100 MeV Ni and 100 MeV Ag irradiated Te/Bi/Si samples

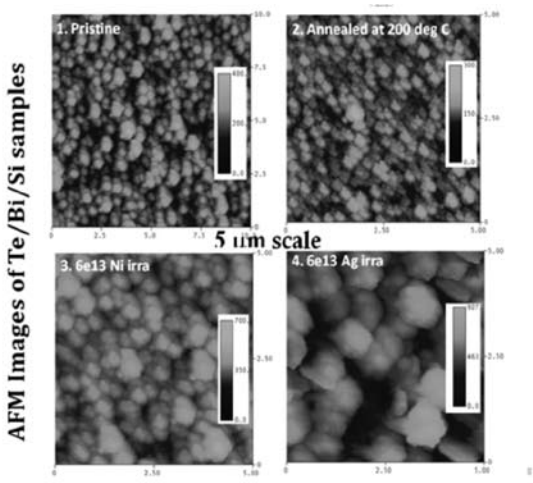

Fig. 2. AFM images of pristine, annealed, 100 MeV Ni and 100 MeV Ag irradiated Te/Bi/Si samples

The atomic transport along the interface were studied using RBS. The RBS spectra of Te/Bi/Si samples are shown in Fig. 1. The contributing layer mass number being close to each other, their corresponding signal peaks lie very near. Bi being beneath the Te layer, its signal peak shifts towards the lower energy side and merge with the Te peak. On SHI irradiation, Bi is found to exist in the top layer which clearly indicates interdiffusion across the interface.

Surface morphology and roughness were studied using AFM. Fig. 2 shows the AFM images of Te/Bi/Si pristine, annealed at 200°C, Ni and Ag irradiated samples. It can be observed that grain size as well as roughness increases to a large extent on 100 MeV Ag ion irradiation. Thus during analysis of RBS spectra for extraction of depth profiles, roughness should be taken into account.

Further investigation is underway to extract the depth profile from RBS data fit using RUMP software. The electrical measurements IV characteristics and RT measurements are also being analysed.

5.2.5 SHI IRRADIATION EFFECTS ON FUNCTIONALIZATION PROPERTIES OF WELL ALIGNED SWNTS

P. Ghosh, K. Datta, M. D. Shirsat

Intelligent Material Research Laboratory (Sensors Division), Dr. Babasaheb Ambedkar Marathwada University, Aurangabad, M. S. India

Smart and reliable sensing gadgets for monitoring of ambient air quality, at a formidable cost, have become a need of the hour due to fast growing complexity in atmospheric conditions. Most importantly, the designing aspects for modern sensing gadgets ask for efficient power management at smallest possible footprint. To meet these demands, novel materials that can be coupled with lowest possible ancillary electronics, are at the forefront of investigation. Nanomaterials can meet these demands to a large probable extent. However, most efficient nanomaterials explored for gas sensing till date (viz. Carbon Nanotubes, Conducting Polymers etc.) are having their inherent drawbacks. Single Wall Carbon Nanotubes (SWNTs) have been

regarded as one of the most stimulating sensing backbone [1-4] because of the highly electrochemically active surface [4-5] and ultra high aspect ratio [6] . However, high surface binding affinity (aroused due to honeycomb surface structure) [7] and limited transduction mechanism available with SWNTs [8] have put a question mark on the applicability of pristine SWNTs as sensing materials. At the same time, dearth of repeatable and reliable methods for spatial control of SWNTs on small footprint substrate remains a practical problem for SWNTs based sensors.

Our investigations deal with spatial control on dispensing SWNTs on a single, small footprint Si/SiO2 substrate and spatially controlled functionalization of SWNTs for multianalyte sensing applications. The substrate we are using for the present investigation plays an important role. On a highly doped p-type substrate (with 300 nm oxide layer), we have patterned 16 Au microelectrode sites with a critical 3 μm gap between two electrode pads of interest. Standard photolithography and lift-off techniques have been adapted for this purpose. In order to achieve a homogenous suspension of SWNTs, ultrasonic agitation has been used for dispersion of SWNTs in various solvents. In due course of investigation, N, N- DMF has been found to be highly effective in producing stable and homogenous suspension of SWNTs. SWNTs (suspension) has been introduced at a quantity of 0.2 – 0.5μL in the 3 μm trench region between Au microelectrodes. SWNTs have been dielectrophoretically, aligned between the microelectrodes – (i) to improve charge transduction capabilities of the device and (ii) to minimize interstitials aroused due to interwining SWNTs in non-aligned modality. In order to introduce selectivity to aligned SWNTs structures, we have electrochemically tailored the surfaces of the aligned SWNTs with metal nanoparticles. But the control over deposition was not regular. In order to overcome this problem, SHI irradiation can be a fascinating way out since irradiation induces moieties on the surface of SWNTs where metal nanoparticles can be well attached to the SWNTs surface [9]. Apart from this, irradiation induces interstitials on the SWNTs surface which may be interesting for non-covalent attachment of Conducting Polymers (CPs) and probable filling of CPs into the SWNTs. During our investigations, we have achieved excellent aligned SWNTs and we have subjected the same for irradiation under Ni^{10+} (120 MeV) and O^{16+} (100 MeV) beams at various ion fluences. In case of Ni^{10+}, the results were quite discouraging because we observed destructive peeling effect on the Au electrodes and breakage of SWNTs at higher fluences (as revealed by SEM images). However, at lower fluences (3×10^{10} ions/cm^2 and 1×10^{11} ions/cm^2) encouraging results were obtained in terms of enhancement of device resistance. In case of O^{16+}, however we got excellent results for the fluence range of 1×10^{10} ions/cm^2 to 5×10^{11} ions/cm^2. The enhancement in device resistance is due to breakage of SWNTs and most importantly creation of interstitials on SWNTs surface leading to inferior surface conduction. This sacrifice is greatly mitigated by highly efficient entrapment of CPs on the SWNTs surface, as we have observed.

REFERENCES

[1] S.E. Moulton, A. I. Minett, and G.G. Wallace, Sensor Letters, 3 (2005) 183
[2] T. Zhang, S. Mubeen, N.Myung, and M.A.Deshusses, Nanotechnology, 19 (2008) 332001
[3] W.D. Zhang and W.H. Zhang , Journal Of Sensors, 160698 (2009)
[4] D.R. Kauffman and A. Star, Angewandte Chemie Int. Ed. 47 (2008) 6550.
[5] M. Meyappan (ed.), Carbon Nanotube- Synthesis, Properties and Application CRC PRESS (2003).
[6] K.R. Ratinac, W. Yang, S.P. Ringer, and F. Braet, Environmental Science & Technology 44 (2010) 1167.
[7] K.A.Williams, P.C. Eklund, Chemical Physics Letters 326 (2000) 352.
[8] L. Dai, Energia 16 (2005) 2.
[9] M. S. Raghuveer, A. Kumar, M. J. Frederick, G. P. Louie, P. G. Ganesan, and G. Ramanathan, Advance Materials 18 (2006) 547

5.2.6 HYDRO-DYNAMICS OF SURFACE PATTERNING BY ION BEAM IRRADIATION: AN INTERFACE PHENOMENON

Tanuj Kumar, D. C. Agarwal, S. A. Khan, N. P. Lalla, and D. Kanjilal

Inter-University Accelerator Centre, Aruna Asaf Ali Marg, New Delhi -110067, India

Fabrication of self-organized nano-structures such as ripples, dots, holes etc. over the surface of semiconductors by using energetic ion bombardment have drawn much attention due to immense importance in the field of optoelectronic, photonic and recording media applications [1-2]. Low energy ion beam sputtering has proven to be a very elegant and cost-effective single step approach for the generation of well controlled nanostructures of different topographies by varying the ion beam parameters viz. energy, fluence and angle of irradiation etc [3-4].

The present work was performed on n-Si (100) wafers having root mean square roughness of 0.2 nm. In order to study the amorphous/crystallin interface role in surface patterning of Si (100) surface using ion irradiation, the thickness of the amorphous layer is varied. The thickness variation is achieved by irradiating the Si surface using 50 keV Ar^+ ion fluence of 5×10^{15} ions/cm^2 at different incidence angle viz. 60º and 0º with respect to surface normal. The basic principle used behind the thickness variation is that the ion beam irradiation at normal incidence having higher penetration depth as compared to oblique irradiation. These two sets of samples having different thickness of amorphous layer are named as set-A (60º) and set-B (0º) respectively. Then both the type of samples were irradiated at room temperature at an angle of 60º with respect to surface normal using 50 keV Ar^+ ion beam. The fluence was varied from 3×10^{17} ions/cm^2 to 9×10^{17} ions/cm^2. During the irradiation the base pressure of chamber was maintained at ~10^{-7} mbar. The ion beam current density was kept constant at 15 μA/cm^2. After irradiation, the samples were analyzed by Nano Scope IIIa atomic force microscope (AFM) under ambient conditions in tapping mode.

AFM images of ion beam irradiated samples from both the sets at the fluences of 3×10^{17} ions/cm^2, 5×10^{17} ions/cm^2, 7×10^{17} ions/cm^2 and 9×10^{17} ions/cm^2 are presented in Fig. 1. From Fig. 1(a-d), it can be clearly seen that for the set-A, the increase in ion fluence leads to formation of ripples, and which are oriented perpendicular to ion beam direction. However, in set-B samples, minor signature of ripples formation with much smaller amplitude is observed under same irradiation fluences.

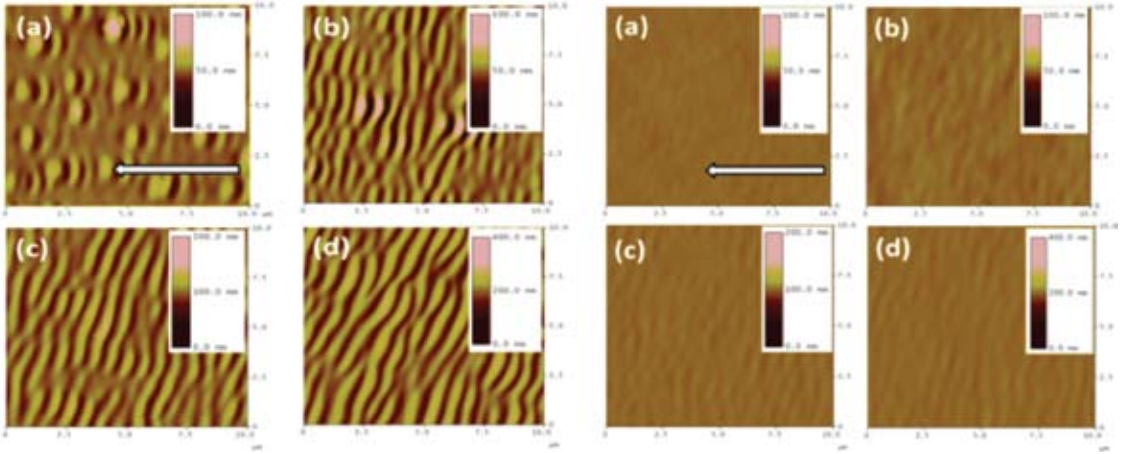

Fig. 1. AFM images for the 50 keV Ar+ irradiated set-A and set-B samples at an angle of 60° with respect to surface normal at the fluences of (a) 3×1017 ions/cm2 (b) 5×10^{17} ions/cm2 (c) 7×10^{17} ions/cm^2 (d) 9×10^{17} ions/cm^2 respectively. The arrows in the figures indicate the projection of ion beam direction on the surface.

REFERENCES

[1] D. Whang, S. Jin, Y. Wu, and C. M. Lieber, Nano Lett. 3 (2003) 1255
[2] J. Lindner, P. Poulopoulos, M. Farle, and K. Baberschke, J. Magn. Mater. 218 (2000) 10
[3] S. Facsko, T. Dekorsy, C. Koerdt, C. Trappe, H. Kurz, A. Vogt, H.L. Hartnagel, Science 285 (1999) 1551.
[4] R. Gago, L. Vazquez, R. Cuerno, M. Varela, C. Ballesteros, and J. M. Albella, Appl. Phys. Lett. 78 (2001) 3316

5.2.7 EXPERIMENTAL AND ATOMISTIC SIMULATIONS STUDIES OF EFFECT OF 350 keV Ar ION IRRADIATION ON SANDWICHED THIN METAL LAYER

Saif A. Khan[1], S. K. Srivastava[2], and D. K. Avasthi[1]

[1]Inter-University Accelerator Centre, Aruna Asaf Ali Marg, New Delhi -110067, India
[2]Department of Physics and Meteorology, Indian Institute of Technology, Kharagpur, India

Nanometer-sized metallic particles embedded in dielectric matrices are useful in several applications and they have been synthesized by many methods [1]. Energetic ions have been widely used for the fabrication of embedded metal nanoparticles by the process of ion implantation [2, 3]. However, use of ion irradiation to engineer existing metallic inclusions is a better method of such synthesis as it involves smaller ion fluence and thermal budget while being a reproducible and clean method. Moreover, a judiciously chosen beam species offering higher ion flux can be used in this method.

Synthesis of two-dimensional assembly of metal nanoparticles embedded in silica was achieved by 350 keV Ar ions irradiation of sandwiched percolating metal layer as shown in Fig. 1(a). Low Energy Ion Beam facility of IUAC was used for ion irradiation and the films were deposited by electron-beam evaporation technique. $SiO_2/Au/SiO_2$ and $SiO_2/Ag/SiO_2$ tri-layered films, with oxide thicknesses of 40 nm and metal layer thickness of 2 nm, were irradiated to synthesize well isolated nanoparticles without the need of annealing. The nanoparticles have average diameter of about 6 nm as revealed by Transmission Electron Microscopy (TEM) as shown in Fig. 1 (b). Calculations based on thermal spike model [4], considering nuclear stopping power and electronic stopping power, suggest that an incident ion produces local transient temperature rise. The mechanism of synthesis is investigated using kinetic Monte Carlo (KMC) simulations [5] taking into account the ion induced local temperature rise. It is clear from Fig. 1(c) that the predictions from simulations agree well with the TEM plan-view observations. Also, the simulations show that the diffusion of material during local transient temperature rise helps in attaining the configuration with minimum energy by formation of nanoparticles assembly.

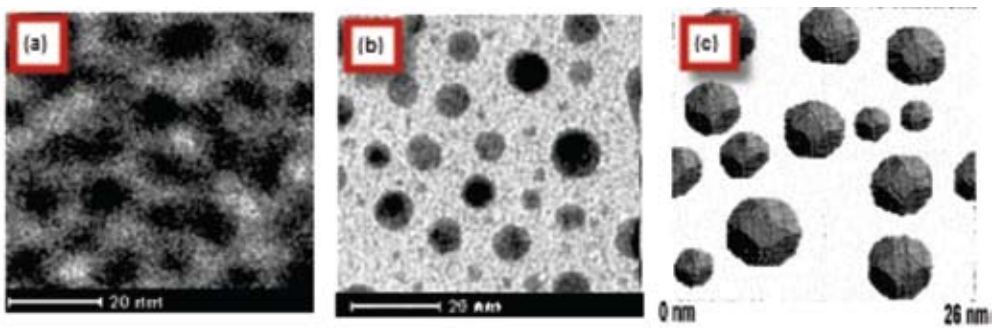

Fig. 1. Plan-view TEM images of (a) pristine $SiO_2/Au/SiO_2$ trilayers on TEM grid, (b) irradiated $SiO_2/Au/SiO_2$ trilayers on TEM grid with 350 keV Ar ions at the fluence of 2×10^{16} ions/cm^2. (c) shows a snapshot from KMC simulations showing nanoparticles formation due to ion irradiation.

REFERENCES

[1] S.A. Khan, K.H. Heinig, and D.K. Avasthi, J. Appl. Phys. 109 (2011) 094312.
[2] M. Strobel, K.H. Heinig, W. Moller, A. Meldrum, D.S. Zhou, C.W. White, and R.A. Zuhr, Nucl Instr. and Meth B 147 (1999) 343-349.
[3] A. Meldrum, L.A. Boatner, and C.W. White, Nucl. Instr. and Meth. 178 (2001) 7-16.
[4] M. Toulemonde, W.J. Weber, G. Li, V. Shutthanandan, P. Kluth, T. Yang, Y. Wang, and Y. Zhang, Phys. Rev. B 83 (2011) 054106.
[5] S.A. Khan, D.K. Avasthi, D.C. Agarwal, U.B. Singh, and D. Kabiraj, Nanotechnology 22 (2011) 235305.

5.2.8 MODIFICATIONS OF SILVER-SILICA NANOCOMPOSITE FILMS BY SWIFT HEAVY ION IRRADIATION: CORRELATION BETWEEN SURFACE PLASMON RESONANCE AND ELECTRONIC SPUTTERING

Fouran Singh[1] and J. C. Pivin[2]

[1]Inter-University Accelerator Centre, Aruna Asaf Ali Marg, New Delhi -110067, India
[2]CSNSM, IN2P3, Bâtiment 108, 91405 Orsay Campus, France.

Plasmonic properties of the silver nanoparticles (AgNPs) have been studied extensively as they offer many potential applications in optical labels, near-field optical probes, biological/chemical sensors, and substrates for surface-enhanced Raman spectroscopy [1]. The tunability of SPR depends on their size, shape and the surrounding dielectric environment of the isolated nanoparticles and is well accounted by Mie theory [2]. It also depends on the distance and spatial ordering of neighboring particles and is well modelled by the Maxwell Garnett's effective medium theory. In this study, it is shown that SPR of the AgNPs can be tailored by the electronic excitations induced by swift heavy ion irradiations. This tailoring depends on the electronic excitations and ion fluences, but from the reported results it difficult to described the exact dependence and more experiments needed. Nevertheless, for an in-depth understanding about the change in SPR peak shape could be made by performing the SPR measurements using polarized light.

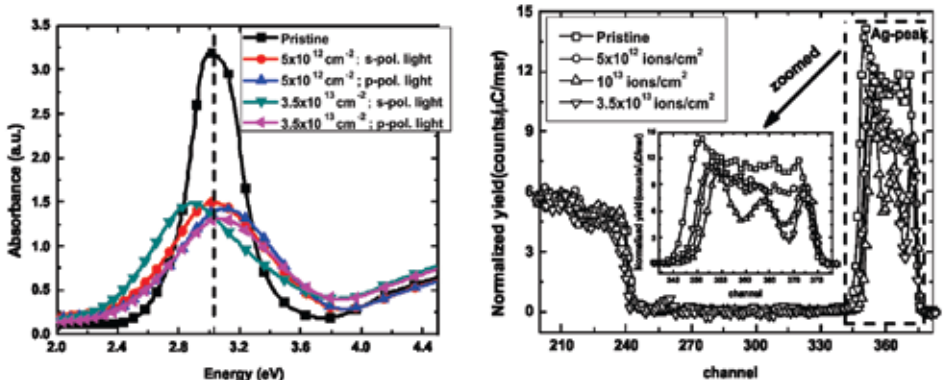

Fig. (left) SPR measurements using polarized light and (right) RBS spectra of silver silica nanocomposite films irradiated using 120 MeV Au ions

Therefore, the NC films containing 10 at.% Ag and annealed at 700°C were also irradiated with 120 MeV Au ions for fluences of 5×10^{12}, 1×10^{13} and 3.5×10^{13} ions/cm^2 at an oblique angle of 45° with respect to the surface. The SPR spectra of these NC films with *s*- (parallel) or *p*- (perpendicular) polarization are shown in left figure and the Rutherford backscattering spectrometry (RBS) spectra on such NC films are shown in right figure. From our detailed study [3], it is concluded that the dipolar interactions in such NC films with high filling fractions is tailored by strong fluctuations of sizes and re-arrangement of nanoparticles by the process of melting, sputtering and re-precipitation in the tracks in agreement with thermal spike calculations.

REFERENCES

[1] P. Alivisatos, Nat. Biotechnol. 22 (2004) 47 and T.A. Taton, C.A. Mirkin, and R.L. Letsinger, Science 289 (2000) 1757
[2] U. Kriebig and M. Vollmer, Optical properties of metal clusters (Springer Series in Material Science 25, Berlin, Heidelberg, 1996)
[3] Fouran Singh and J.C. Pivin et al, J. Phys. D: Appl. Phys. 44 (2011) 325101

5.2.9 EFFECT OF 200 MeV Ag IONS ON THE TRANSPORT PROPERTY OF YBCO/Ag COMPOSITE THIN FILM

A. Kujur[1], D. Behera[1], K. Asokan[2]

[1]Department of Physics, National Institute of Technology, Rourkela-769 008
[2]Inter-University Accelerator Centre, Aruna Asaf Ali Marg, New Delhi -110067, India

Ag (1 wt. %) is added to YBCO to produce YBCO/Ag composite thin film grown by pulsed laser deposition. These composite films were subjected to 200 MeV Ag ions irradiation. The structural disorder in microstructure was studied using XRD and Raman Spectroscopy techniques. The intensity of the XRD

peaks decreases immensely after irradiation giving a clue of amorphization occurring in the sample [1]. Raman spectra clearly indicate the loss of apical oxygen O (4) at 500 cm^{-1} and a defect peak appearing at 600 cm^{-1} on irradiation as shown in Fig. 1(a) [2]. Transport property was analyzed using Magnetization vs. field loop recorded at 40 K. Synergetic effect of Ag and columnar defect deteriorates material property and impedes the flow of supercurrent thereby resulting in decrease in critical current density and flux pinning. In this report we analyze the combined effect of Ag (secondary phase -3D APCs) composite to YBCO and SHI irradiation (1D –APCs) to composite film. The whole idea behind this is to visualize the pinning mechanism and report the value of J_c. Nevertheless the results show decline of J_c (as shown in Fig 1(b)) providing substantial evidence of damage occurring in quality of thin films after doses of irradiation. We support our results by Raman interpretations where spectrum shows a strong oxygen loss depicted by the Raman shift of 500 cm^{-1} and the local formation of impurity phases upon irradiation where the temperature during irradiation is expected to be significantly enhanced.

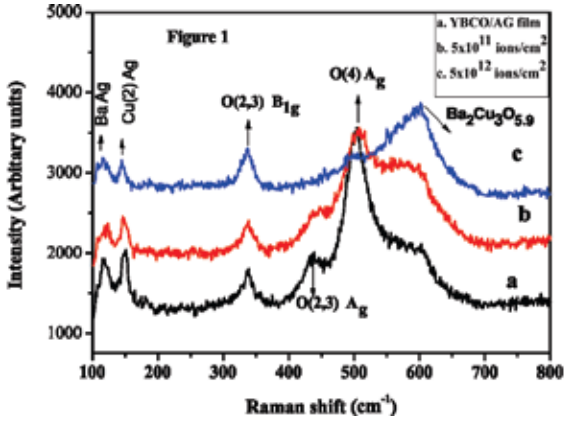

Fig. 1. Micro-Raman spectra of (a) unirradiated YBCO/Ag film (b) irradiated YBCO/Ag films with 200 MeV of Ag ions using dose 5×10^{11} ions/cm^2 (c) ion dose 5×10^{12} ions/cm^2

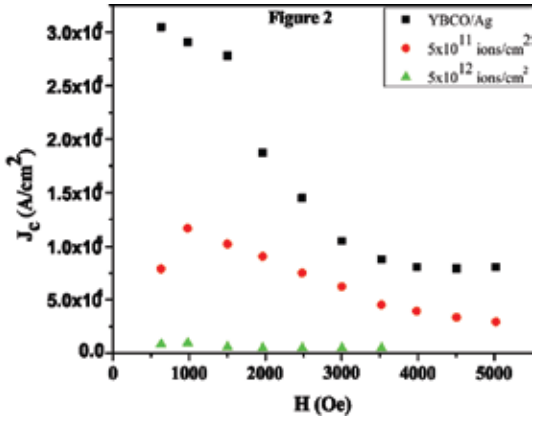

Fig. 2. The curve depicts J_c vs H for pristine and irradiated samples with ion doses 5×10^{11}ions/cm^2 and 5×10^{12} ions/cm^2 of Ag

REFERENCES

[1] R. Biswal, J. John, P. Mallick, B. N. Dash, P. K. Kulriya, D. K. Avasthi, D. Kanjilal, D. Behera, T. Mohanty, P. Raychaudhuri, and N. C. Mishra, J. of Appl Physics 106 (2009) 053912

[2] M. K. Choi, N. V. Minh, J. S. Bae, W. Jo, I. -S. Yang, R. Ko, H.S. Ha, and C. Park, Prog. Supercond. 6 (2005) 95

5.2.10 SWIFT HEAVY ION IRRADIATION ON Ag:ZrO_2 NANOCOMPOSITE THIN FILMS

Manish Kumar[1], P.K. Kulriya[1], J.C. Pivin[2] and D.K. Avasthi[1]

[1]Inter-University Accelerator Centre, Aruna Asaf Ali Marg, New Delhi -110067, India
[2]CSNSM-IN2P3, Baˆtiment 108, 91405 Orsay Campus, France

Using swift heavy (120 MeV O and 100 MeV Ag) ions, we have studied its effect on sol-gel derived Ag_2O_3:ZrO_2 composite films, and found the electronic energy loss and fluence dependent evolution and tailoring of plasmonic properties of Ag:ZrO_2 nanocomposites. The optical studies exhibit the change in color of films from transparent in pristine film to shiny yellow when films are irradiated by 100 MeV Ag ions at a fluence of 3×10^{12} ions/cm^2. However, irradiation by 120 MeV O ions up to the fluence of 1×10^{14} ions/cm^2 does not induce any coloration in films. The coloration is attributed to the evolution of plasmonic feature resulting in a surface plasmon resonance (SPR) induced absorption peak in the visible region as shown in Fig. 1. Increase in fluence from 3×10^{12} to 6×10^{13} ions/cm^2 of 100 MeV Ag ions induces a redshift in SPR induced peak position from 434 to 487 nm. Microstructural studies confirm the conversion of Ag_2O_3 (in pristine films) into cubic phase of metallic Ag and the increase of average size of particles with the increasing fluence up to 6×10^{13} ions/cm^2. Further increase in fluence leads to the dissolution of Ag atoms in the ZrO_2 matrix.

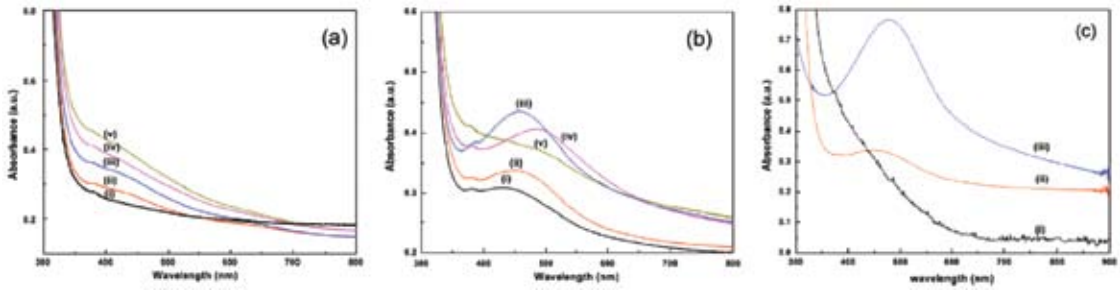

Fig. 1. (a) Absorption spectra of films (i) pristine and irradiated with 120 MeV O ions of fluences, (ii) 3×10^{12}, (iii) 1×10^{13}, (iv) 6×10^{13}, and (v) 1×10^{14} ions/cm^2. (b) Absorption spectra of films irradiates with 100 MeV Ag ions of fluences (i) 3×10^{12}, (ii) 1×10^{13}, (iii) 3×10^{13}, (iv) 6×10^{13}, and 1×10^{14} ions/cm^2. (c) Absorbance spectra of films having Ag precursor concentrations (i) 0 M, (ii) 0.05 M, and (iii) 0.1 M, irradiated with 100 MeV Ag ions at fluence 1×10^{13} ions/cm^2.

REFERENCE

[1] Manish Kumar, P.K. Kulriya, J.C. Pivin, and D.K. Avasthi, J. of Appl. Phys. 109 (2011) 044311

5.2.11 ROLE OF DEFECTS AND INTERFACE MODIFICATION ON THE FERROMAGNETISM IN THE NANOSTRUCTURED Pd

P. K. Kulriya[1, 2] B. R. Mehta[1], D. C. Agarwal[2], Praveen Kumar[3], S.M.Shivaprasad[3], J.C.Pivin[4], D. K. Avasthi[2]

[1]Department of Physics, Thin Film Laboratory, Indian Institute of Technology, New Delhi 110 016, India
[2]Inter-University Accelerator Centre, Aruna Asaf Ali Marg, New Delhi -110067, India
[3]CPMU, Jawaharlal Nehru Centre for Advanced Scientific Research, Bangalore
[4]CSNSM, Bâtiment 108, IN2P3-CNRS, 91405 Orsay Campus, France

The origin of the ferromagnetism in the non-magnetic material at nano-dimensions is not clearly understood despite observation in a number of materials systems such as Pd, [1-3] Pt, Au, [4] Ag, and Cu, and metal oxides such as Al_2O_3, In_2O_3, ZnO and SnO_2. Theoretical reports predicted that ferromagnetism in Pd arises due to quantum well states, lattice expansion, crystal defects and surface effects, structural transformation from fcc to hcp and icosahedral crystal structure. The ferromagnetic properties in the Pd based nanocomposite materials at nano-dimensions has been investigated by a novel approach of intentionally creating defects and interface modifications. The investigations involve studying the (a) effect of interfacial interaction between Pd nanoparticles (NPs) in carbon or silica matrix having different structural properties and (b) effect of structural defects induced by swift heavy ion irradiation and hydrogen loading deloading cycles [5]. The well separated and uniformly distributed as-deposited (Fig. 1(a)) and hydrogen cycled (Fig. 1(b)) Pd nanoparticles dispersed in the a:C and a:silica matrix, used in present study are synthesized by atom beam sputtering technique. The magnetic properties of these nanoparticles have been studied using x-ray magnetic circular dichroism (XMCD) and superconducting quantum interference device (SQUID) magnetometry measurements. Detailed structural and electronic properties of Pd NP and NP-matrix interface have been investigated using glancing angle x-ray diffraction, and x-ray photoelectron spectroscopy techniques. Efforts have been made to correlate interfacial and structural defects with the electronic changes in Pd and detailed results on magnetic properties are given in Ref. [5]. The ferromagnetic response of Pd is found to increase by 20 times for NP dispersed in carbon matrix [1] and by about 3.5 times in case of Pd nanoparticles dispersed in a:SiO_2 matrix, as a result of ion irradiation. Ferromagnetic response is found to increase by about 9.3 times (Fig. 2) on subjecting the Pd NPs to hydrogen loading-deloading cycle (HC). Ferromagnetic properties of Pd NPs dispersed in a:C and a:SiO_2 matrices despite having same size and concentration are observed to be drastically different due to matrix effect [5]. These changes in ferromagnetic properties have been related to shift in position of Pd $3d_{5/2}$ main peak and interfacial peak which leads to the change in the electronic structure due to matrix, creation of

defects in the nanoparticle core and at NP-matrix interface during post deposition treatments. The present study clearly established that ferromagnetism in the non-magnetic materials is linked to interface and defects which may having different origins.

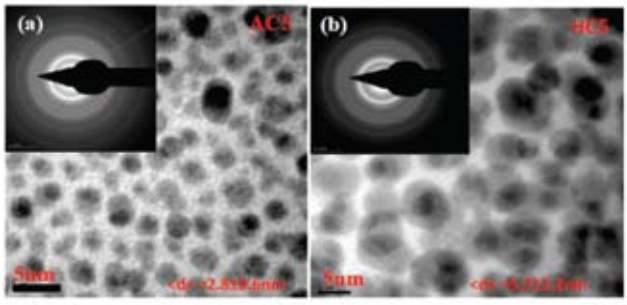

Fig. 1. HRTEM images for (a) as-deposited and (b) hydrogen cycled Pd NPs in carbon matrix.

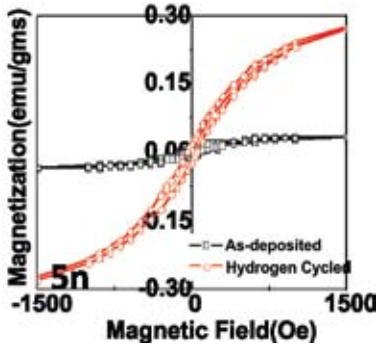

Fig. 2. SQUID magnetometer spectrum for (a) as-deposited and (b) hydrogen cycled Pd NPs in carbon

REFERENCES

[1] P. K. Kulriya, B. R. Mehta, D. K. Avasthi, D. C. Agarwal, P. Thakur, N. B. Brookes, A. K. Chawla, and R. Chandra, Appl. Phys. Lett. 96(2010) 053103
[2] T. Shinohara, T. Sato, and T. Taniyama, Phys Rev Lett 91 (2003) 197201
[3] B. Sampedro, P. Crespo, A. Hernando, R. Litra´n, J. C. Sa´nchez Lo´pez, C. Lo´pez Cartes, and A. Fernandez, Phys. Rev. Lett. 91 (2003) 237203
[4] Jose de la Venta, Andrea Pucci, Enrique Fernández Pinel, Miguel A. García, Cesar de Julián Fernandez, Patricia Crespo, Paolo Mazzoldi, Giacomo Ruggeri, and Antonio Hernando, Adv. Mater. 19, (2007) 875
[5] P. K. Kulriya, B. R. Mehta, D. C. Agarwal, Praveen Kumar, S. M. Shivaprasad, J. C. Pivin, and D. K. Avasthi, J. of Appl. Phys. (under review)

5.2.12 THERMOELECTRIC ENHANCEMENT OF PbTe THIN FILM USING SHI IRRADIATION

Srashti Gupta[1], D. C.Agarwal[2], S. K. Tripathi[3], S. Neeleshwar[1], A. Jacquot[4], B. Lenoir[5], D. K. Avasthi[2]

[1]University School of Basic and Applied Sciences, G.G.S. Indraprastha University, Delhi 110403, India
[2]Inter-University Accelerator Centre, Aruna Asaf Ali Marg, New Delhi -110067, India
[3]Department of Physics, Panjab University, Chandigarh-160 014, India
[4]Fraunhofer Institute for Physical Measurement Technique, D–79110 Freiburg, Germany
[5]Institut Jean Lamour, UMR 7198 CNRS-Nancy Université-UPVM, Parc de Saurupt, F-54042 Nancy, France

PbTe is one of the most favorable thermoelectric materials due to its stability over a wide temperature range (500-900 K) for converting waste heat or solar heat into electricity. The efficiency of a thermoelectric material can be defined by a dimensionless quantity called figure of merit $ZT = S^2\sigma T/k$; where, S is the thermopower or Seebeck coefficient, σ is the electrical conductivity, k is the thermal conductivity and T is the absolute temperature at which the properties are measured [1]. PbTe can easily absorb oxygen, which affects its physical properties in uncontrolled manner [1]. Swift Heavy Ion (SHI) irradiation is a possible way to desorb oxygen from the materials [2]. An enhancement in thermoelectric properties using 5 MeV Si ion irradiation in superlattices namely Bi_2Te_3/Sb_2Te_3 was reported with increase in the thermopower from 30 to 55 μV/K at 300 K [3]. Thus, ion irradiation is an effective tool to modify thermoelectric properties in a controlled manner without any requirement of external doping or self doping. In the present study, the superiority of SHI irradiation over thermal annealing process for the enhancement of thermoelectric properties of PbTe thin film is demonstrated.

PbTe thin films (~190 nm in thickness) were synthesized by thermal evaporation of PbTe powder on quartz

at room temperature. A set of these films were annealed at 250ºC under inert (Ar + H_2) atmosphere for 1 hr. Another set of these films were irradiated by 100 MeV Ag^{7+} ion at fluence 1×10^{13} ions/cm^2 using 15UD Pelletron at IUAC. The thermoelectric power of the samples was measured in the temperature range 300 – 630 K on a IPM-SR4 set-up at Institut Jean Lamour, CNRS, France.

The variation of the thermopower with temperature of pristine, annealed and irradiated samples is shown in Fig. 1. The thermopower of pristine, annealed and irradiated samples at room temperature are ~ 189, ~ 232 and ~ 266 µV/K respectively, which increases to ~ 260, ~ 240 and ~ 343 µV/K at 525 K. S is positive which suggesting a p-type behaviour of sample. The enhancement in thermopower in SHI irradiated sample as compared to the pristine and annealed thin films is likely to be due to the enhanced density of states near the Fermi level or also may be due to a change of the scattering mechanisms of the charge carrier. Present results are motivating for further investigation on the enhancement of TE material by SHI irradiation.

In summary, swift heavy ion irradiation (at a fluence of 1×10^{13} ions/cm^2) of p-type PbTe thin film leads to ~ 40% enhancement in thermopower upto high temperature (~525 K). On the other hand, thermal annealing of the PbTe thin film results in a decrease of thermopower.

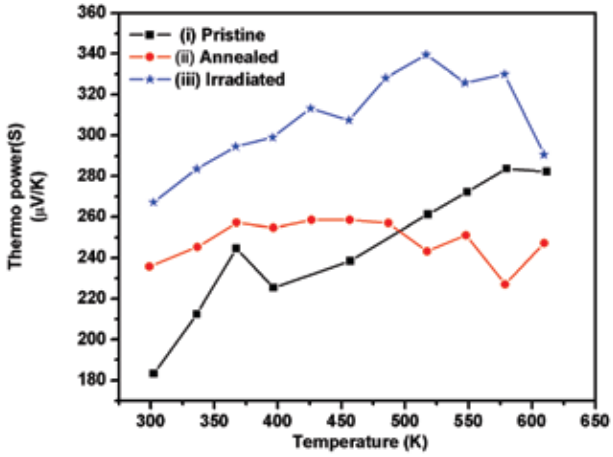

Fig. 1. Temperature dependence of thermopower of PbTe thin film pristine, annealed and irradiated sample using 100 MeV Ag ions at fluence 1×10^{13} ions/cm^2.

REFERENCES

[1] Donald E. Bode and Henry Levinstein, Phys. Rev. 96 (1954) 259-265.
[2] Y. Batra et al., Nucl. Instrum. Methods Phys. Res. Sect. B. 266 (2008) 1697-1700.
[3] S. Budak, Nucl. Instrum. Methods Phys. Res., Sect. B. 261 (2007) 608-611.

5.2.13 SWIFT HEAVY ION IRRADIATION INDUCED MODIFICATIONS IN OPTICAL PROPERTIES OF Si-RICH a-S_iN_x:H FILMS

Ravi Kumar Bommali[1], S. Ghosh[1], G. V. Prakash[1], Saif A. Khan[2], D. Kanjilal[2] and P. Srivastava[1]

[1]Department of Physics, IIT Delhi, Hauz Khas, New Delhi – 110016
[2]Inter-University Accelerator Centre, Aruna Asaf Ali Marg, New Delhi -110067, India

Modification of Si-nanostructures embedded in dielectric matrix has been of considerable interest to the scientific community as a possible candidate for optoelectronic applications [1]. Our earlier irradiation results reveal that the dissolution and re-precipitation of Si-nanostructures embedded in hydrogenated amorphous silicon nitride (a-SiN_x:H) matrix is quite sensitive to the swift heavy ion irradiation and can pave way to obtain Si-nanostructures of uniform size and distribution [2].

Extending our earlier work, in the present experiments as-deposited and SiO_x capped, Si-rich a-SiN_x:H samples of various compositions prepared by PECVD (Plasma Enhanced Chemical Vapour Deposition) technique were irradiated with 100 MeV Ni^{7+} ions at different fluences using a 15 UD Pelletron Accelerator at IUAC. As-deposited and irradiated samples have been characterised by UV-vis reflectance spectroscopy and photoluminescence spectroscopy. Shown below are the reflectance and photoluminescence results for two samples S1 and S2 having refractive indices 2.3 and 1.9 respectively. The Si content is more in S1 as compared to S2. Reflectance results reveal a compaction of the films, with increasing fluence (Fig.1).

This is attributed to hydrogen desorption under irradiation as revealed by Residual Gas Analysis (not shown here). The photoluminescence spectra indicate modification in optical emission of irradiated films (Fig. 2). Further, characterization such as Raman spectroscopy and cross-sectional transmission electron microscopy are being carried out to correlate structural modifications with optical emission.

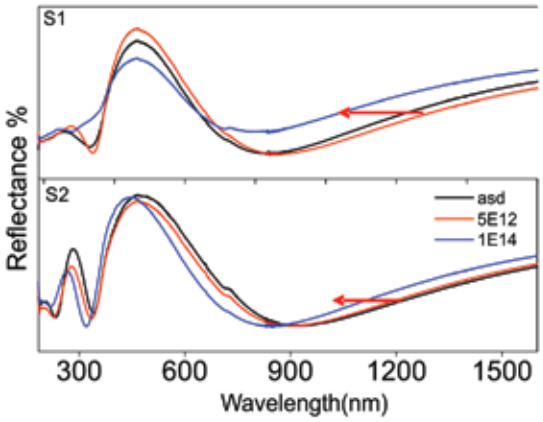

Fig. 1. Normal reflectance spectra for as- deposited and irradiated films.

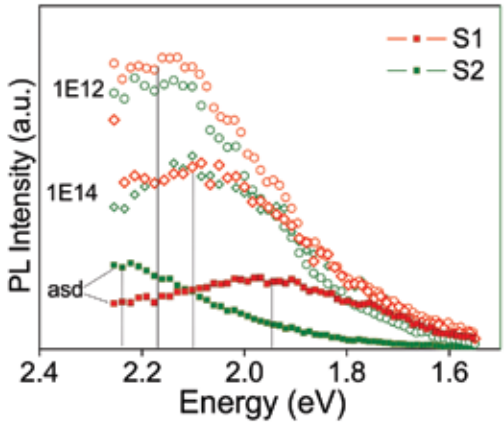

Fig. 2. Photoluminescence spectra for as-deposited and irradiated films.

REFERENCES

[1] T. Mohanty, A. Pradhan, S. Gupta, and D. Kanjilal, Nanotechnology, 15 (2004) 1620

[2] Sarab Preet Singh, Santanu Ghosh, G. Vijaya Prakash, Saif A. Khan, D. Kanjilal, A. K. Srivastava, Himanshu Srivastava, and P. Srivastava, Nucl. Instr. and Meth. B, 276 (2012) 51

5.2.14 EFFECT OF 120 MeV Ag^{9+} ION IRRADIATION ON STRUCTURAL AND OPTOELECTRONIC PROPERTIES OF ZnS/TiO_2 CORE-SHELL QUANTUM DOTS

Prabha Sana[1], Shammi Verma[2], K. Phaneendra[2], and M.M. Malik[1]

[1]Physics Department, Maulana Azad National Instituite of Technology, Bhopal- 462 051
[2]Inter-University Accelerator Centre, Aruna Asaf Ali Marg, New Delhi -110067, India

This work aims to study the structural, electrical and optical modifications of ZnS/TiO_2 core-shell quantum dots under SHI irradiation to find their suitability in photo device applications in radiation harsh environment. The ZnS/TiO_2 core shell quantum dots (QDs) were synthesized by colloidal technique and irradiated with 120 MeV Ag^{9+} ions at fluence 3×10^{12} and 3×10^{13} ions/cm^2. The UV-visible absorption spectra of these QDs show strong absorption band edge at 234 nm in pristine sample which further shifts towards 240 nm at higher fluence 3×10^{13} ions/cm^2. At higher fluence the band edge becomes sharp showing the uniform distribution of QDs. X-ray diffraction pattern shows increase in crystallinity of these QDs at higher fluence 3×10^{13} ions/cm^2, which is further confirmed by electron diffraction patterns of pristine and irradiated samples observed in TEM measurement as shown in Fig. 1. Bright field TEM images of pristine and irradiated samples at fluence 3×10^{13} ions/cm^2 show the nanoparticles of size distribution approximately 1-10 nm and analysis reveales that the sizes of QDs' increased at higher fluence which is confirmed by red shifting in the UV absorption band edge at higher fluence compared to pristine. The photoluminescence spectra of as-prepared QDs show emission at 414 nm and 436 nm due to sulphur vacancies or interstitial lattice defects. The PL emission intensity increased after SHI irradiations at fluence 3×10^{12} and 3×10^{13} ions/cm^2 which may be due to production of more sulphur vacancies/interstitial defects under the ion irradiation.

To observe the optoelectronic characteristics of ZnS/TiO_2 QD's under SHI irradiation, these QD's were deposited on 1×1 cm^2 ITO (Indium Tin Oxide) coated glass substrate in the form of thin film of thickness of 2 μm. The as-prepared cells were annealed at 400°C for ½ hour with heating rate 2°/minute. I-V characteristics of pristine and 120 MeV Ag^{9+} ions irradiated ZnS/TiO_2/ITO cells (Fig. 2) show that after irradiation current density is increased. This high forward current density could be attributed to the following causes in irradiated cell: 1) due to SHI irradiation the large interface existing between ZnS/TiO_2 QDs and ITO substrate, 2) big built-in-potential across the ZnS/TiO_2/ITO heterojunction is formed, 3) the phenomena of charge transport in ZnS/TiO_2/ITO system could be explained by the trap limited model. As the large quantity of sulphur vacancies have been formed in ZnS/TiO_2, these vacancies might play the role of charge traps and control the charge transport process. Photoconductivity measurements of pristine and irradiated ZnS/TiO_2 cells show increase in conductivity in response to 60 W visible light, although minute short circuit current I_{sc} has been observed in order of μA at zero bias.

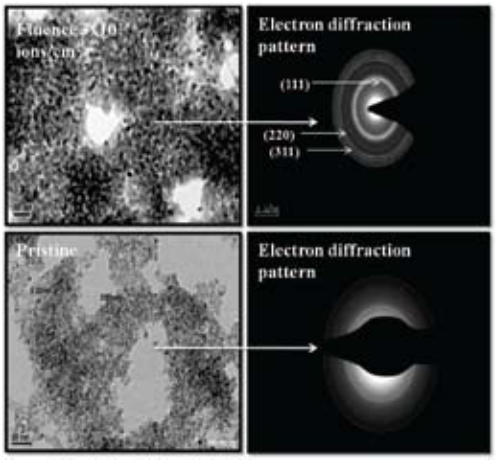

Fig. 1. TEM and SAED pattern of pristine and irradiated samples.

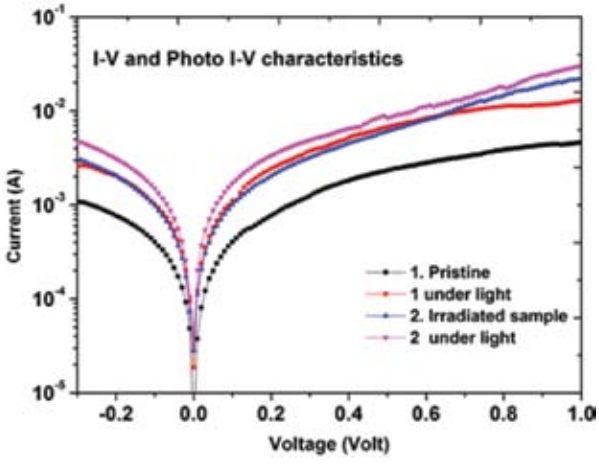

Fig. 2. IV and Photo-IV characteristics of pristine and irradiated samples.

REFERENCES

[1] Hai Jun Xu, Hai Shun Jia, Zhi TaoYao, and Xin Jian Li ; J. Material Research Society Vol 23, No.1 Jan 2008
[2] S. Sarmah and A. Kumar, Phys. Status Solidi A 207(10) (2010) 2279

5.2.15 FORMATION OF ZnO BY PHASE SPLITTING OF $ZnMoO_4$ UNDER DENSE ELECTRONIC EXCITATION

D C Agarwal, D K Avasthi and D. Kabiraj

Inter-University Accelerator Centre, Aruna Asaf Ali Marg, New Delhi -110067, India

The interesting aspects of material modification by swift heavy ion beam as a result of electronic and atomic collision-cascades close to the ion path; a rapidly quenched thermal spike is formed leaving behind a cloud of interstitial atoms and vacancies. The major outcomes of electronic energy loss due to the drastic atomic rearrangement in the irradiated material lead to different manifestations independently on its crystal structure. In this study, 100 MeV Ag -ion induced structural phase transition of thermally-evaporated $ZnMoO_4$ thin films has been reported [1, 2]. $ZnMoO_4$ thin films were grown on Si substrates by electron-beam evaporation method at room temperature (RT) in high vacuum of $5x10^{-6}$ mbar. The as-deposited films were amorphous in nature. Therefore, the films were post annealed at 600°C in oxygen ambiance for 6 hr to get crystalline nature. These annealed films were uniformly bombarded with 100 MeV Ag ions with different fluences.

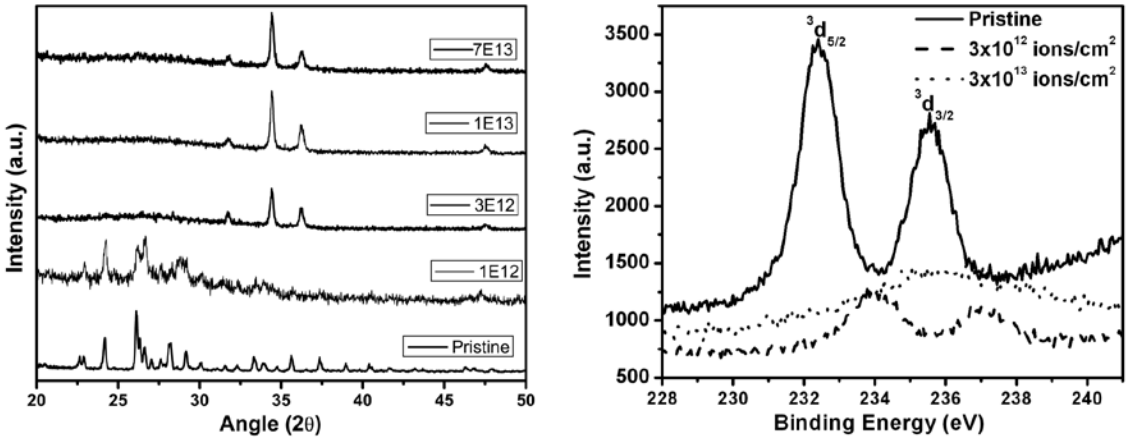

Fig. 1. XRD spectra (Left) and XPS of Mo 3d doublet of pristine and irradiated $ZnMo_4$ (Right)

X-ray diffraction (XRD) spectrum of pristine film reveals the formation of polycrystalline $ZnMoO_4$ film. All peaks are well matched with the $ZnMoO_4$ anorthic (triclinic) structure. There is no reflection observed for the phase of zinc, zinc oxide, molybdenum, and molybdenum oxide. Ion beam irradiation of these films changes the structure gradually with ion fluence and ZnO phase progressively evolved. Mixed phase of ZnO and $ZnMoO_4$ is observed at low fluence of 1×10^{12} ions/cm^2, and further irradiation of $ZnMoO_4$ shows complete conversion of $ZnMoO_4$ to ZnO phase at fluence of to 1×10^{13} ions/cm^2 as seen from Fig. 1 (left). The XRD pattern of the thermally annealed films also shows a polycrystalline nature with no preferred orientation, exhibiting the (1 0 0), (0 0 2) and (1 0 1) reflections at 2θ value of 31.5, 34.4 and 36.2 respectively. Irradiation at higher fluences from 1×10^{13} to 7×10^{13} ions/cm^2 do not affect the crystal structure and films retained the ZnO crystal structure. Moreover, the intensity of (002) reflection of ZnO is increased with ion fluence at the expense of other reflections. Raman spectroscopy is also in good agreement with XRD result. The doublet of Mo 3d peak appeared at 232.37 and 235.60 eV, which correspond to Mo $3d^{5/2}$ and $3d^{3/2}$ respectively. Spin-orbit splitting of Mo 3d levels give rise to $3d^{5/2}$ and $3d^{3/2}$ levels (Fig. 1 (right)) with an energy separation of 3.2 eV, which is well matched with the present result, implying that Mo is present in +6 state. It is clear that Mo atomic fraction decreased with ion fluence. Rutherford Backscattering Spectroscopy analysis confirms that Mo is not present up to the depth of 100 nm even at very high fluence 7×10^{13} ions/cm^2. The phase splitting of $ZnMoO_4$ in hot ion track takes place which transforms it to ZnO upon cooling down. SHI irradiation results in the local annealing of the film under the effect of transitory heating within tracks through electron–phonon coupling, known as thermal spikes [3]. The formation of ZnO and absence Mo reveals the fact that MoO_3 is evaporated from the hot ion track during thermal spike due to the volatile nature of MoO_3. The energy deposited by SHI irradiation helps to raise the temperature locally and results in a phase transition of the film.

REFERENCES

[1] A. Kumar et al., J. Appl. Physics 101(2007)14308
[2] A. Benyagoub, Nucl. Instr. and Meth. B, 206 (2003) 132
[3] M. Toulemonde, J. M. Costantini, Ch. Dufour, A. Meftah, E. Paumier, and F. Studer,1996 Nucl. Instr. and Meth. B 116 (1996) 37

5.2.16 ENHANCEMENT OF LPG SENSING PROPERTIES IN NANOCRYSTALLINE ZINC OXIDE THIN FILM BY HIGH ELECTRONIC EXCITATION

Ravikiran Birajadar[1], Farha Siddiqui[1], S.Shaikh[1], Ravikiran Late[1], Anil Ghule[2], Fouran Singh[3], Ramphal Sharma[1, 2]

[1]Thin Film and Nanotechnology Laboratory, Department of Physics, Dr. Babasaheb Ambedkar Marathwada University, Aurangabad 431004, Maharashtra, India

[2]Department of Nanotechnology, Dr. Babasaheb Ambedkar Marathwada University, Aurangabad 431004, Maharashtra, India.
[3]Inter-University Accelerator Centre, Aruna Asaf Ali Marg, New Delhi -110067, India

Zinc oxide (ZnO) with wurtzite structure is an important and promising material, with many typical properties such as transparency in the visible range, direct band gap of 3.37 eV, resistivity of semiconductor (usually in the range of 10^{-3}–10^{5} Ωcm), electrochemical stability and absence of toxicity. ZnO thin films have been used in gas sensors. Some of the important aspects about gas sensors are the cost of manufacturing and raw materials employed, which are directly associated with the selection of deposition technique. Among all the techniques, Successive Ionic Layer Adsorption and Reaction (SILAR) is simple, low cost, and effective technique, which does not require any sophisticated instrumentation for deposition of films. The present article focuses on tailoring the surface morphology and electrical properties of these ZnO thin films, deposited on ITO by SILAR method, by using 120 MeV Au^{9+} ions with different fluence and its effect on sensitivity of the sensor.

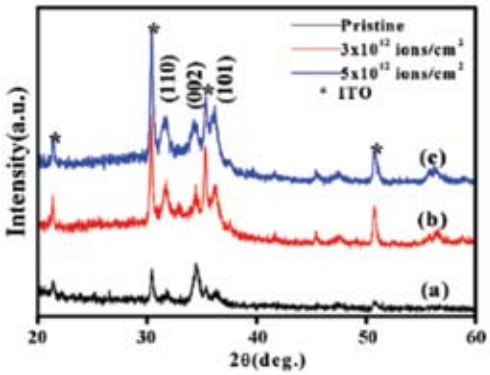

Fig.1. Representative XRD patterns of pristine and irradiated ZnO thin films with different fluence 3×10^{12}Ions/cm^2 and 5×10^{12} ions/cm^2.

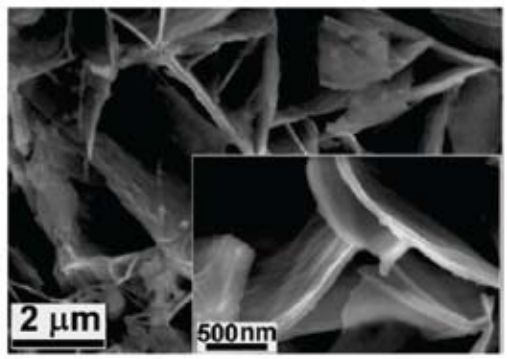

Fig. 2. Representative SEM image of ZnO thin film irradiated with fluence 3×10^{12} ions/cm^2.

The XRD spectra reveal that the material deposited on to the ITO is polycrystalline in nature. The XRD pattern for ZnO thin films showed diffraction peaks along (1 0 0), (0 0 2), and (1 0 1) as shown in Fig. 1. The average value of lattice parameters are found to be a = 3.258Å and c = 5.207 Å, which are in close agreement with the standard values confirming hexagonal wurtzite structure (JCPDS DATA CARD 79-0206). It is found that at low fluence i.e. 3×10^{12} ions/cm^2, full width at half maxima (FWHM) of the peak decreases and the intensity increases, which implies that the crystallite size of the material increases from 16 nm to 20 nm. Thus, it is noted that the crystallinity, crystallite size and quality of the film improve with ion irradiation at low fluence. This might be due to the releasing of strains between the grains at low fluence and also due to decrease in concentration of oxygen vacancies in ZnO thin film improving the crystalline quality of the film. While at higher fluence i.e. at 5×10^{12} ions/cm^2, the FWHM of peaks is found to increase and the intensity decreases, which reflects that the crystallite size is affected implying decrease and is noted to be 15 nm. At higher fluence, according to Coulomb explosion model, the SHI produces cylindrical shock waves of charged ions pushing the atoms from their original positions and distorting their lattices resulting in the observed increase in FWHM of peaks. SEM images (Fig. 2) obtained show uniformly deposited cabbage leaf-like ZnO nanostructures, which were randomly oriented and are not well developed. The randomly oriented pristine ZnO cabbage leaf-like structures show improved crystallinity and increase in crystallite size (20 nm) on irradiation with fluence 3×10^{12} ions/cm^2 as a result of annealing effect. On the other hand, the cabbage leaf-like structures were found to open wide and were observed to be well spaced after irradiation with fluence 5×10^{12} ions/cm^2. Opening of the cabbage leaf-like structures creates deep hollow region resulting in increased surface area, especially after irradiation. These observations are in good agreement with those noted in XRD studies, in which, the crystallite size of the material decreases from 20 nm to 15 nm at higher fluence. This implies increase in surface to volume

ratio.This type of surface morphology is promising in gas sensing applications because the large surface area available for gas interaction leads to improved gas sensitivity in short response time.

Optical absorption shows that the pristine sample has direct band gap of 3.22 eV; while the representative irradiated sample with fluence 3×10^{12} ions/cm^2 and 5×10^{12} ions/cm^2 shows a direct band gap of 3.20 and 3.18 eV, respectively. Therefore there is no significant change in band edge after the irradiation, except for slight increase in absorbance in the visible region. This implies that basic crystal structure of ZnO is intact.

The resistivity decreases with the increase in irradiation fluence from 3×10^{12} to 5×10^{12} ions/cm^2. It is observed that, at lower fluence (3×10^{12} ions/cm^2), the crystallite size increases while at higher fluence (5×10^{12} ions/cm^2) the crystallite size is found to decrease, consequently the resistivity is expected to increases but is not observed in this case. This clearly indicates that the grain boundary scattering is not dominating here. The drastic change in resistivity is observed after irradiation.

We observed an enhancement of LPG gas sensing properties in nanostructured ZnO thin films irradiated using 120 MeV Au^{9+} ions with fluence 5×10^{12} ions/cm^2, resulting in excellent LPG sensing properties. In particular, irradiated ZnO thin film gas sensor shows a highly sensitive and reversible response to LPG gas at relatively lower temperature and even at low LPG concentrations. The observed enhancement can be attributed to the evolution of cabbage leaf-like structures with irradiation and increase in fluence helps to the increase the surface area with formation of deep hollow porous region within the leaf-like ZnO nanostructures. These results along with a simple growth process demonstrate that the ZnO thin film irradiated using 120 MeV Au^{9+} ions with fluence 5×10^{12} ions/cm^2 are promising for large scale fabrication of cost-effective and high performance LPG gas sensors operating at low LPG concentration and temperature.

REFRENCES

[1] M. Suchea, S. Christoulakis, K. Moschovis, N. Katsarakis, and G. Kiriakidis, Thin Solid Films 515 (2006) 551
[2] R. Zhang and L. L. Kerr, J. Solid State Chem. 180 (2007) 988
[3] G. K. Mehta, Vacuum 48 (1997) 957
[4] D. C. Agarwal, A. Kumar, S. A. Khan, D. Kabiraj, F. Singh, A. Tripathi, J. C. Pivin, R. S. Chauhan, and D. K. Avasthi, Nucl. Instr. and Meth. 244 (2006) 136

5.2.17 SHI INDUCED MODIFICATIONS OF CdS–Bi_2S_3 NANOCOMPOSITE THIN FILM BY SUCCESSIVE IONIC LAYER ADSORPTION AND REACTION (SILAR) METHOD

Farha Siddiqui[1], S.Shaikh[1], Ravikiran Late[1], Anil Ghule[2], F. Singh[3], and Ramphal Sharma [1, 2]

[1]Thin film and Nanotechnology Laboratory, Department of Physics, Dr. Babasaheb Ambedkar Marathwada University, Aurangabad 431 004, Maharashtra, India
[2]Department of Nanotechnology, Dr. Babasaheb Ambedkar Marathwada University, Aurangabad 431 004, Maharashtra, India
[3]Inter-University Accelerator Centre, Aruna Asaf Ali Marg, New Delhi -110067, India

Cadmium sulphide (CdS) and Bismuth sulphide (Bi_2S_3) thin films have received considerable attention during the recent years because of their potential application in conversion of solar energy into electrical energy and in variety of semiconductor devices. The energy band gap of CdS and Bi_2S_3 is 2.4 and 1.4 eV, respectively. To achieve higher mobility and increased life time of charge carriers, in the present work, we synthesized CdS–Bi_2S_3 composite semiconducting thin film. We have synthesized CdS, Bi_2S_3 and CdS–Bi_2S_3 nanocomposite thin film using successive ionic layer adsorption and reaction (SILAR) technique. This comparative study gives better insight on the properties of the individual material and its composite CdS–Bi_2S_3. The effect of SHI on CdS and Bi_2S_3 thin film is also investigated. The CdS and Bi_2S_3 thin films were irradiated using 100 MeV Au^{9+} ions at the fluence of 5×10^{12} ion/cm^2.

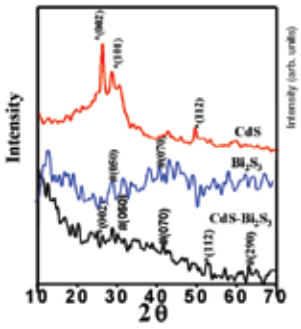

Fig. 1. XRD patterns of as deposited CdS, Bi_2S_3 and CdS- Bi_2S_3 thin films.

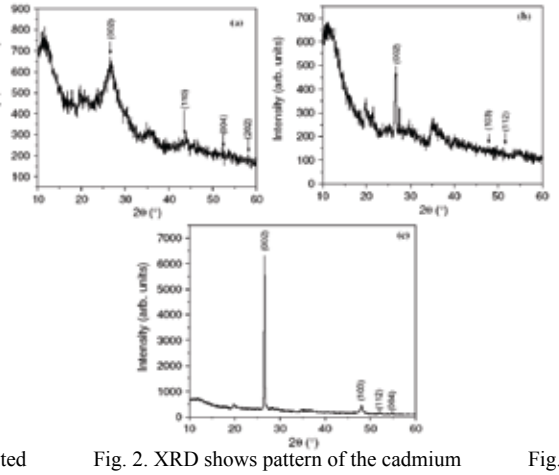

Fig. 2. XRD shows pattern of the cadmium sulfide thin films :(a) as deposited, (b) annealed at 300ºC for 1 h in air and (c) 100 MeV Au SHI irradiated.

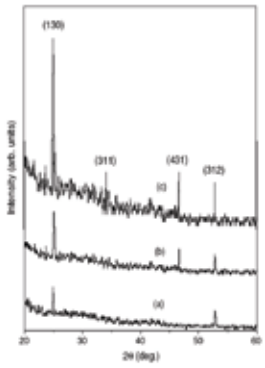

Fig. 3 shows XRD patterns of (a) as deposited, (b) annealed and (c) SHI irradiated bismuth sulphide thin films.

In Fig. 1 the peaks in XRD patterns of the samples CdS, Bi_2S_3 and CdS–Bi_2S_3 nanocomposite thin film have been assigned in accordance with the JCPDS references of CdS (No 01-783) and Bi_2S_3 (No 79 2384). In present investigation it was observed that the CdS film was polycrystalline in nature and Bi_2S_3 films was amorphous in nature. The planes observed at (0 0 2), (1 0 1), (1 1 2) were due to hexagonal phase of CdS and the planes at (0 5 0), (0 7 2) and (2 9 0) were due to the orthorhombic phase of Bi_2S_3. Furthermore, CdS–Bi_2S_3 showed mixed structure, which means combination of hexagonal CdS and orthorhombic Bi_2S_3 structure in CdS–Bi_2S_3 nanocomposite thin film. The crystallite size of CdS, Bi_2S_3 and CdS–Bi_2S_3 thin film were found to be 11 nm, 5 nm and 7 nm, respectively.

Fig. 2 shows the XRD pattern of the as-deposited, annealed 300ºC and 100 MeV Au^{9+} ion irradiated CdS thin films with 5×10^{12} ions/cm^2. The intrinsic peak of (0 0 2) for hexagonal CdS is observed at 2θ = 26.5° for all three samples. The peak is broad for the as-deposited sample due to fine particle (nano) structure of CdS. The crystallite size of as deposited CdS is 11 nm. After annealing, this peak gets more pronounced indicating the improvement in the crystallite size from 11 to 21.3 nm. Irradiation may cause the coalescence of particles and result in the increase in the particle size to 69.2 nm. Hence the XRD pattern shows a highly orienting peak of (0 0 2). There are also some small peaks of hexagonal phase indicating the polycrystalline nature of the films. Fig. 3 shows XRD patterns of as-deposited, annealed in air at 300ºC for 1 h and Au^{9+} ion irradiated Bi_2S_3 thin film onto glass substrate are shown which have some broad and low intensity peaks. The intensity of (130), (311), (431) and (312) peaks increases after annealing and Au ion irradiation. This is attributed to the improvement in crystallinity and enhancement in crystallite size after irradiation.

Surface morphological studies play an important role to determine surface profile and nature of the films. Results indicate CdS thin film have spherical crystallites distributed over the substrate and it shows Bi_2S_3 thin film demonstrating cellular network. From this, it is observed that the as-deposited Bi_2S_3 thin film is homogenous, without cracks or pinholes and covers the entire glass substrate. The deposited CdS–Bi_2S_3 nanocomposite thin film shows highly porous compact nanowalled structures. Small nanosized grains are uniformly distributed over smooth background. This clearly indicates the nanocrystalline nature of the film and smooth background may possess the amorphous phase of Bi_2S_3 thin film. The grains are very small and have unequal circular size and shape.

Optical absorption of as deposited CdS, as deposited Bi_2S_3, and as deposited CdS–Bi_2S_3 nanocomposite thin films were studied in the wavelength range of 400–1100 nm. The optical absorption edge is found to shift towards higher wavelength. The optical studies revealed that the energy band gap of CdS–Bi_2S_3

nanocomposite thin film has close match with the solar spectrum, which is useful in fabrication of optoelectronic devices. Furthermore, the as deposited CdS, as deposited Bi_2S_3 and as deposited CdS–Bi_2S_3 nanocomposite thin films demonstrated good response to the light indicating the fact that the film can be employed in photosensor applications.

REFERENCES

[1] R. R. Ahire, B. R. Sankpal, and C. D. Lokhande, Mater. Chem. Phys. 72 (2001) 48
[2] K. M. Gadve, C. D. Lokande, and P. P. Hankare, Mater. Chem. Phys. 38 (1994) 393
[3] A. Jana, C. Bhattacharya, and J. Datta, Electrochim. Acta 55 (2010) 6553

5.2.18 EFFECT OF SWIFT HEAVY ION IRRADIATION ON THE PROPERTIES OF SPRAY PYROLYTICALLY DEPOSITED Ti DOPED In_2O_3 FILMS

V. Gokulakrishnan[1], S. Parthiban[2], K. Jeganathan[3], K. Asokan[4], K. Ramamuthi[1]

[1]Crystal Growth and Thin Film Laboratory, School of Physics, Bharathidasan University, Tiruchirappalli 620 024, India.
[2]CENIMAT/I3N, Departamento de Ciência dos Materiais, Faculdade de Ciências e Tecnologia, FCT, Universidade Nova de Lisboa and CEMOP-UNINOVA, 2829-516 Caparica, Portugal.
[3]Centre for Nanoscience and Nanotechnology, School of Physics, Bharathidasan University, Tiruchirappalli 620 024, India
[4]Inter-University Accelerator Centre, Aruna Asaf Ali Marg, New Delhi -110067, India

Ti (2 at. %)doped indium oxide thin films were prepared by spray pyrolysis method at 400 °C and irradiated with 100 MeV O^{7+} ions at different fluences. The effect of irradiation on the structural and surface morphological properties of these thin films is reported for different ion fluences.

X-ray diffraction (XRD) studies on the as-deposited and irradiated In_2O_3:Ti films confirmed the cubic bixbyite structure of the polycrystalline indium oxide (IO) and the diffraction peaks were identified by matching with the ICDD data [1] and shown in Fig. 1. XRD peaks observed for In_2O_3: Ti at the diffraction angles (2θ) 30.5° and 35.4° belong to (222) and (400) planes of cubic IO. An additional peak of (321) was introduced at 33.9° due to irradiation with 5×10^{11} ions cm^{-2}. But the (321) peak disappeared and the intensity of (222) peak reduced significantly when irradiated with higher fluence ($\geq 1\times10^{12}$ ions cm^{-2}). The intensity of (400) diffraction peak is significantly increased for the fluence of 1×10^{12} ions cm^{-2} but tend to decrease later when the fluence is increased to 5×10^{13} ions cm^{-2}. The film has only the weak (222) peak when irradiated with the fluence of 5×10^{13} ions cm^{-2}; thus shows the tendency towards amorphization. The crystallite size was estimated from the (222) XRD peak, using Scherrer's formula [2] and it decreases from 59 (as-deposited) to 30 nm on irradiation with ion fluence of 5×10^{13} ions cm^{-2}.

Surface microstructures (2.5 μm×2.5 μm) obtained from atomic force microscope (AFM) analysis of In_2O_3:Ti films irradiated with various fluences are comparatively shown in Figs. 2(a)-(d) as a function of irradiation ion fluence. Irradiation at higher ion fluence seems to fragment the grains into smaller size. The grain size is reduced from 87 nm of the as-deposited films to 48 nm, when the films are irradiated with the fluence of 5×10^{13} ions cm^{-2}. For the fluence of 1×10^{13} ions cm^{-2} and 5×10^{13} ions cm^{-2} the agglomerated grains were loosely packed due to the thermal annealing of irradiation. The AFM study reveals that the crystalline quality of the film is modified following a significant change in the surface roughness due to irradiation with O^{7+} ions of various fluences. The root mean square (rms) values of surface roughness obtained from the AFM analysis is 16, 13, 10 and 8 nm for the as-deposited film and for the films irradiated with different fluences of 1×10^{12}, 1×10^{13} and 5×10^{13} ions cm^{-2}, respectively.

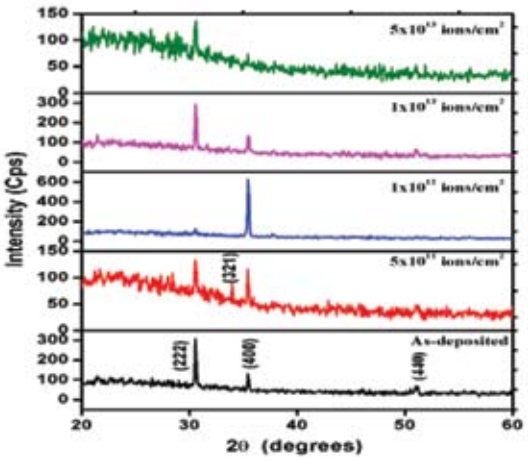

Fig. 1. XRD patterns of the as- deposited and SHI irradiated In_2O_3: Ti films

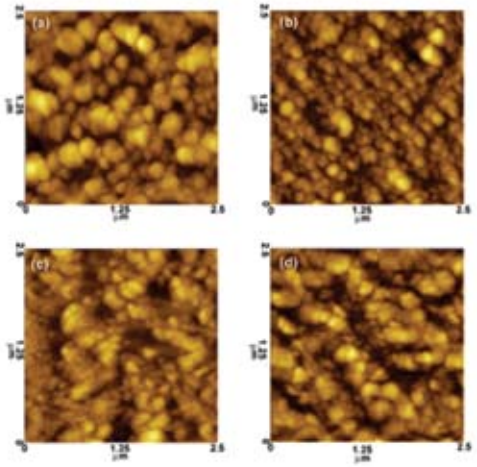

Fig. 2. AFM microstructures obtained from (a) as-deposited, irradiated In^2O^3: Ti films with fluence of (b) 1×10^{12}, (c) 1×10^{13} and (d) 5×10^{13} ions cm^{-2}

REFERENCES

[1] Powder Diffraction File, JCPDS-International Centre for Diffraction Data-ICDD, Card No. 06-0416, Philadelphia, PA, (2005).
[2] B.D. Cullity, Elements of X-ray diffraction, Addison-Wesley, Massachusetts, 1956.

5.2.19 SWIFT HEAVY ION PROVOKED STRUCTURAL AND ELECTRICAL PROPERTIES IN SnO_2 THIN FILMS

K. M. Abhirami[1], R. Sathyamoorthy[1], D.Kanjilal[2], K. Asokan[2]

[1]Kongunadu Arts and Science College, Coimbatore, Tamil Nadu- 641 029, India.
[2]Inter-University Accelerator Centre, Aruna Asaf Ali Marg, New Delhi -110067, India

SnO_2 thin films grown on glass substrates at 300°C by reactive thermal evaporation and sintered at 600 °C were irradiated by 120 MeV Ag^{9+} ions. Though irradiation is known to induce lattice disorder and suppression of crystallinity, we observe grain growth at some fluence of irradiation. The films are irradiated at fluences of 1×10^{11}, 5×10^{11}, 1×10^{12}, 5×10^{12} and 1×10^{13} ions/cm^2. The electrical, optical, morphological and structural properties of the irradiated and pristine films were studied using Hall effect measurement, UV–visible absorption spectroscopy, atomic force microscopy (AFM) and X-ray diffraction (XRD). The composition of the films and sputtering due to irradiation are disclosed by Rutherford Backscattering Spectroscopy (RBS) spectra as shown in Fig. 1(a). From XRD patterns in Fig. 1(b), it is observed that intensity of diffraction peak increases for the film irradiated upto the fluence of 1×10^{11} ions/cm^2 whereas beyond that the peak intensity decreases with fluence. The increasing peak intensity and narrowing of the peaks could be indicative of irradiation induced grain growth. But the observed decrease in the peak intensity at higher fluences could be due to an increase of the micro-strains generated by irradiation-induced lattice defects [1].

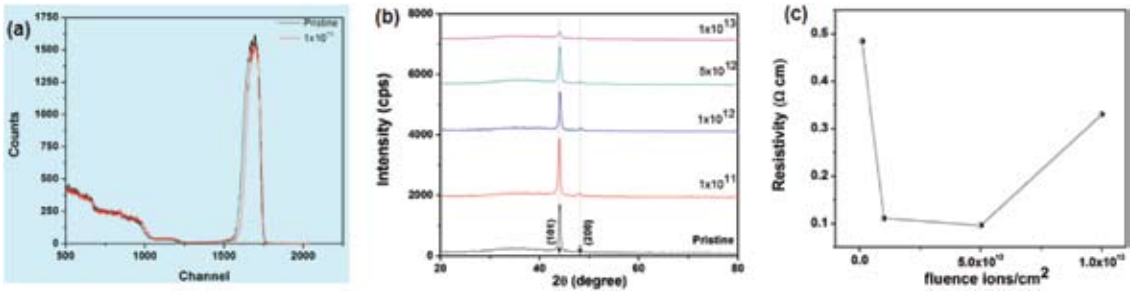

Fig. 1. (a) RBS spectra of pristine and irradiated samples, (b) XRD pattern of pristine and irradiated samples, and (c) variation of resistivity of samples at different fluences.

Tuning of the surface morphology on nanometric scale by ion bombardment can be achieved by ion- solid interaction. The roughness increases with increase in fluence upto 1×10^{12} ions/cm^2 and decreases beyond that. Agglomeration of grain becomes more noticeable with increase in ion fluence and could be ascribed to the multiple ion impacts. A significant decrease in band gap was noticed with increase in ion dose. The band gap varies between 3.56 eV to 4.01 eV for 1×10^{11} ions/cm^2 to 1×10^{12} ions/cm^2. The decrease in transmission could arise due to the increase in absorption associated with the creation of intermediate energy levels during irradiation [2].

The as-deposited SnO_2 film has a quite high resistivity as shown in Fig. 1(c). As the fluence increases, the resistivity of the films decreases drastically and reaches a minimum at 5×10^{12} ions/cm^2. With further increase of the ion fluence, a reversed behavior of the resistivity emerged, which may be due to creation of more defects or decline in the crystallinity [3]. The negative sign of the hall coefficient implies the n-type conductivity of the material.

In the case of pristine sample, the width of Sn peak in the RBS spectrum is high compared to the irradiated sample as can be seen in Fig. 1(a). RBS spectra of Ag ion irradiated (1×10^{13} ions/cm^2) samples shows the decrease in width of peak may be due to the loss of Sn atoms which may result due to the sputtering of SnO_2 compound.

REFERENCES

[1] S. Chandramohan, R. Sathyamoorthy, P. Sudhagar, D. Kanjilal, D. Kabiraj, K. Asokan, V. Ganesan, T. Shripathi, and U.P. Deshpande, Appl. Phys. A 94 (2009) 703
[2] V.K. Miloslavskij, Phys. Solid State 7 (1965) 1550
[3] M. Batzill and U. Diebold, Prog. Surf. Sci. 79 (2005) 47

5.2.20 SOFTENING OF PHONONS BY LATTICE DEFECTS AND STRUCTURAL STRAIN IN SWIFT HEAVY ION IRRADIATED NANOCRYSTALLINE ZINC OXIDE FILMS

Fouran Singh[1], R. G. Singh[2], Vinod Kumar[1], S. A. Khan[1], J. C. Pivin[3]

[1]Inter-University Accelerator Centre, Aruna Asaf Ali Marg, New Delhi -110067, India
[2]Maharaja Agrasen College, University of Delhi, New Delhi- 110096, India
[3]CSNSM, IN2P3, Bâtiment 108, 91405 Orsay Campus, France.

Origin of the SHI induced phonon mode in a good nanocrystalline ZnO films having wurtzite structure is studied. Particularly, the induced *A*1 (LO) phonon mode is very interesting as it evolves and red shifted with increase in irradiation fluence. Therefore, the induced phonon mode could be attributed to the surface phonon mode or deformation potential (intrinsic lattice defects) in structure under the heavy ion irradiation in terms of electric field induced Raman scattering [1]. On the other hand, indirectly UV-Vis studies (as shown in left figure) evidenced that the concentration of oxygen vacancies are increased with increase in the ion fluence and oxygen vacancies are supposed to be the electron carriers in ZnO. So, the high carrier

concentration and large band bending in near band edge absorption due to accumulation of defects at grain boundaries generate a built in electric field within the grains, and hence enhance the Raman active optical phonons [2].

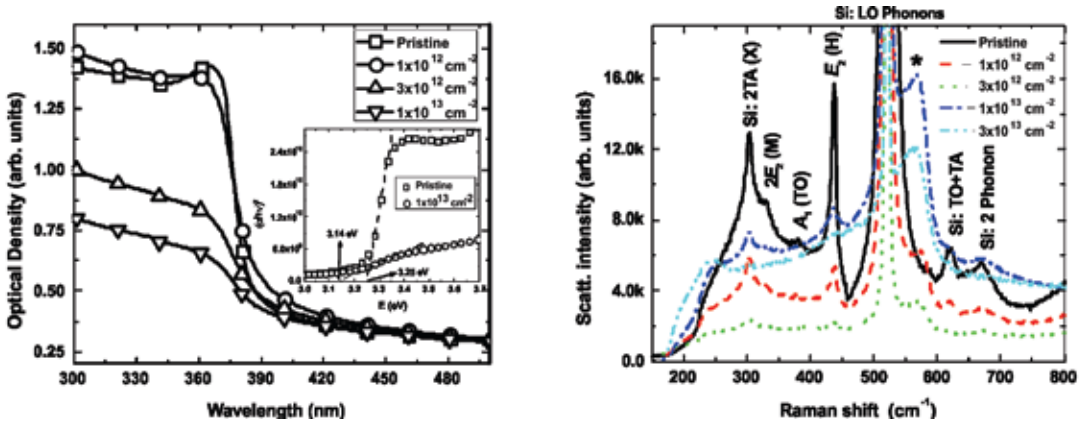

Fig. (left) UV-Vis absorption spectra and (right) micro-Raman spectra of 120 MeV Au irradiated nanocrystalline ZnO films

The reduction in the grain size and increase of grain boundary density enhances the build in electric field and consequently the intensity of the evolved phonon mode around at 573 cm^{-1} (as shown in right figure). Indeed the intensity of this mode is affected by the concentration of oxygen vacancies since it involves only the vibrations of the oxygen sub-lattice in agreement with ERDA studies. The softening of about 11 cm^{-1} cannot be attributed to the size of crystallites [3]. Therefore, it is explained in terms of the combined effects of phonon localization by lattice defects and structural strain in the lattice induced by energetic heavy ions [4].

REFERENCES

[1] T.C. Damen, S.P.S. Porto, and B. Tell, Phys. Rev. 142 (1966) 570
[2] J. Serrano, A.H. Romero, F.J. Manjón, R. Lauck, M. Cardona, and A. Rubio, Phys. Rev. B 69 (2004) 094306
[3] A.G. Rolo and M.I. Vasilevskiy, J. Raman Spectroscopy 38 (2007) 618
[4] Fouran Singh, P.K. Kulriya and J.C. Pivin, Solid State Commun 150 (2010) 1751; and Fouran Singh, R.G. Singh, Vinod Kumar, S.A. Khan, and J.C. Pivin, J. Appl. Phys., 110 (2011) 083520

5.2.21 INVESTIGATIONS ON 120 MeV Au^{9+} IRRADIATED PRASEODYMIUM INCORPORATED ZnS/TiO_2 CORE-SHELL NANOSTRUCTURES

Prabha Sana[1], M.M. Malik[1]

[1]Physics Department, Maulana Azad National Instituite of Technology, Bhopal- 462 051

In the present work, the colloidal method has been successfully employed for the preparation of Pr^{3+} doped ZnS/TiO_2 core-shell nanostructures. In this study, we used 120 MeV Au^{9+} ions to check the radiation hardness, and to observe the modifications produced in structural and optical properties of synthesized Pr^{3+} doped ZnS/TiO_2 core-shell nanostructures. The irradiation effect has been observed at three fluences 3×10^{12}, 1×10^{13} and 3×10^{13} ions/cm^2. The uniqueness of this work is the selection of energy and fluence of the ion species (gold). The total electronic energy density deposited by the gold ions with fluence of 3×10^{12} to 3×10^{13} ions/cm^2 is above the electronic energy deposition threshold. The XRD analysis of pristine sample reveals the hexagonal structure of core ZnS with reflection planes (101) and (102). Reflections planes (220)* and (101)* are predicted for β-ZnS phase having cubic system and face-centred lattice, therefore XRD analysis shows the mixed phase of ZnS nanostructure. The X-ray diffraction pattern corresponding to the pristine and irradiated films seem to be similar. SEM analysis of pristine sample shows cubical microstructures, which are the aggregation of Pr^{3+} doped ZnS/TiO_2 NC's. SEM micrograph shows the fragmentation and agglomeration of the cubical morphology after irradiation to a fluence of 3×10^{12} ions/

cm^2. For fluence 1×10^{13} ions/cm^2, growth of nanorods have been observed on the surface of cubes and these cubes are disintegrated simultaneously. At the highest fluence 3×10^{13} ions/cm^2, cubic morphology of Pr^{3+} doped ZnS/TiO_2 disappeared and complete growth of nanorods are observed as seen from Fig. 1.

The photoluminescence spectrum of pristine sample shows the luminescence peak at 485 nm, 525 nm and 665 nm for corresponding transition energy levels $^3P_0$- $^3H_4$, $^3P_0$- $^3H5$ and $^3P_0$- $^3F_2$ of Pr^{3+} ions in ZnS host matrix as shown in Fig. 2. The characteristic blue emission due to sulphur vacancies at 379 nm in ZnS has been observed with less intensity suggesting the transfer of excitons to deep trap level of Pr^{3+} ions, also effective TiO_2 coating may prevent the surface defects, vacancies and dangling bonds. At fluence 3×10^{12} ions/cm^2 and 1×10^{13} ions/cm^2 emission intensity of photoluminescence (PL) spectra have increased. The PL intensity is sensitive to the damage created by SHIs. At initial irradiation fluence 3×10^{12} ions/cm^2 and 1×10^{13} ions/cm^2 the fragmentation of crystal might have produce colour centres, increased the radiative transition at grain boundaries, therefore increased intensity is observed. However, at higher fluence 3×10^{13} ions/cm^2 the intensity of emission spectra has been slightly degraded, it may be due to higher dislocation density produced in nanocrystalline Pr^{3+} doped ZnS/TiO_2 core-shell structure, because higher dislocation density attributes to the destruction of photo generated carriers by non-radiative recombination centres.

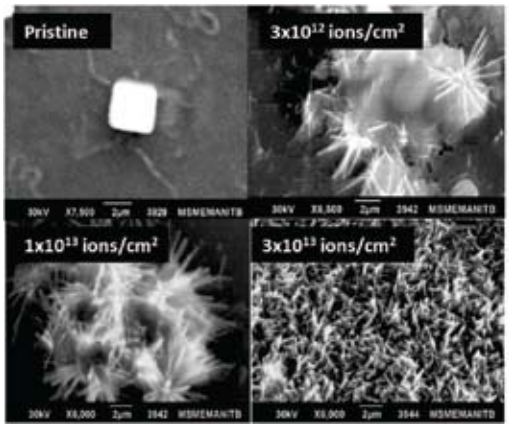

Fig. 1. SEM images of pristine and irradiated samples.

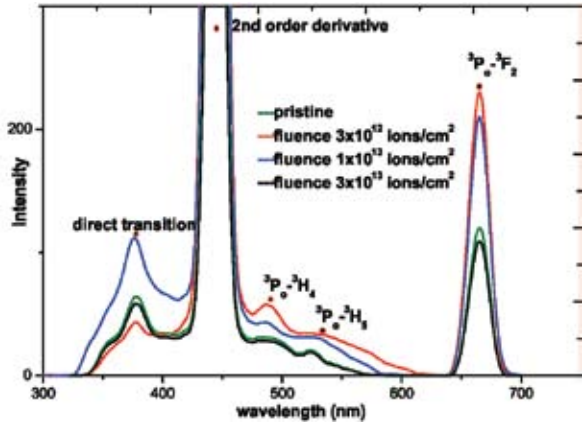

Fig. 2. Photoluminescence spectra of pristine and irradiated samples.

REFERENCES

[1] Jeong Ho You and H. T. Johnson, J. Appl. Phys. 101 (2007) 023516
[2] S. Wageh, Zhao Su Ling, Xu Xu-Rong, J. of Crystal Growth 255 (2003) 332

5.2.22 STRUCTURAL AND MAGNETIC PROPERTIES OF 100 MeV Ag^{+7} ION IRRADIATED Co DOPED TiO_2 THIN FILMS

P. Mohanty[1], N. C. Mishra[2], P. K. Kulriya[3], D. Kanjilal[3] D. K. Avasthi[3] and Chandana Rath[1],*

[1]School of Materials Science and Technology, Institute of Technology, Banaras Hindu University, Varanasi 221005, India
[2]Department of Physics, Utkal University, Vani Vihar, Bhubaneswar, Odisha, India
[3]Inter-University Accelerator Centre, Aruna Asaf Ali Marg, New Delhi -110067, India

In this work we have studied the structural and magnetic properties of $Ti_{1-x}Co_xO_{2-d}$ (x= 0.015) thin films deposited by PLD technique on Si (100) substrate. The oxygen partial pressure during deposition was varied to study its effect on phase and magnetic properties. We observe that with increasing oxygen partial pressure, rutile to anatase phase transformation in the films. Magnetic measurements using SQUID

magnetometer revealed that all the films are ferromagnetic at room temperature. From XPS studies we infer the phase transformation is due to oxygen vacancies which triggers the magnetic ordering at RT. MFM of film deposited at 0.1 mT oxygen pressure, confirms the magnetic signals throughout the film surface. To study the effects of defects (columnar) on structural and magnetic properties we irradiated the films with 100 MeV Ag^{+7} ions with fluence ranging from 5×10^{10} to 1×10^{12}. All the films amorphized at fluence 1×10^{12} but the crystallinity persists in the film deposited at 0.1 mT oxygen partial pressure (Fig. 1). We observe morphological changes with ion irradiation. At 1×10^{12} fluence, micrometer sized craters are observed along with nano-rod like structures on the surface. Fig. 2 shows the comparison of magnetization as a function of applied magnetic field for the film deposited at 0.1 mT and similar film irradiated with fluence 1×10^{12}. The coercivity of the pristine and irradiated films remains unchanged while the saturation magnetization decreases after irradiation. We believe that with ion irradiation the amorphized latent tracks were created as S_e is more than S_{eth}. Those amorphized regions do not contribute to the observed magnetization rather decreases the M_s.

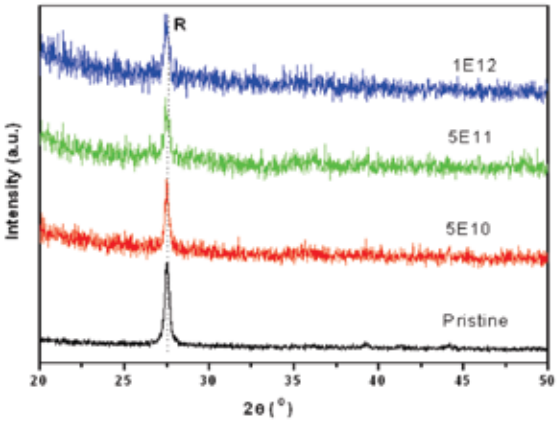

Fig. 1. GAXRD of the film irradiated with different ion fluence.

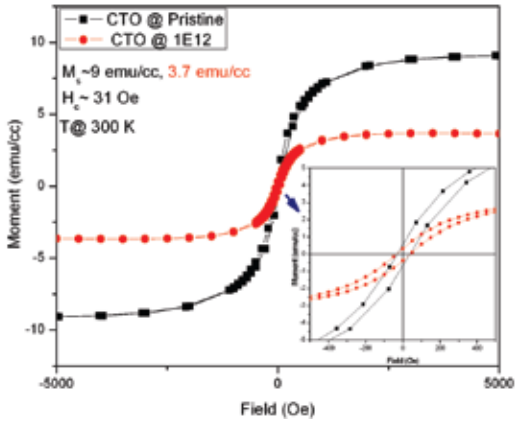

Fig. 2. Magnetization as a function of applied magnetic field at 300 K of pristine (black) and irradiated with 1×10^{12} (red)

REFERENCE

[1] P. Mohanty, Chandana Rath, N. C. Mishra, P. K. Kulriya, D. Kanjilal and D. K. Avasthi, (unpublished)

5.2.23 DECOMPOSITION OF NANOCRYSTALLINE ZINC SILICATE PHASE AT THE ZnO-Si INTERFACE BY SWIFT HEAVY ION IRRADIATION

Sanjeev Kumar[1], A. Kapoor[1] R. G. Singh[2], Vinod Kumar[3] and Fouran Singh[3]

[1]Department of Electronic Science, University of Delhi South Campus, New Delhi– 110021, India
[2]Maharaja Agrasen College, University of Delhi, New Delhi- 110096, India
[3]Inter-University Accelerator Centre, Aruna Asaf Ali Marg, New Delhi -110067, India

The structure, optical and transport properties of zinc oxide (ZnO) thin films and nanostructures on silicon substrates can be controlled by thermal annealing for their potential applications in optoelectronic devices [1]. But, the annealing at high temperature on partially oxidized Si-substrates leads to the formation of nanocrystalline zinc silicate at the interface of ZnO-Si as confirmed by x-ray diffraction (XRD) pattern and Fourier transform infrared (FTIR) spectroscopy for the pristine films and shown in Figure left and right respectively. However, it affects the transport of the carriers across the junction for various devices. Nevertheless, this phase of silicates is having applications in advanced optoelectronic devices such as solid state white light and flat panel display devices. Therefore, for the detailed study on the formation of this phase and its mechanism under thermal annealing is reported recently by our group [2].

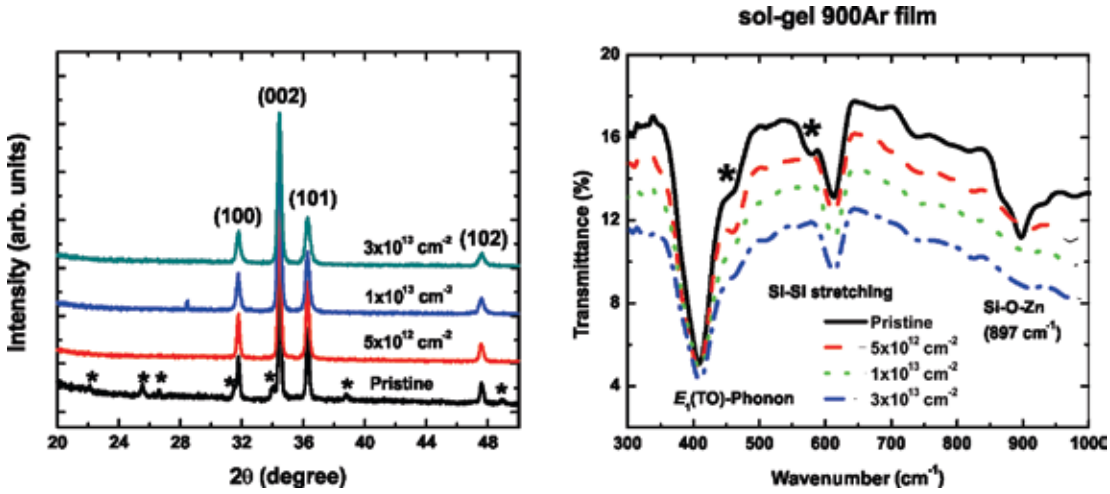

Fig. (left) XRD pattern and (right) FTIR spectra of pristine and 120 MeV Au irradiated nanocrystalline ZnO films on Si substrates

Peak marked with star sign in the XRD pattern are the peak of zinc silicate, which disappears after the irradiation. Similarly, shoulder marked with star sign and vibrational mode Si-O-Zn is characteristics of the discussed phase, which disappears after the irradiation. Therefore, one can say that XRD and FTIR results clearly show that the thin layer of this unwanted phase can be dissolved by 120 MeV Au ion irradiations. The decomposition mechanism in terms of bond breaking and diffusion processes are reported elsewhere [3]. However, the detailed decomposition mechanism by SHI irradiation will be reported later.

REFERENCES

[1] R.G. Singh, Fouran Singh, Vinod Kumar, and R.M. Mehra, Current Appl. Phys. 11 (2011) 624.
[2] R.G. Singh, Fouran Singh, R. M. Mehra, D. Kanjilal, and V. Agarwal, Solid State Comm. 151 (2011) 701.
[3] R.G. Singh, Fouran Singh, I. Sulania, D. Kanjilal, K. Sehrawat, V. Agarwal, and R.M. Mehra, Nucl. Instr. and Meth. B 267 (2009) 2399

5.2.24 ROLE OF DOPING IN THE SHI INDUCED MODIFICATIONS OF OPTICAL PROPERTIES OF NANOCRYSTALLINE ZINC OXIDE FILMS

Vinod Kumar[1], R. G. Singh[2], L. P. Purohit[3] and Fouran Singh[1]

[1]Inter-University Accelerator Centre, Aruna Asaf Ali Marg, New Delhi -110067, India
[2]Maharaja Agrasen College, University of Delhi, New Delhi- 110096, India
[3]Department of Physics, Gurukula Kangri University, Haridwar-249 404

Modifications of structural and optical properties of ZnO and ZnO:B films on Corning glass substrate with 120 MeV Ag ion irradiation have been investigated. Effect of boron doping in the structural, electrical and optical properties is reported in our previous work [1]. The structural properties were studied using X-ray diffraction and it shows that the average crystallite size of ZnO films is observed to increase by the irradiation [2]. The atomic force microscopy (AFM) study of films shows that the roughness of the films varies with increase in fluence. Optical transmittance of doped ZnO pristine and irradiated films is observed to be higher than 85% in the visible region. The transparency of ZnO and ZnO:B changed after irradiation. Variation in bandgap of undoped and ZnO:B is shown in Fig. 1. Bandgap narrowing and widening is observed in ZnO:B with change in ion fluence from 1×10^{11} to 3×10^{13} ion /cm^2. It is also shown that the bandgap of undoped and doped ZnO films can be tuned by SHI irradiation. Jain et al. have reported that bandgap of ZnO films can be varied with doping concentration [3]. The modifications of structural and optical properties are explained in terms of thermal spikes induced by SHIs [4].

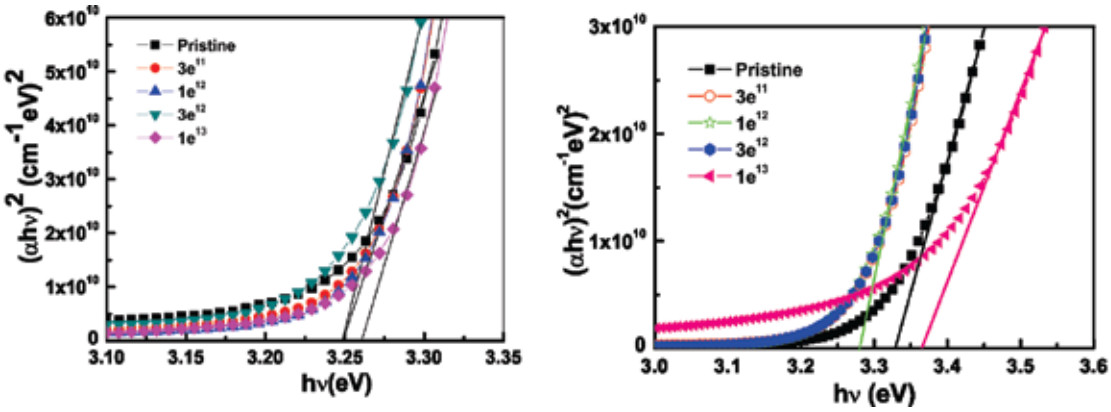

Fig. 1. Tauc's plots of undoped ZnO (left figure) and ZnO:B films (right figure) for different fluences of 120 MeV Ag ions.

We have also proposed to explore undoped and doped ZnO by bromine and iodine ion beams for photodiode application. We have synthesized ZnO and ZnO:B films on silicon substrate for this purpose using sol-gel and RF-sputtering. We have explored these samples by 80 MeV Br ion beam. The characterization and analyses part of these samples is in progress.

REFERENCES

[1] Vinod Kumar, R. G. Singh, L. P. Purohit and R. M. Mehra, J. Mater. Sci. Technol. 27 (2011) 481.
[2] Fouran Singh, R. G. Singh, Vinod Kumar, S. A. Khan, J. C. Pivin, J. Appl. Phys. 110 (2011) 083520.
[3] Anubha Jain, P. Sagar, R.M. Mehra, Solid-State Electronics 50 (2006) 1420.
[4] Vinod Kumar, R. G. Singh, L. P. Purohit and Fouran Singh, Adv. Mat. Lett. (2012) (submitted after revision).

5.2.25 CONDUCTING NANO-CHANNELS IN INDUCED PIEZOELECTRIC POLYMERIC MATRIX USING SWIFT HEAVY IONS AND SUBSEQUENT FUNCTIONALIZATION

Karun Kumar Jana[1], Biswajit Ray[2], Devesh K. Avasthi[3] and Pralay Maiti*,[1]

[1]School of Materials Science and Technology, Institute of Technology, Banaras Hindu University, Varanasi 221 005, India
[2]Department of Chemistry, Banaras Hindu University, Varanasi 221 005, India
[3]Inter-University Accelerator Centre, Aruna Asaf Ali Marg, New Delhi -110067, India

Nanohybrids of poly-(vinylidene fluoride) with layered silicates have been synthesized by melt extrusion and nano-channels have been fabricated by swift heavy ions *(SHI)* irradiation followed by chemical etching of the selective amorphous zones in the latent tracks. The channel diameter is reduced to 30 nm from the value of 40 nm corresponding to pristine *PVDF* which in presence of nanoclay in nanohybrid makes it suitable for membrane application. Grafting with styrene was carried out inside the nano-channel using the free radicals created by the *SHI* exposure. Sulphonation on the grafted polystyrene has been made to increase the conductivity of the membrane to the semiconducting range through ion channel conduction. The grafting and sulphonation inside the nano-channels have been confirmed through spectroscopic techniques e.g. *NMR, FTIR, UV* and molecular weight measurement. The dimension of the channels is controlled by *SHI* fluence and thereby dictates the properties including 10 orders higher in magnitude of conductivity by creating greater number of channels and hence, the surface area required for enhanced grafting and sulphonation. The matrix *PVDF* crystallizes in piezoelectric β-phase in presence of nanoclay and promotes the formation of smart membrane.

REFERENCE

[1] K. K. Jana. B. Ray. D. K. Avasthi. P. Maiti. J. Mater. Chem. 22 (2012) 3955

5.2.26 HETERO-EPITAXIAL GROWTH OF Si/SiO_2 USING 100 MeV Ni^{7+} BEAM

P. K. Sahoo[1], T. Som[2], I. Karn[3], D.Kanjilal[3]

[1]School of Physical Sciences, National Institute of Science Education and Research (NISER) Bhubaneswar
[2]Institute of Physics, Bhubaneswar
[3]Inter-University Accelerator Centre, Aruna Asaf Ali Marg, New Delhi -110067, India

The term dynamic epitaxy is used when simultaneous recovery of the damage is achieved by irradiating the substrate with desired species at elevated temperatures. In a way, dynamic epitaxy is a variant of ion beam induced epitaxial crystallization (IBIEC). It has been used to make variety of compounds in silicon including silicon oxide, silicon nitride, and metal silicide buried layers for silicon on insulator (SOI) device application and SIMOX technology. Another important material for opto-electronic and micro-sensors applications is alpha-quartz. Martin *et al*. [1] have described as to how ion implantation was used to manufacture micro-sensor by implanting quartz with 40 keV titanium ions. However, the difficulties of epitaxially recovering ion amorphized alpha quartz still remain a bottleneck in achieving a good quality material for opto-electronic applications. We have a series of papers published in low energy IBIEC of alpha quartz using alkali ions [2-4], which involves well understood S_n dependant recrystallization mechanism. However, the Se dominant mechanism involved in shift heavy IBIEC (SHIBIEC) remains unexplored in case of this important material.

In this study, the electronic energy loss dependant recrystallization of α-SiO_2 and Si/SiO_2 were observed at room temperature and elevated temperature in the range of 373-625 K. The relationship between the crystallization and processing conditions are discussed in the light of electronic and nuclear energy loss dependence. We try to understand the fundamental issues related to the underlying mechanism of ion beam induced epitaxial growth in SiO_2 both on amorphous SiO_2 (a-SiO_2) and a-Si. We also want to know the threshold temperature and fluence at which the re-crystallization starts in these systems. It has been observed that different mechanisms are involved in Si/SiO_2 and SiO_2/a-SiO_2 re-crystallization due to different interface.

Samples with 80 nm of SiO_2 layers on n-type Si substrates were grown by dry oxidation process. These Si/SiO_2 samples and α-quartz were irradiated with 200 keV Kr+ beam at a fluence of 1×10^{15} ions/cm^2 using low energy facility at IUAC. The Kr+ energy was chosen to amorphize both Si and SiO_2 layer to create an a-Si/SiO_2 interface. Here we show results of Si/SiO_2 system only and the SiO_2 recrystallization studies were still under detailed analysis.

Fig. 1 shows the RBS-Channeling spectra of Si/SiO_2 samples before and after irradiation with 100 MeV Ni beams. It has been observed from the channeling data that at RT the sample hardly recrystallized, whereas at elevated temperature it shows systematic recrystallization with activation energy of 1.9 eV, which is less as compared with low and high energy ion beam induced epitaxy [5-7]. The SiO_2 capping layer has some role on this low activation. The AFM image also shows very interesting surface morphology. It can be seen from Fig. 2 that RT irradiated sample show a hole like structure, which can be attributed as ion tracks on the SiO_2 layer. We are still investigating the details of the interface and underneath microstructure of the sample. As we increase the irradiation temperature to 100°C, the surface shows molten layer of SiO_2 and further increase in temperature smoothens the surface. It also gives an indication of recrystallization of the SiO_2 layer at higher irradiation temperature. The mechanism of recrystallization and the role of electronic and nuclear energy loss are still under investigation.

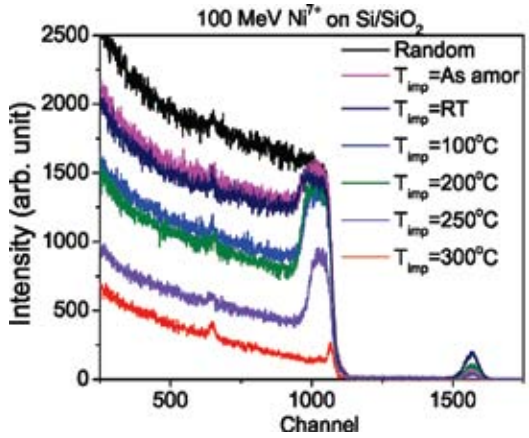

Fig. 1. RBS-Channeling of Si/SiO_2 samples irradiated with 100 MeV Ni^{7+} at different temperature in the range of RT to 300°C.

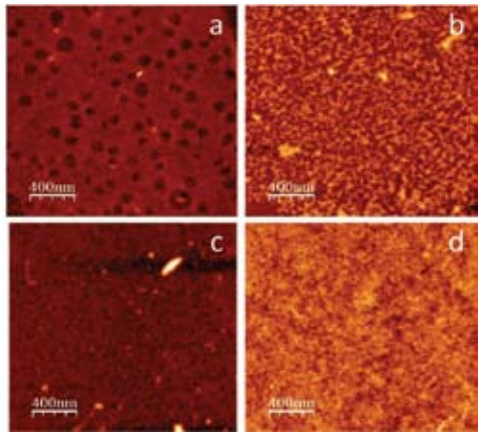

Fig. 2. The AFM image of Si/SiO_2 samples irradiated at (a) RT, (b) 100°C, (c) 200°C and (d) 300°C

REFERENCES

[1] P. Martin, M. Dufour, A. Ermolieff, S. Marthon, F. Pierre, andM. Dupov, J. Appl. Phys 72 (1992) 2907
[2] J. Keinonen, S. Gąsiorek, P. K. Sahoo, S. Dhar, and K. P. Leb. Appl. Phys. Lett. 88 (2006) 26110
[3] P. K. Sahoo, S. Gąsiorek, and K. P. Lieb, Appl. Phys. Lett. 87 (2005) 021105
[4] P. K. Sahoo, S. Gąsiorek, and K. P. Lieb, Nucl. Instr. and Meth. B, 249 (2006) 109
[5] Pratap. K. Sahoo, Ph.D. Thesis Department of Physics, Indian Institute of Technology Kanpur-208016, India (2004)
[6] P. K. Sahoo, T. Mohanty, D. Kanjilal, A. Pradhan and V. N. Kulkarni, Nucl. Instr. and Meth. B 257 (2007) 244
[7] P. K. Sahoo, T. Som, D. Kanjilal, and V. N. Kulkarni, Nucl. Instr. and Meth. B 240 (2005) 239

5.2.27 SWIFT HEAVY ION IRRADIATION INVESTIGATIONS ON POLYETHERETHERKETONE (PEEK)

Rajesh Kalia[1], Sapna Kalia[1], J K Sharma[1] and Indra Sulaniya[2]

[1]Department of Physics, M M University, Mullana (Ambala), Haryana, PIN-133207
[2]Inter-University Accelerator Centre, Aruna Asaf Ali Marg, New Delhi -110067, India

Organic polymers have been broadly used as electrical insulating materials and have large applications in power supply industries. The electrical performance of these materials is affected by their working environments such as nuclear reactor and radiation facilities [1]. Polyetheretherketone (PEEK) is an engineering thermoplastic with high performance. The Polyetheretherketone (PEEK) films of thickness 25 μm [EK301025] and 50 μm [EK301050] were procured from Goodfellow Cambridge Ltd., UK. These films are transparent pale amber in color. PEEK is an aromatic polyether and has good thermal, chemical, mechanical strength and radiation resistance [2]. Therefore, PEEK is expected to be applied in electrical insulation as well as in various other industrial fields [3].

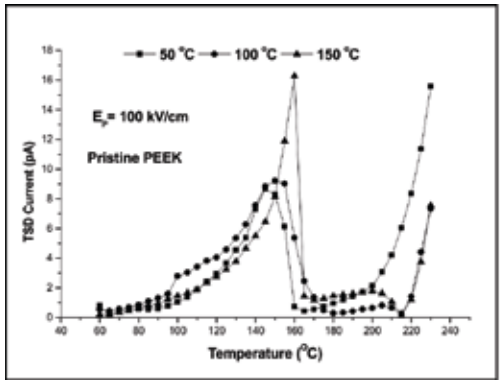

Fig. 1. TSDC spectra of 50 μm Pristine PEEK

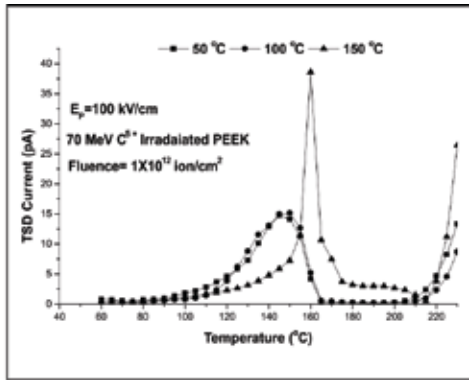

Fig. 2. TSDC spectra of 50 μm irradiated PEEK

Various researchers have investigated the dielectric relaxation phenomena in polymer electrets using the thermally stimulated discharge current (TSDC) technique [4]. The charge storage mechanism in polymer electrets is strongly dependent on the structure of electrets material [5]. However, only a few reports have been published on electrical and dielectric properties of PEEK [1, 3]. To study the TSDC behavior of irradiated samples, the samples of PEEK (25 μm and 50 μm) were irradiated with 70 MeV C^{5+} ion beam and 100 MeV Si^{8+} ion beam for fluence 1×10^{10} ions/cm^2, 1×10^{11} ions/cm^2, 1×10^{12} ions/cm^2 and 1×10^{13} ions/cm2 from the 15 MV Pelletron at IUAC.

The TSDC spectra of pristine and irradiated samples are shown in Fig. 1 and Fig. 2. The magnitude of α-relaxation peak in irradiated samples has increased as compared to that in pristine samples at similar conditions. The possible mechanisms for this increase may be either an increase in dipole concentration within the polymer, or increase in either electronic or ionic mobile charge concentration near the glass transition temperature.

REFERENCES

[1] S. Fujita, K. Shinyama, and M. Baba (1999) 10th international symposium on electrets. IEEE, pp. 115–118
[2] W. K. Sakamoto WK, Electica Quimica 28(2) (2003) 49
[3] J. R. Atkinson, J. N. Hay, and M. J. Jenkins, Polymer 43 (2002) 731
[4] C. Bucci and R. Fieschi, Phys. Rev. Lett. 12(1) (1964) 16
[5] M. M. Perlman (1973) Electrets charge storage and transport in dielectrics. The Electro Chemical Society, Princeton.

5.2.28 IRRADIATION INDUCED EFFECTS IN MgO BY X-RAY ABSORPTION NEAR-EDGE STRUCTURE SPECTROSCOPY

Jitendra Pal Singh[1], K. Asokan[1], D. Kabiraj[1], D. Kanjilal[1], and W. F. Pong[2]

[1]Inter-University Accelerator Centre, Aruna Asaf Ali Marg, New Delhi -110067, India
[2]Department of Physics, Tamkang University, Taiwan

Swift heavy ions (SHI) induce phase transformation in materials, removal of impurity phase, texturing in thin film, magnetization in Pd thin films etc. Recently, MgO has become important material due to evidences of ferromagnetism that can be tuned due to presence of defects [1] and it is an important material in magnetic tunnel junctions [2]. Hence creating defects and to understand nature of these defects induced by irradiation will be an important task. Understanding the effect of irradiation in the electronic structure of materials provides an opportunity to know the mechanism of ion beam interactions.

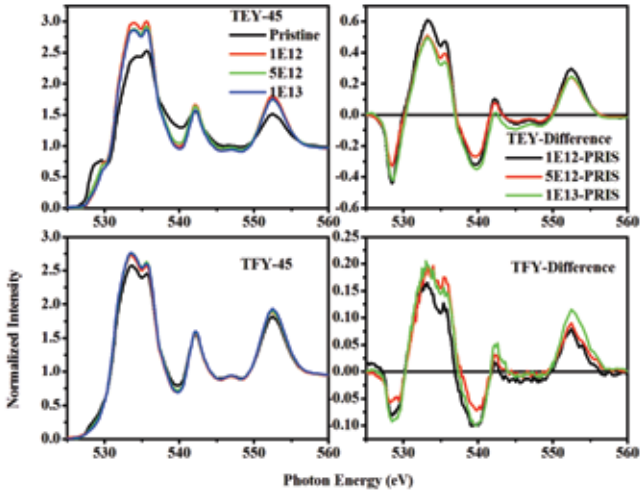

Fig. 1. (a) XANES spectra of the MgO film irradiated at different fluence.

In the present work MgO thin film deposited by e-beam evaporation has been irradiated by 100 MeV O^{7+} ion. Irradiation experiment has been carried out by using Pelletron Accelerator at IUAC at different fluencies 1×10^{12}, 5×10^{12} and 1×10^{13} ions/cm^2. XAS measurements were performed at the high energy spherical grating monochromator 20A1 XAS (HSGM) beamline in the National Synchrotron Radiation Research Center (NSRRC), Taiwan.

Fig. 1 shows the X-ray absorption near-edge structure spectra at O K-edge measured both in total electron yield and total fluorescence mode. These O-K edge spectra for all samples in TEY and TFY mode exhibit major spectral features at ~532.7, 535.0, 541.8 and 552.7 eV [1, 2]. Pre-edge region observed in TEY mode consists of two peaks around ~528.3 and 529.5 eV and arises due to the excitation to the localized bound state (Fig. 1). A visual inspection shows that the intensity of peaks (532-552 eV) increases after irradiation and may be due to evolution of empty states by irradiation. Decrease in intensity with irradiation and almost no change with fluence indicate surface state pining due to presence of defects. These modifications occur due to simultaneous fragmentation, grain growth, surface diffusion, viscous flow, sputter redeposition, and sputter removal affected by shadowing processes [2, 3]. The detailed investigation has been carried out by performing XANES study at different angles 10º, 45º and 70º.

REFERENCES

[1] J. P. Singh, K. Asokan, D. Kabiraj, D. Kanjilal and W. F. Pong (under preparation)
[2] S. Ikeda, K. Miura, H. Yamamoto, K. Mizunuma, H. D. Gan, M. Endo, S. Kanai, J. Hayakawa, F. Matsukura , and H. Ohno, Nature Materials 9 (2010)721
[3] J. P. Singh, K. Asokan, D. Kabiraj, D. Kanjilal, S. Gautam, and K. H. Chae, Adv. Mater. Lett. 3 (2012) 112 and ref within.

5.2.29 SWIFT HEAVY ION INDUCED MODIFICATIONS IN $NdNiO_3$ THIN FILMS DEPOSITED ON $SrTiO_3$ SUBSTRATE

Yogesh Kumar[1], R. J. Choudhary[2], Ravi Kumar[3]

[1]Inter-University Accelerator Centre, Aruna Asaf Ali Marg, New Delhi -110067, India
[2]UGC-DAE Consortium for Scientific Research, Indore – 452 001, India
[3]Centre for Materials Science & Engineering, National Institute of Technology, Hamirpur – 177 005, India

We report here the growth and the effect of 200 MeV Ag^{15+} ion beam on the structural properties of NdNiO3 (NNO) thin films deposited on c-axis oriented $SrTiO_3$ (STO) single crystals using the technique of pulsed laser ablation. The KrF excimer laser source (λ = 248 nm and pulse duration ~ 20 ns) was used for the deposition of thin films by ablating $NdNiO_3$ bulk target. Further the thin films were irradiated using Ag^{15+} ion beam at different fluence values of 1×10^{11}, 5×10^{11} and 1×10^{12} ions/cm^2. Growth and effect of swift heavy ion irradiation on the structure of NNO/STO films were studied using X-ray diffraction (XRD). Along with the substrate STO, XRD $\theta - 2\theta$ pattern of all the NNO/STO films are displayed in Fig. 1. Highly c-axis oriented growth of NNO film on STO single crystals is evident from this figure. It is maintained even up to the highest value of irradiation fluence. Further, in order to study the in-plane growth and hence to check the epitaxy of films, ϕ-scan measurements are performed. Along with the substrate, results obtained for pristine film and that of irradiated at highest fluence value of 1×10^{12} ions/cm^2 are shown in Fig. 2. Apparently, we obtain four peaks in each case, indicating the cube-on-cube growth of samples. Hence, it is obvious that the films not only have the oriented growth but are also epitaxial in nature. The close matching of pseudocubic unit cell parameter of NNO (~ 3.81 Å) with cubic unit cell parameter of STO (~ 3.903 Å) would have resulted in such a growth [1]. Besides this, an increase in out-of-plane lattice parameter after irradiation is evident from the vertical line shown in Fig. 1. It would have been due to the high pressure zones created in the target material by the energetic ions while passing through it [2].

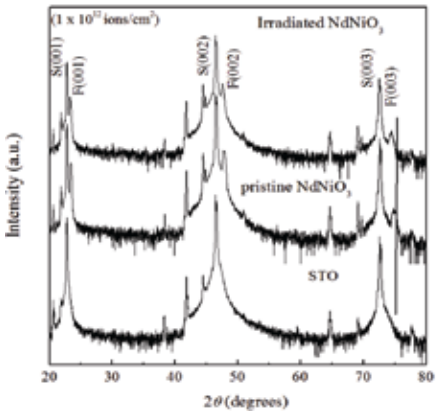

Fig. 1. XRD θ-2θ patterns of pristine and the irradiated $NdNiO_3$ films. Some of the peaks are indicated by symbols 'S' and 'F' which represent the peaks of substrate and film, respectively.

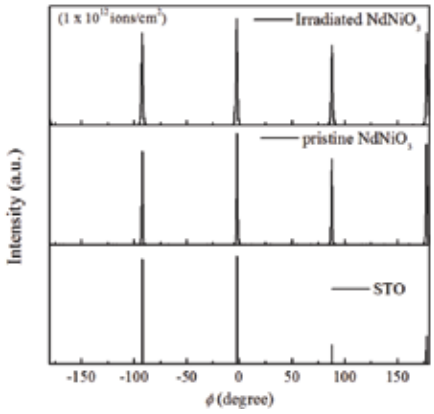

Fig. 2. ϕ-scans along (110) planes of $SrTiO_3$ (STO) substrate and that of pristine and irradiated $NdNiO_3$ thin films.

REFERENCES

[1] A. Tiwari, C. Jin, and J. Narayan, Appl. Phys. Lett. 80 (2002) 4039
[2] G. Szenes, Phys. Rev. B 51 (1995) 8026

5.2.30 EFFECT OF 200 MeV Ag ION IRRADIATION ON MULTIFERROIC $GdMnO_3$ THIN FILMS

Puneet Negi[1], Gagan Dixit[2], H. M. Agarwal[1], R. C. Srivastava[1] and K. Asokan[2]

[1]G. B. Pant University of Agriculture and Technology Pantnagar, 263145 Uttarakhand, India
[2]Inter-University Accelerator Centre, Aruna Asaf Ali Marg, New Delhi -110067, India

The modification of magnetic oxides and manganites by swift heavy ion (SHI) got interest since last two decades [1, 2]. SHI irradiation with suitable energy and fluence generates structural strain as well as columnar amorphization in these materials. Presently, we are reporting the effect of irradiation of 200 MeV Ag^{15+} beam on structural properties of multiferroic $GdMnO_3$ thin films grown on (110) oriented $SrTiO^3$ substrate by using pulsed laser deposition technique. The films were at four fluences 5×10^{11} 1×10^{12}, 5×10^{12} and 1×10^{13} ions/cm^2. X-ray diffraction (XRD) of pristine sample confirms the (200) oriented growth of the film as can be seen from Fig. 1(a). The asymmetric stretching mode appearing at 483 cm^{-1} in Raman spectrum (Fig. 1(b)), is associated with MnO_6 and confirms the $GdMnO_3$ phase. XRD pattern shows small shifting of (200) peak towards lower angle side with the increasing fluence values. XRD and the Raman spectra show that films lose their crystallinity at higher fluences (5×10^{12} and 1×10^{13} ions/cm^2). The observed structural disorder may be due to strain as well as columnar amorphization induced by SHI.

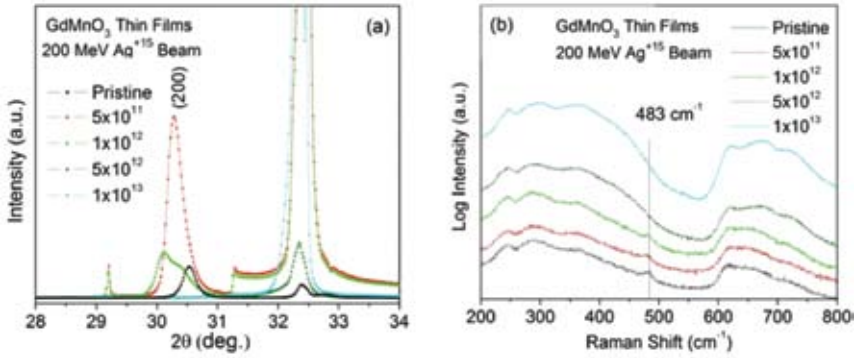

Fig. 1. (a) XRD pattern and (b) Raman Spectra of pristine and irradiated multiferroic $GdMnO_3$ thin films at different fluence values

REFERENCES

[1] R. Kumar, S. K. Arora, D. Kanjilal, G. K. Mehta, R. Bathe, S. K. Date, S. R. Shinde, L. V. Saraf, S. B. Ogale, and S. I. Patil, Radiation Effects and Defects in Solids 147 (1999) 187

[2] R. N. Parmar, J. H. Markna, D. G. Kuberkar, R. Kumar, D. S. Rana, V. C. Bagve, and S. K. Malik, Appl. Phys. Lett. 89 (2006) 202506

5.2.31 LOW TEMPERATURE DIELECTRIC BEHAVIOUR OF 100 MeV O^{7+} IRRADIATED NCO TERMINATED LIQUID CRYSTALLINE POLYURATHANE

Sohan Lal and J. K. Quamara

Physics Department, National Institute of Technology, Kurukshetra

The liquid Crysalline Polyurathane (LCPU) is quite versatile from application point of view. The thermotropic LCPUs have many commercial and scientific applications, particularly in display and optical storage devices. In present study we report the dielectric properties of 100MeV O^{7+} ion irradiated LCPU samples. The LCPU samples were synthesized based on NCO terminated polybutadiane and bi-phinol [1]. The dielectric constant and loss studies of pristine as well as O^{7+} ion irradiated samples (fluence: 3×10^{10}, 3×10^{11} and 1×10^{12}) have been made in temperature range 80 K to 300 K for different frequencies using Agilent 4285 LCR meter at IUAC.

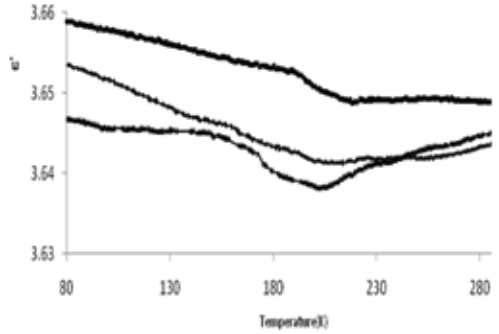

Fig. 1. A plot of dielectric Constant (ε′) versus temperature for the pristine (-×)and O^{7+}irradiated LCPU samples at different fluence of irradiation (-■- 3×10^{10} , -♦- 3×10^{11} ions/cm^2) at 10 KHz frequency.

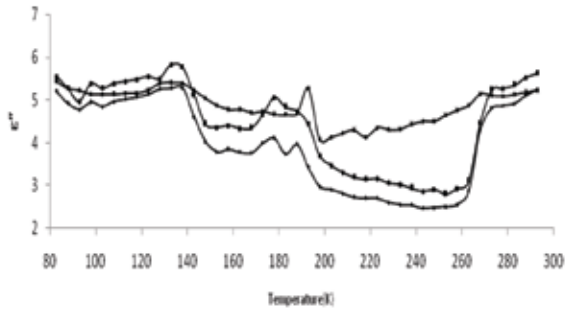

Fig. 2. A plot of dielectric loss (ε′′) versus temperature for the pristine (-×) and O^{7+}irradiated LCPU samples at different fluence of irradiation (-■- 3×10^{10} , -♦- 3×10^{11} ions/cm^2) at 10 KHz frequency.

The variation of dielectric constant and loss spectrum for samples has been shown in Fig. 1 and Fig. 2 respectively. From the figure it can be seen that the dielectric constant initially decreases rapidly with the increase in temperature up to 190 K and becomes almost temperature independent for 190 K to 220 K but again increases with temperatures after 220 K. The nature of curves can be associated to various relaxation processes, namely, γ-relaxation around 130 K, β- relaxation around 180-190 K and α relaxation polarization around 260 K which occur in this PLC [2]. These relaxation processes are revealed in ε′-T curves. The dielectric constant (ε′) values for the irradiated samples are more than those for the pristine samples and increases with increasing fluence. This may be due to increase in water absorbing capacity due to irradiation.

REFERENCES

[1] Pushkar Raj, Sohan Lal, A. B. Samui, S. K. Mahna, and J. K. Quamara, IJPAC: 3 (2011) 211

[2] G. Georgoussis, A. Kyritsis, P. Pissis, Yu. V. Savelyev. E. R. Akranovich, and E. G. Privalko. Eur. Polymer Jour. 35 (1999) 2007

5.2.32 RECTIFYING RESPONSE OF SCHOTTKY DEVICES USING ZnO-NANORODS IRRADIATED WITH 80-MeV OXYGEN IONS

Sayan Bayan and Dambarudhar Mohanta

Nanoscience and Soft Matter Laboratory, Department of Physics, Tezpur University, PO Napaam, Tezpur 784 028, Assam.

The metal/semiconductor junction of high quality is vital for the development of semiconductor nanostructure based opto-electronic devices. The Schottky response was studied in Ag/ZnO junctions having 80-MeV O^{6+} ion irradiated ZnO nanorods. The ZnO nanorods, grown on Al_2O_3/Al substrates [1], were irradiated at IUAC with different ion fluence viz. as 3×10^{10}, 6×10^{10}, and 9×10^{10} ions/cm^2.

In the room temperature photoluminescence (PL) spectra (at λ_{ex}=325 nm), the presence of donor defects like oxygen vacancy (V_O^+) and zinc interstitial related defects (Zn_i and Zn_i^+) were traced out in the Gaussian fitted PL spectrum of the unirradiated sample (Fig. 1(a)). Upon irradiation with different fluences, the evolution of oxygen interstitial and zinc vacancy related acceptor defects (O_i, V_{Zn} and V_{Zn-}) were witnessed (Fig. 1(b), (c), (d)).

As shown in the current-voltage (*I-V*) characteristic curve (Fig. 2), the forward current for the Ag/ZnO junction was found to get enhanced upon irradiating the nanorods with the fluences of 3×10^{10} and 6×10^{10} ions/cm^2. The enhancement in current conduction can be attributed to the increase in defect concentration due to irradiation as observed in the PL spectra (Fig. 1). The Schottky barrier height (ϕ_B) and ideality factor (η) of the junctions [2] can be determined for Ag/ZnO system from the respective I-V curves [3]. The values of ϕ_B for the Ag/ZnO systems, comprising the nanorods irradiated with 3×10^{10} and 6×10^{10} ions/cm^2, show substantial enhancement in the values (0.95 eV and 0.9 eV; respectively) as compared to the unirradiated one (0.78 eV). Again, the respective values of η were found to be 6.9 and 7.3, which are comparatively lower than the unirradiated case (17.7). The evolution of V_{Zn} and O_i acceptor type defects can be assigned for the observed modification [3]. Finally, at the highest fluence of 9×10^{10} ions/cm^2, the decreasing trend of the concentration of native defects compared to the unirradiated one has led to the lowering of the forward current. In this situation, the Ag/ZnO junctions are characterized by moderate values of ϕ_B and η (0.87 eV and 8.0 respectively) than the unirradiated one, owing to the prevalence of V_{Zn}^- defects.

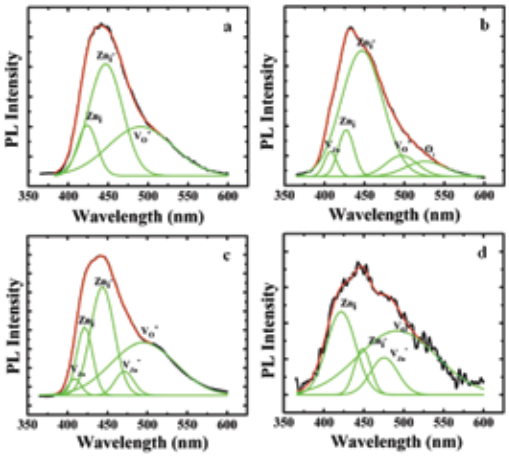

Fig. 1. PL spectra of the nanorods a) before, and after irradiation at (b) 3×10^{10} ions/cm^2, (c) 6×10^{10} ions/cm^2, and (d) 9×10^{10} ions/cm^2.

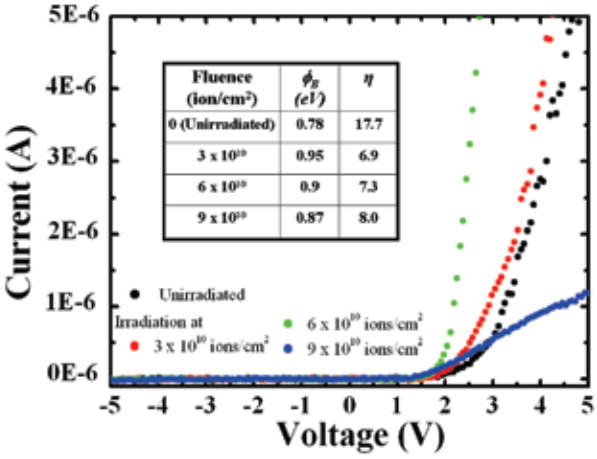

Fig. 2. Room temperature *I-V* characteristic curve of the Ag/ZnO system before and after irradiation.

REFERENCES

[1] S. Bayan and D. Mohanta, J. Appl. Phys. 108 (2010) 023512.
[2] S. M. Sze and K.K. Ng, Physics of Semiconductor Devices, Wiley , New York, 2007.
[3] S. Bayan and D. Mohanta, J. Electron. Mater. (In press) DOI: 10.1007/s11664-012-1995-8.

5.2.33 EFFECTS OF 30 AND 60 MeV BORON ION IRRADIATION ON ELECTRICAL CHARACTERISTICS OF BIPOLAR TRANSISTOR

K. S. Krishna Kumar, C.M. Dinesh, Ramani

Department of Physics, Bangalore University, Bangalore-560056

The transistors studied for total fluence effects for 30 and 60 MeV boron ion irradiation in the present investigation are silicon NPN overlay RF Power transistor (BEL 2N 3866) used for high power gain driver for VHF/UHF applications in space, military and communication equipments. The irradiation was performed in vacuum chamber with decapped transistor in unbiased condition with grounding all leads and exposing directly to beam with ion fluence ranging from 1×10^{10} to 1×10^{12} ions/cm^2 at IUAC.

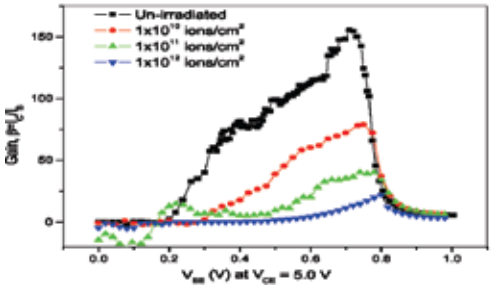

Fig. 1. Variation of gain for different fluences 30 MeV B^{4+} ion irradiated. 2N 3866 transistor.

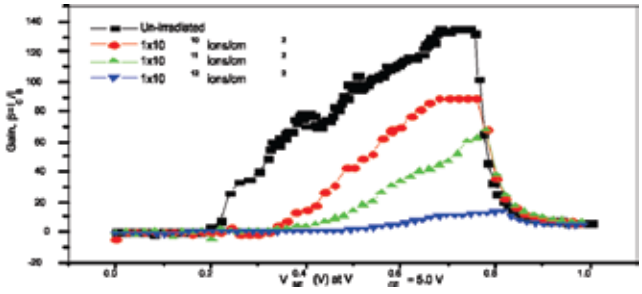

Fig. 2. Variation of gain for different fluences 60 MeV B^{4+} ion irradiated. 2N 3866 transistor.

Fig. 1 and 2 shows the Gummel characteristics of the transistor before and after irradiation by 30 and 60 MeV B ions respectively. Exposure of the transistor to B ion decreases I_C but increases I_B with the increase in ion fluence. The atomic displacements and vacancies produced upon irradiation in the bulk of the transistor reduce the minority carrier lifetime. A decrease in the minority carrier lifetime is reflected in the degradation of forward current gain of the transistor. The other important characteristic that influences the total-dose response of bipolar transistors is the output or collector characteristics (I_C-V_{CE}). Fig. 3 and 4 show the output I_{CE}-V_{CE} characteristic curves for unirradiated and irradiated transistor for different fluences at a constant base current of I_B = 50 μA. The collector current reduces considerably as the fluence increases. Further, there is a decrease in I_{Csat} with increase in fluence. The boron ions induced defects reduce the minority carrier lifetime and may be responsible for the increase in series resistance and thereby reducing I_{Csat}.

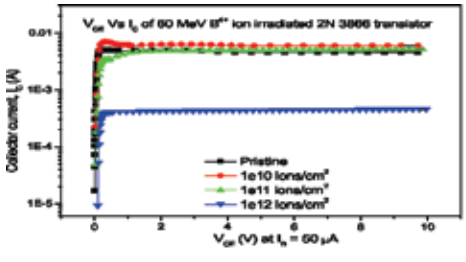

Fig. 3. Collector characteristics of the transistor 2N 3866 at different fluences at const I_B=50μA and different V_{CE}

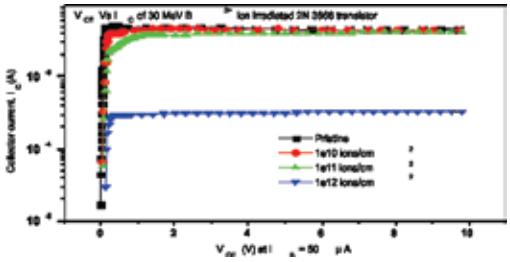

Fig. 4. Collector characteristics of the transistor 2N 3866 at different fluences at const I_B=50μA and different V_{CE}

Fig. 5 and 6 shows the plot of capacitance versus collector-base voltage for B^{4+} ion irradiated transistor and for unirradiated transistors. The plot shows that there is a considerable degradation in the C–V characteristics of the transistor after irradiation. This would indicate that there is a partial loss of charge carriers in the base-collector junction of the transistor upon irradiation [2, 3].

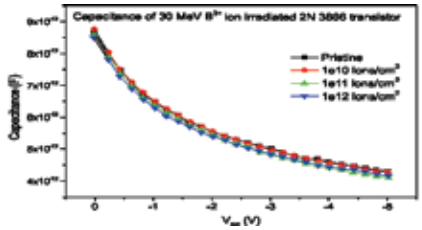

Fig. 5. Capacitance variation of collector-base junction at different fluences of 30 MeV B^{4+} ion irradiated 2N 3866.

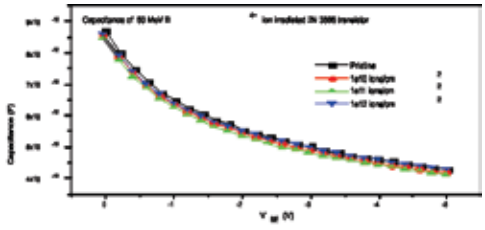

Fig. 6. Capacitance variation of collector-base junction at different fluences of 60 MeV B^{4+} for 2N 3866

The results reveal considerable degradation of the electrical characteristics leading to reduction in the forward current gain. The I-V, C-V measurements reveal that the defects and recombination centers generated in the emitter-base region as well as in the neutral base region are largely responsible for the reduction in the collector current and increase in base current.

REFERENCES

[1] Kanjilal D, Curr. Sci. 80 (2001) 1560
[2] C.M. Dinesh, Ramani, M. C. Radhakrishna, R. N.Dutt, S. A.Khan, and D. Kanjilal, Nucl. Instr. and Meth.B 266 (2008) 17138
[3] K. V. Madhu, S. R. Kulkarni, and R. Damle, Pramana-J. of Phys. 74 (2010) 97

5.2.34 INFLUENCE OF 175 MeV NICKEL ION AND 75 MeV BORON ION IRRADIATION ON THE I-V CHARACTERISTICS OF NPN RF POWER TRANSISTORS

N. Pushpa[1], K. C. Praveen[1], A. P. Gnana Prakash[1], Ambuj Tripathi[2], S.K.Gupta[3] and D. Revannasiddaiah[1]

[1]Department of Studies in Physics, University of Mysore, Manasagangotri, Mysore-570 006, India
[2]Inter-University Accelerator Centre, Aruna Asaf Ali Marg, New Delhi -110067, India
[3]Technical Physics Division, Bhabha Atomic Research Centre, Mumbai- 400 085, India

The bipolar devices and circuits used for space applications encounter different types of radiations like gamma, neutrons, protons and heavy ions. In case of use in high energy physics experiments like Large Hadron Collider (LHC), the bipolar devices/circuits need to be radiation tolerant up to 100 Mrad of total doses in their 5 year lifetime. In literature there is a lack of understanding, whether the different Linear Energy Transfer (LET) radiation creates same amount of degradation or different while keeping identical total doses. To understand the deterioration on silicon NPN overlay *RF* Power transistors (BEL 2N 3866) we choose two different LET ions i.e., 175 MeV Ni^{13+} ions and 75 MeV B^{5+} ions in the total dose range of 100 krad to 100 Mrad and the ratio of LET of these ions is around 25:1 in silicon. The different electrical characteristics like Gummel characteristics, excess base current (ΔI_B), DC current gain (h_{FE}) and output characteristics were studied before and after ion irradiation. For brevity, ΔI_B and h_{FE} results are presented in this report. Fig. 1 illustrates the change in ΔI_B for 175 MeV Ni^{13+} ion and 75 MeV B^{5+} ion irradiated transistors. We can observe from the figure that, as the ion dose increases the base current also increases to around two orders of magnitude after 100 Mrad of total dose. The increase in IB at low injection is the result of increased recombination current in the emitter-base (E-B) depletion region due to radiation-induced generation-recombination (G-R) centers. In addition to G-R centers, high energy ions can also create various types of defects and their complexes in the transistor structure and they reduce the minority carrier lifetime and this in turn increases the I_B of the transistor. Fig. 2 illustrates the DC current gain (h_{FE}) for 175 MeV Ni^{13+} ion irradiated transistors. From the figure it is clear that the h^{FE} of the irradiated transistors reduces almost to a negligible value after a total dose of 100 Mrad. Similar degradation was observed in 75 MeV B^{5+} ion irradiated transistors. The normalized current gain as a function of total dose for 175 MeV $Ni1^{3+}$ ion and 75 MeV B^{5+} ion irradiated transistors is shown in Fig. 3. From Fig. 1 and 3, it is clear that the degradation in I-V characteristics of transistor is almost same for both types of ions with similar total doses even though there is a large difference in the LET.

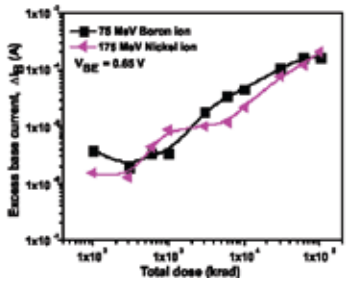

Fig. 1. The variation in excess base current after 175 MeV Ni^{13+} and 75 MeV B^{5+} ion irradiation

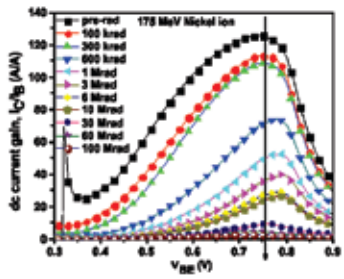

Fig. 2. The variation in dc current gain after 175 MeV Nickel ion irradiation

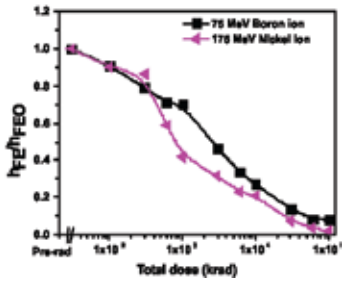

Fig. 3. The normalized current gain as a function of total dose

REFERENCE

[1] N. Pushpa, K. C. Praveen, A. P. Gnana Prakash, P. S. Naik, John. D. Cressler, S. K. Gupta and D. Revannasiddaiah. Nucl. Instrum. Meth. A. 273 (2012) 36

5.2.35 A COMPARISON OF 175 MeV NICKEL AND 75 MeV BORON ION IRRADIATION EFFECTS ON SUBTHRESHOLD CHARACTERISTICS OF N-CHANNEL DEPLETION MOSFETS

N. Pushpa[1], K. C. Praveen[1], A. P. Gnana Prakash[1], Ambuj Tripathi[2], S. K. Gupta[3] and D. Revannasiddaiah[1]

[1]Department of Studies in Physics, University of Mysore, Manasagangotri, Mysore-570 006, India
[2]Inter-University Accelerator Centre, Aruna Asaf Ali Marg, New Delhi -110067, India
[3]Technical Physics Division, Bhabha Atomic Research Centre, Mumbai- 400 085, India

The N-channel metal oxide semiconductor field effect transistors (3N187 MOSFETs) considered for the present work are used in space, military and communication equipments. Therefore understanding the radiation effects on these devices is important. The N-channel MOSFETs were exposed to 175 MeV Ni^{13+} ions and 75 MeV B^{5+} ions in the dose ranging from 100 krad to 100 Mrad. The major radiation effects in MOS devices occur due to charge generation, transport and trapping in the SiO_2. The degradation of MOS devices is mainly due the radiation induced interface (N_{it}) and oxide trapped charges (N_{ot}) at Si/SiO_2 interface and eventually make the device malfunction. The subthreshold characteristics of 175 MeV Ni^{13+} ions irradiated MOSFET is shown in Fig. 1. Similar type of degradation was observed in 75 MeV B^{5+} ion irradiation [1-2]. We observed that the threshold voltage (V_{Th}) of the irradiated MOSFET was found to decrease significantly after ion irradiation. The densities of oxide-trapped (ΔN_{ot}) charge and interface trapped charge (ΔN_{it}) in irradiated MOSFETs were estimated from the subthreshold measurements and are shown in Fig. 2 and Fig. 3 respectively. It can be seen that ΔN_{it} and ΔN_{ot} were found to increase after irradiation and ΔN_{ot} in irradiated MOSFETs was found to be higher than that of ΔN_{it}. The net threshold voltage shift (ΔV_{th}) and contribution to that shift due to the interface traps (ΔVN_{it}) and the trapped oxide charge (ΔVN_{ot}) were calculated by the subthreshold measurements using the technique proposed by McWhorter and Winokur [3]. The ΔN_{ot} is calculated using the standard expression $\Delta N_{ot} = \Delta V_{ot}$ Cox/q and the ΔN_{it} is calculated by the expression $\Delta N_{it} = \Delta V_{it} C_{ox}/q$ where $q = 1.6\times10^{-19}$ C. From the Fig. 2 and 3 it can be seen that the degradation in ΔN_{it} and ΔN_{ot} is almost same for both 175 MeV Ni^{13+} ion and 75 MeV B^{5+} ion irradiated MOSFETs.

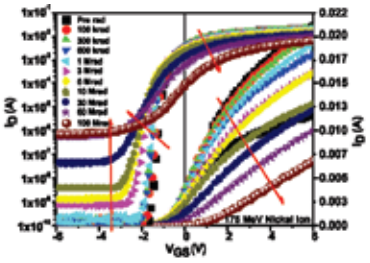

Fig. 1. I_D-V_{GS} characteristics of 175 MeV Ni ion irradiated MOSFET (V_{DS} = 1 V)

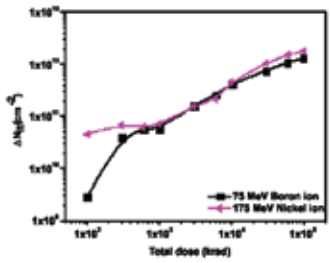

Fig. 2. Variation in ΔN_{it} after 175 MeV Ni^{13+} ion and 75 MeV B^{5+} ion irradiation

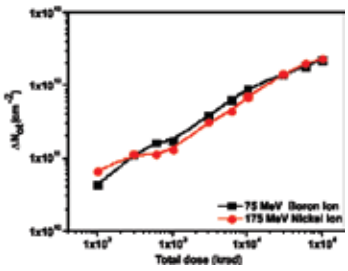

Fig. 3. Variation in ΔN_{ot} after 175 MeV Ni^{13+} ion and 75 MeV B^{5+} ion irradiation

REFERENCES

[1] N. Pushpa, K. C. Praveen, A. P. Gnana Prakash, Y. P. Prabhakara Rao, A. Tripathi, G. Govindaraj, and D. Revannasiddaiah, Nucl. Instr. and Meth. A. 613 (2010) 280

[2] N. Pushpa, K. C. Praveen, A. P. Gnana Prakash, P. S. Naik, Ambuj Tripathi, S. K. Gupta, and D. Revannasiddaiah, Nucl. Instr. and Meth. B 273 (2012) 40

[3] P. J. McWorter and P. S. Winokur, J. Appl. Phys. 48 (1986) 133

5.3 RADIATION BIOLOGY

5.3.1 STUDY OF RADIOSENSITIVITY OF HUMAN CERVICAL CANCER CELL LINE TREATED WITH GLUCOSE STABILIZED GOLD NANOPARTICLE

Harminder Kaur[1], Geetanjali Pujari[1], Manoj Semwal[2], A. Sarma[1] and D.K. Avasthi[1]

[1]IUAC, New Delhi
[2]Army Hospital [Research & Referral], New Delhi

In the present study, we show the radiosensitization effect of Glucose stabilized Gold nanoparticle (Glu-AuNP) on Human cervical cancer cell line HeLa. Glu-AuNP treated cells were irradiated with ^{60}Co gamma and carbon beam (LET 290 KeV//μm). It is seen that gamma as well as carbon ion irradiation of Glu-AuNP treated HeLa cells lead to a steeper survival curve as compared to that of irradiation of untreated cells. The result suggests an enhancement of radio-sensitization induced by Glu-AuNP.

The Glu-AuNP of 5 - 9 nm diameter were synthesized in the Radiation Biology laboratory and characterized by UV-Vis Spectroscopy and Transmission Electron Microscopy (TEM). The internalization of Glu-AuNP into the cell was confirmed by TEM of ultra-microtome sections of the cells. The TEM studies were carried out at the AIRF, JNU, New Delhi.

The γ-irradiation was carried out at Army Referral Hospital, New Delhi using Theratron 1000E Telecobalt machine. Carbon ion irradiation was carried out using ASPIRE system at the Radiation Biology beamline of IUAC.

After irradiation, the clonogenic assay was performed to study the effect of γ –radiation and Carbon ion beam on HeLa cells with and without Glu-AuNP pre-treatment. Results of colony forming assay of γ as well carbon ion-irradiated HeLa cells with Glu-AuNP pre-treatment in form of a survival curve are shown in Figure 1. The experimental survival fraction [S/So] data points were fitted with Linear Quadratic dose [D] dependent relation given by $S/So = \exp -[\alpha D + \beta D^2]$, where α and β are constants.

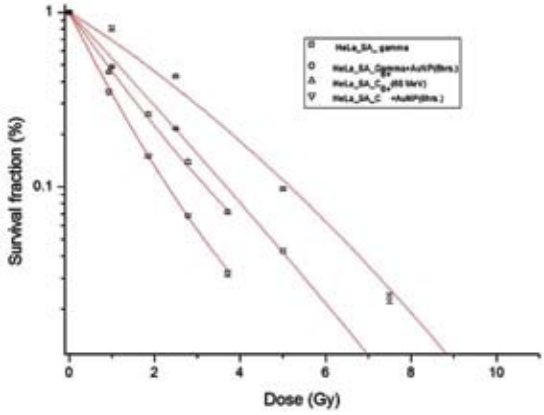

Fig. 1. Survival Fraction of HeLa cells and the γ-irradiated/^{12}C irradiated HeLa cells pre-treated with Glu-AuNP for 6 h.

We observed a significant decrease in survival fraction on combined treatment of Glu-AuNP and γ as well as carbon radiation in comparison to the cells exposed to only γ and carbon ion irradiation. Thus by carrying the AuNP to cancer cells, the tumour cell killing efficiency during radiation therapy can be enhanced and more killing is observed at lesser dose of radiation. Thus this result can contribute towards clinical application in radiation therapy.

5.3.2 ROLE OF PARP-1 IN CELL CYCLE REGULATION OF HUMAN CERVICAL EPITHELIAL CARCINOMA (HELA) CELLS IN RESPONSE TO HIGH LET RADIATION $^{12}C^{6+}$

A. Ghorai[1], A. Sarma[2], N.P. Bhattacharyya[3], U. Ghosh[1]

[1]Department of Biochemistry & Biophysics, University of Kalyani, WB-741235
[2]Inter-University Accelerator Center, Aruna Asaf Ali Marg, New Delhi, 110067
[3]Saha Institute of Nuclear Physics, 1/AF Bidhannagar, Kolkata- 700064

High LET (linear energy transfer) radiations are known to have more pronounced biological effectiveness than low LET X-ray or γ-ray. Besides other consequences of DNA damage by high LET radiations alteration in cell cycle pattern is one of them [1]. Poly (ADP-ribose) polymerase (PARP) is a DNA repair enzyme but it has a great impact on cell cycle progression [2]. Here we are interested to find out the role of PARP-1 in cell cycle progression after DNA damage by heavy ion beam which produces cluster damage.

Our preliminary data showed that HeLa cells were arrested at S phase up to 2.0 Gy of $^{12}C^{6+}$ (62 MeV, average LET 287 kev/μm, fluence $4\times10^6/cm^2$) as detected in FACS Calibur™ (BD Bio- science, USA), fluorescence-activated cell sorter. Conversely, PARP-1 knock down cells (HSiI) were arrested at G_2/M phase dose dependently and also arrested at higher doses (2.0 Gy and 4.0 Gy) at S phase like normal HeLa cells (Table- 1). All were done for 24 hrs growth after irradiation. We need to find out the detail mechanism behind this observation further.

Dose (Gy)	HeLa (% of Cell Population with standard deviation)			HSiI (% of Cell Population with standard deviation)		
	G_0/G_1	S	G_2/M	G_0/G_1	S	G_2/M
0	40.77±0.36	43.87±1.08	15.35± 0.72	37.33±0.07	47.46± 0.38	15.19± 0.40
0.5	28.49± 0.16	53.58± 0.82	17.92± 0.78	34.30±0.80	48.85± 1.58	16.84± 0.87
1.0	26.89± 0.27	57.57± 0.94	15.53± 1.11	30.69±1.29	46.68± 1.27	22.62± 0.89
2.0	32.66± 2.43	57.73± 3.42	9.59± 0.99	19.16±0.48	58.12± 0.71	22.71± 0.52
4.0	41.51± 2.01	41.34± 4.94	17.14± 2.92	26.36±9.08	55.32±12.12	18.98± 4.04

Table- 1: Cell Cycle analysis by FACS after $12C^{6+}$ irradiation.

REFERENCES

[1] B.C. Woodhouse & G.L. Dianov. DNA Repair (Amst). 7(7) 2008 1077-86. Review
[2] C. Boehler et al. Proc Natl Acad Sci U S A. 2011 Feb 15; 108(7):2783-8.

5.4 ATOMIC & MOLECULAR PHYSICS

5.4.1 ION ENERGY LOSS IN THE WAKE FIELD IN SOLID FOILS

T. Nandi[1], K. Haris[2], Pankaj Kumar[1], S. A. Khan[1], Anil Batra[3], Bhawna Arora[3], Akhil Jhingan[1], P. Verma[4] and H G Berry[5]

[1] Inter-University Accelerator Centre, JNU New Campus, New Delhi 11 0067
[2] Dept. of Physics, Aligarh Muslim University, Aligarh 20 2002
[3] Dept. of Physics, Delhi University, Delhi 11 0007
[4] Dept. of Physics, Kalindi College, East Patel Nagar, New Delhi-110008.
[5] Dept. of Physics, University of Notre Dame, Notre Dame, Indiana 46556

Our atomic lifetime measurements has found the signature of surface wake field at the exit surface due to passage of highly charged ion beam through a solid thin foil [1]. Further, another study shows that highly charged slow ions lose a lot of their energy at the entry surface [2]. Recently, we have measured the stopping powers of several fast, highly-ionized atoms passing through thin bi-layer targets made up of polypropylene and aluminum. We were surprised to find that the energy loss depends on the ordering of the target (PP/Al or Al/PP) and is significantly different for the two cases. We measure an average differential energy loss of 458 ± 31keV. We tentatively ascribe to the differing wake fields as the beam exits the target in the two cases. Our differential energy loss results are about two orders of magnitude greater than the theoretical predictions of Neelavati et al [3] for energy losses due to the wake potential for fast ions in solids. However, theoretical estimates, from the work of Vager and Gemmell [4], show reasonably close agreement with our results.

Table 1: Energy loss contributions due to wake potentials (from definition)

Ion species	Ion-beam Energy (MeV)	Al/PP E_{out} (MeV)	PP/Al E_{out} (MeV)	Difference in energy loss (keV)	Average difference
56 Fe 10+	115.084±0.021	86.860±0.023	86.447±0.029	413 ± 37	458 ± 31
58 Ni 10+	111.185±0.017	79.369±0.030	78.914±0.028	455 ± 41	
58 Ni 11+	134.204±0.010	104.036±0.034	103.553±0.045	483 ± 57	
58 Ni 12+	159.970±0.014	130.923±0.040	130.442±0.030	481± 50	

The experimental set up has already been discussed; the major result is given here. Further measurements with bi-layer foils of differing thicknesses and conductivity are expected to elucidate the origin of the differential energy loss further, and verify or negate our suggestion that it is due to the exit wake field.

REFERENCES

[1] T. Nandi and B.P. Mohanty, "Measurement of Wake Field Intensity", *J. Phys. B: At. Mol. Opt. Phys,* 42, 225402 (2009)

[2] T. Nandi,"Role of Ion-Surface Interaction at the Entry Surface on the Energy Loss of Highly Charged Slow Ions in Solids" Open Journal Microphysics, Vol. 1, 53-57 (2011).

[3] N. Neelavati, R.H. Ritchie and W. Brandt, "Bound Electron States in the Wake of Swift Ions in Solids", Phys. Rev. Lett. 33, 670 (1974); and 34, 560 (1975).

[4] Z. Vager and S. Gemmell, "Polarization Induced in a Solid by the Passage of Fast Charged Particles", Phys. Rev. Lett. 37, 1352 (1976).

5.4.2 FULLY STRIPPED IONS IN NUCLEAR REACTION

T. Nandi[1], B.J.Roy[2], Biraja Mohanty[3], Mumtaz Oswal[3], Sunil Kumar[3], B. Kumar[4], K. Haris[5], V. Jha[2], D.C. Biswas[2], and Akhil Jhingan[1]

[1]Inter-University Accelerator Centre, New Delhi-110 067
[2]Nuclear Physics Division, Bhabha Atomic Research Centre, Mumbai-400085
[3]Department of Physics, Panjab University, Chandigarh – 160014
[4]Department of Physics, J. P. University, Chapra - 841301, Bihar
[5]Department of Physics, A.M.U., Aligarh -202002, U.P.

It is evident from our work [1] that the projectile like ions are most likely formed as the fully stripped ions. Also in another study [2] it is observed that the ions do capture up to circular Rydberg states in the H and He-like ions while passing through the target. It can be noted here that no Rydberg states can survive while passing through a solid matrix indicating that they can only be formed at the exit surface [1, 2]. This demands that the starting ion must be a fully stripped ion. In order to substantiate it, several measurements were done recently in direct as well as inverse kinematics.

For the direct kinematic experiments, ^{12}C beams of energies in the range of 45-70 MeV were bombarded on enriched target of ^{56}Fe. Elastic events and light particles were detected using silicon surface barrier detectors in ΔE-E telescope while X-ray spectra from the target like particles were recorded by a low energy germanium detector using a suitable X-ray absorber. Iron Kα and K_β lines were observed due to the K-shell vacancy creations by ion impact. However, the X-ray lines from target like ions (TLI) such as Ni and Ga originated from Lyα and Lyβ structures; no Kα and K_β lines belonging to Ni and Ga have been noticed at all. It means the X-rays from only H-like ions and no X-rays from neutral atoms. These H-like ions are produced from α-transfer reactions or p-evaporation from the compound nuclei or from compound nuclei. Reaction product would lose all electrons except one in excited state is an utter unphysical proposition. Rather, fully stripped ions are formed in the first place and then electron capture takes place. Hence, both nuclear and atomic phenomena are responsible for production of H-like TLI.

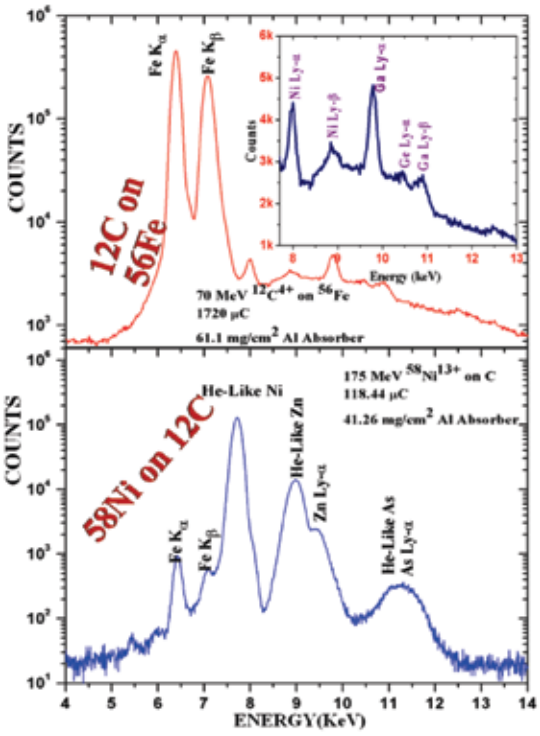

Fig. 4. A detailed comparison of the observed X-ray spectra as obtained in direct (upper panel) and inverse (lower panel) kinematics.

In the inverse kinematic experiments 173 & 175 MeV ^{58}Ni beams were bombarded on the natural carbon target and X-ray spectra obtained from this experiment display X-ray lines from H and He-like Zn and As ions producing from a-transfer reaction and p-evaporation residues, respectively. Whereas He and Li – like ions are formed from the projectile ions, but only H and He –like ions are formed from PLI. This reveals that higher charge states are created with PLI. Here also above mentioned two-step process hold true that firstly the fully stripped ions are formed from nuclear reaction in the time scale of 10^{-22} sec and then electron capture occurs in 10^{-18} sec. Hence, both nuclear and atomic processes are occurring at different times. Such an experiment in the cross link between atomic and nuclear physics is done for the first time. The area of research is having important implication in astrophysics.

REFERENCES

[1] T. Nandi, J. Phys. B 42 (2009) 125201.
[2] T. Nandi, Astro. Phys. J. Lett 673 (2008) L103.

5.4.3 A NEW ELECTRON CAPTURE PROCESS

T. Nandi[1], B.J.Roy[2], Biraja Mohanty[3], Mumtaz Oswal[3], Sunil Kumar[3], B. Kumar[4], K. Haris[5], V. Jha[2], D.C. Biswas[2], and Akhil Jhingan[1]

[1]Inter-University Accelerator Centre, New Delhi-110 067
[2]Nuclear Physics Division, Bhabha Atomic Research Centre, Mumbai-400085
[3]Department of Physics, Panjab University, Chandigarh – 160014
[4]Department of Physics, J. P. University, Chapra - 841301, Bihar
[5]Department of Physics, A.M.U., Aligarh -202002, U.P.

Besides the nuclear observables, atomic observables are also observed from any nuclear reactions. Recently detail analysis of the x-ray spectra from nuclear reactions showed that nuclear products are

basically fully stripped ions [1, 2]. Subsequently electron capture needs to take place to result in excited states emanating x-rays. Experimental condition prevailing nuclear reactions does not favor usual electron capture processes. For example, the target–like ions can capture electrons from target atoms; however, electron capture probability from target atoms for projectile-like ions (PLI) is extremely small. The PLI could only capture from the electrons, which are left by the projectile ions at the very moment of the PLI formations.

Very interestingly, this electron capture process leads to larger double-electron capture cross section than single electron capture cross section. X-ray spectra due to 175 MeV $^{58}Ni^{13+}$ beam on ^{12}C exhibit x-rays from both projectile ions and PLI. Considering the fact that projectile x-rays are formed due to electronic excitation of the concerned charge state, whereas the x-rays from PLI is a result of electron capture followed by production of PLI from a nuclear transfer reaction as follows:

$CSF \times \sigma_{exc} \times N_p = \sigma_{tran} \times N_t \times N_p \times \sigma_{sec} \times R$

Where CSF= Total charge state fractions of He & Li-like ions through 50 μg/cm^2 C-foil leading to x-rays = (9.2 + 26*0.7)= 27.4%. Here 0.7 is the branching ratio of M2 x-ray transition from 1s2s2p $^4P_{5/2}$ state in Li-like ions.

σ_{exc} = 1s to 2p excitation cross section= 0.3 x 10^{-20} cm^2. Both CSF and σ_{exc} are taken from ETACHA code [3].

σ_{tran} = α transfer cross section = 16.5±0.16 mb as measured from this experiment

N_t = Number of target atoms = 2.6x10^{18} cm^2

N_p = Number of projectile ions falling on the target

σ_{sec} = Single electron capture cross section for $^{62}Zn^{30+}$ from left over electrons by $^{58}Ni^{13+}$ after nuclear reaction.

R= He-&Li-like peak of projectile/Ly-α peak of projectile like ion as measured in the experiment = 92

Assuming 10% uncertainty in the theoretical CSF and σ_{exc} values and experimental measured errors in other quantities, the unknown quantity σ_{sec} in the above equation turns out to be 2.08 ± 0.77 x10^{-16}cm^2. If we replace R now by the He-&Li-like peak of projectile/X-ray peak of He-like PLI as measured in the experiment = 12.27; σ_{sec} will be replaced by σ_{dec} , which is the double electron capture cross section of $^{62}Zn^{30+}$ from the left over electrons by $^{58}Ni^{13+}$. Then we find σ_{dec}= 1.50 ± 0.57 x10^{-15} cm^2. Double electron capture cross section is 7.2 times higher than the single electron cross section. In order to understand this process, theoretical works are in progress.

REFERENCES

[1] T. Nandi, J. Phys. B 42 (2009) 125201.
[2] The article no 5.4.2 in this annual report.
[3] J.P. Rozet, C. Stéphan, and D. Vernhet, Nucl. Instr. Meth. B 107 (1996) 67.

5.5 ACCELERATOR MASS SPECTROMETRY

5.5.1 ^{10}Be IN THE SEDIMENT CORE FROM CENTRAL INDIAN OCEAN BASIN

J.N.Pattan[1], Pankaj Kumar[2], Archna Bohra[2], G. Parthiban[1] and S.Chopra[2]

[1]CSIR-National Institute of Oceanography, Dona Paula, 403004, Goa.
[2]Inter-University Accelerator Centre, Aruna Asaf Ali Marg, 110067, New Delhi.

^{10}Be is the cosmogenic radionuclide mainly produced in the upper atmosphere by spallation of nitrogen and oxygen atoms by secondary cosmic rays. ^{10}Be in the marine is mainly sourced from cosmogenic and terrestrial. It is produced in the atmosphere and washed by the rainwater, transported and get absorbed to the fine clay particles in the marine sediments. ^{10}Be has a half life of 1.387 Ma hence; it is a potential tool for dating sediment cores in the time range upto ~12 Ma.

Sediments in the Central Indian Ocean Basin (CIOB) are mostly derived from the Himalayas and Indian peninsula through major rivers such as Ganges-Brahmaputra [1, 2]. Since, these sediments are below the carbonate compensation depth (>4400m), hence, there is no presence of calcium carbonate. However, a significant quantity of biogenic opal is present in these sediments. The sediment accumulation in CIOB is 1-2 mm/ka [3]. Therefore dating of any long sediment core in CIOB is difficult mainly because ^{14}C technique is not possible due to their location below Carbon Compentation Depth (CCD) and U-Th technique does not exceed 300 ka. Therefore, ^{10}Be is only reliable dating tool for CIOB long sediment cores which are few million years old.

For the ^{10}Be chronology, we have used a 5 m long sediment core (AAS-V/GC-02) collected at a water depth of 5000m in CIOB from siliceous domain (Fig.1). This sediment core was analyzed for major, trace and ultra-trace elements earlier [4]. The present core showed large variation in the intensity of monsoonal precipitation (Al, Ti, Zr content), biogenic productivity (biogenic opal content) and weathering processes (K/Al and Mg/Al ratio). To understand chronology of these events ^{10}Be chronology is being investigated for the sediment core in CIOB. Initially we have selected six sediment subsamples from the sediment core, one duplicate sediment sample and a blank to monitor background. To know the variation between leached (atmospheric produced) and bulk (both atmospheric and terrigenous fraction) chemical treatment we have studied both fractions. The procedure of chemical processing of sediments is taken from reference [5]. These processed samples were analyzed for ^{10}Be/^{9}Be ratio using AMS facility of IUAC, New Delhi. The processing of data is under progress.

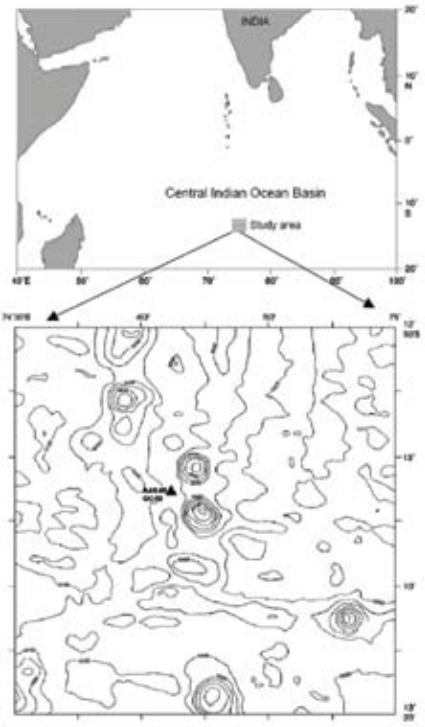

Fig. 1. Map showing study area and location of the sediment core AAS-05/GC-02.

REFERENCES:

[1] Nath et al., 2008, Mar. Geol, 87, 301-313.
[2] Mudholkar et al., 1993. Indi. J. Mar.Sci, 22, 241-246
[3] Banakar et al., 1991.Mar. Geol. 96, 167-173.
[4] Pattan et al., 2005. Chem. Geol. 221, 26-278.
[5] Pankaj Kumar et al., 2011. J. Radio. Nucl.Chem, DOI 10.1007/s10967-011-1184x